OECD/MCCI-2009-TR06

OECD MCCI Project
2-D Core Concrete Interaction (CCI) Tests:
CCI-5 Data Report

Rev. 1 - Final

November 2010

by:

M. T. Farmer, D. J. Kilsdonk, S. Lomperski, and R. W. Aeschlimann

Nuclear Engineering Division
Argonne National Laboratory
9700 S. Cass Avenue
Argonne, IL 60439 USA

Table of Contents

1.0 INTRODUCTION.....1

2.0 FACILITY DESCRIPTION.....2

2.1 Test Apparatus.....3

2.2 Instrumentation and Data Acquisition.....8

2.3 Corium Composition.....15

2.4 Concrete Composition.....15

3.0 TEST PROCEDURES.....17

3.1 Pretest Preparations.....17

3.2 Test Operations.....20

4.0 RESULTS.....27

4.1 Electric Power.....27

4.2 Melt Temperatures.....27

4.3 Concrete Basemat and Sidewall Ablation Rates.....28

4.4 Posttest Debris Examination and Chemical Analysis Results.....30

5.0 REFERENCES.....38

APPENDIX A: Data Acquisition System Channel Assignments.....39

APPENDIX B: Test Data.....52

APPENDIX C: Chemical Analysis Results.....85

List of Figures

Figure **Page**

2-1 Schematic of CCI Test Facility 4
2-2 Top View of Lower Test Section 4
2-3 Side View of Lower Test Section Showing Inert MgO Sidewall Sections 5
2-4 Side View of Lower Test Section Showing Concrete Sidewall 5
2-5 Test Section Water Supply System 7
2-6 Quench and Overflow Tanks 7
2-7 Spray Tank 9
2-8 Off Gas System 9
2-9 Illustration of CCI-5 Crust Lance Assembly Mounted in Test Section 10
2-10 Test Section Pressure Relief System 11
2-11 Photograph of Rupture Disk and Counter-Weighted Check Valve 11
2-12 Plan View of Basemat Instrumentation Layout (dimensions are in cm) 12
2-13 Elevation View of Basemat Type C Thermocouple Locations 13
2-14 Exterior View of Concrete Sidewall Form Showing Instrument Locations 13
2-15 CCI Data Acquisition and Control Systems 14
3-1 Illustration of Thermite Sample Train Installed in Test Section 19
3-2 Voltage Reading Across Thermite Igniter Shunt 22
3-3 Bulk Melt Temperature Data over the First 5 Minutes of the Interaction 22
3-4 Test Section Pressure Response 24
3-5 Quench System Tank Differential Pressure Responses (the range of these units is 0-35 kPad, and they clip at ~ 55 kPad) 24
3-6 Photo of Aerosol Plugging of Offgas Flowmeter Inlet (pipe ID is 10 cm) 25
3-7 Miscellaneous Temperatures in Quench and Off-Gas Systems 25
3-8 Thermal Response in South MgO Sidewall at the +10 cm Elevation 26
4-1 DEH Input Power 27
4-2 Melt Temperatures Measured During CCI-5 28
4-3 Basemat Axial Ablation Front Location 29
4-4 North Sidewall Lateral Ablation Front Location 29
4-5 Top Views of the Test Section (a) After Lid Removal, and (b) After Removal of Top Section, Middle Section, and Test Section Transition Plate 32

List of Figures (Contd.)

Figure **Page**

4-6 Side View of Lower Section (from west) After Removal of MgO Sidewalls.....33
4-7 View from the West of the Solidified Corium over the Basemat.....34
4-8 View from the North of the Solidified Corium over the Basemat 35
4-9 (a) Perspective and (b) Close-up Photographs of Corium on the North Concrete Sidewall 36
4-10 Posttest Debris Renderings as Viewed from the (a) West and (b) South.....37
B-1 Compensator Temperature, Channels B0-B49 and B50-B99.....53
B-2 Basemat Type C "WCL" Array Data.....53
B-3 Basemat Type C "WNW" Array Data.....54
B-4 Basemat Type C "WNE" Array Data 54
B-5 Basemat Type C "WSE" Array Data.....55
B-6 Basemat Type C "WSW" Array Data.....55
B-7 North Sidewall Type C "WN" Array Data 56
B-8 Melt Surface Temperature Optical Pyrometer OP-1 Data.....56
B-9 Basemat Type K "A" Array Data 57
B-10 Basemat Type K "B" Array Data.....57
B-11 Basemat Type K "C" Array Data.....58
B-12 Basemat Type K "D" Array Data 58
B-13 Basemat Type K "E" Array Data.....59
B-14 North Sidewall Type K "SWA" Array Data.....59
B-15 North Sidewall Type K "SWB" Array Data.....60
B-16 North Sidewall Type K "SWC" Array Data.....60
B-17 North Sidewall Type K "SWD" Array Data.....61
B-18 North Sidewall Type K "SWE" Array Data 61
B-19 North Sidewall Type K "SWF" Array Data 62
B-20 North Sidewall Type K "SWG" Array Data.....62
B-21 North Sidewall Type K "SWH" Array Data.....63
B-22 North Sidewall Type K "SWI" Array Data 63
B-23 North Sidewall Type K "SWJ" Array Data 64

List of Figures (Contd.)

Figure **Page**

B-24 North Sidewall Type K "SWK" Array Data 64
B-25 North Sidewall Type K "SWL" Array Data 65
B-26 North Sidewall Type K "SWM" Array Data 65
B-27 North Sidewall Type K "SWN" Array Data 66
B-28 North Sidewall Type K "SWO" Array Data 66
B-29 Thermocouple Compensator Data for Channels Q0-Q49 and Q50-Q99 67
B-30 Test Section Sidewall Heat Loss Data at -17.5 cm Elevation 67
B-31 Test Section Sidewall Heat Loss Data at -10.0 cm Elevation 68
B-32 Test Section Sidewall Heat Loss Data at -7.5 cm Elevation 68
B-33 Test Section Sidewall Heat Loss Data at +2.5 cm Elevation 69
B-34 Test Section Sidewall Heat Loss Data at +10.0 cm Elevation 69
B-35 Test Section Sidewall Heat Loss Data at +12.5 cm Elevation 70
B-36 Test Section Sidewall Heat Loss Data at the +67.5 cm Elevation 70
B-37 Test Section Sidewall Heat Loss Data at the + 92.2 cm Elevation 71
B-38 Test Section Sidewall Heat Loss Data at the + 148.8 cm Elevation 71
B-39 Test Section Sidewall Heat Loss Data at the + 174.7 cm Elevation 72
B-40 Test Section Sidewall Heat Loss Data at the + 193.0 cm Elevation 72
B-41 Test Section Sidewall Heat Loss Data at the + 211.3 cm Elevation 73
B-42 Test Section Sidewall Heat Loss Data at the + 229.6 cm Elevation 73
B-43 Test Section Mainline Thermocouple Data 74
B-44 Test Section Plenum and Insertable Water Probe Thermocouple Data 74
B-45 Quench Tank Water Volume, Coil Inlet, and Coil Outlet Temperatures 75
B-46 Temperatures in Water Supply, Quench, and Off Gas Systems 75
B-47 Crust Lance Load Cell Data 76
B-48 Lance Position Indicator Data 76
B-49 Total Power Supply Power 77
B-50 Power Supply Voltage Data 77
B-51 Total Power Supply Current Data 78
B-52 Power Supply Current Transformer Data 78

List of Figures (Contd.)

Figure **Page**

B-53 Hall Effect Meter Data 79
B-54 Voltage across Igniter Shunt 79
B-55 Pressure Transducer Power Supply Voltages 80
B-56 Tank Water Volume Data 80
B-57 Supply and Quench System Tank Head Data (Backup) 81
B-58 Test Section Water Head Transducer Data 81
B-59 Water Supply Tank Pressure 82
B-60 Test Section Pressure 82
B-61 Quench/Overflow and Spray Tank Plenum Differential Pressures 83
B-62 Water Flow Rates 83
B-63 Test Section Helium Cover Gas Flow Rates 84
B-64 Final Off Gas Flow Rate 84

List of Tables

Table **Page**

1-1 Specifications for CCI-5 3
2-1 Post-Reaction Bulk Composition for CCI-5 Thermite 16
2-2 Detailed Pre- and Post-Reaction Compositions for CCI-5 Thermite 16
2-3 Engineering Composition of CCI-5 Siliceous Concrete Basemat and Sidewall 16
2-4 Chemical Composition of Siliceous Concrete 17
3-1 CCI-5 Event Sequence (times relative to onset of cavity ablation). 21
4-1 Chemical Analysis Results for Samples Collected from CCI-5 Posttest Debris 31
A-1 "Concrete" DAS Channel Assignments for CCI-5 40
A-2 "Power" DAS Channel Assignments for CCI-5 44
A-3 "Quench" DAS Channel Assignments for CCI-5 48
C-1 Raw Data from CCI-5 Sample Analyses 86

1.0 INTRODUCTION

Ex-vessel debris coolability is an important light water reactor (LWR) safety issue. For existing plants, resolution of this issue will confirm the technical basis for severe accident management guidelines (SAMGs). For new reactors, understanding this issue will help confirm the effectiveness of the design and implementation of new accident mitigation features and severe accident management design alternatives (SAMDAs). The first OECD-MCCI program conducted reactor material experiments focused on achieving the following technical objectives: i) provide confirmatory evidence for various cooling mechanisms through separate effect tests and data for severe accident code model development, and ii) provide longer-term two-dimensional core-concrete interaction data for code assessment and improvement.

Debris cooling mechanisms investigated as part of the first MCCI program included: i) water ingression through cracks/fissures in the core debris, ii) melt eruption caused by gas sparging (volcanic-type event), and iii) large-scale crust mechanical failure leading to renewed bulk cooling. The results of this testing and associated analysis provided an envelope (principally determined by melt depth) for debris coolability. However, this envelope does not encompass the full range of melt depths that are calculated for all plant accident sequences. Cooling augmentation by additional means may be needed at the late stage to assure coolability for new reactor designs as well as for various accident sequences for existing reactors. In addition, the results of the CCI tests showed that lateral/axial power split is a function of concrete type. However, the first program produced limited data sets for code assessment. In light of significant differences in ablation behavior for different concrete types, additional data would be useful in reducing uncertainties and gaining confidence in code predictions.

Based on these findings, a workscope was defined for the follow-on MCCI program that can be divided into the following four categories:

1. Combined effect tests to investigate the interplay of different cooling mechanisms, and to provide data for model development and code assessment purposes.
2. Tests to investigate new design features to enhance coolability, applicable particularly to new reactor designs.
3. Tests to generate two-dimensional core-concrete interaction data.
4. Integral tests to validate severe accident codes.

Aside from these various testing categories, an analysis workscope was also defined to develop and validate debris coolability models to form the technical basis for extrapolating the experiment findings to plant conditions.

As one of the steps in satisfying these program objectives, the Management Board (MB) approved the conduct of a fifth longer-term 2-D Core-Concrete Interaction (CCI) experiment designed to provide information in several areas, including: i) lateral vs. axial power split during dry core-concrete interaction, ii) integral debris coolability data following late phase flooding, and iii) data regarding the nature and extent of the cooling transient following breach of the crust formed at the melt-water interface. The first three tests [1] in this experiment series investigated the interaction of fully oxidized PWR core melt compositions with specially designed concrete

test sections that were initially 50 cm x 50 cm in cross-sectional area. Both siliceous and limestone/common sand concrete types were addressed. The fourth test [2] examined the interaction of a partially oxidized BWR melt composition with limestone/common sand concrete.

The overall design objective of CCI-5 was to increase the test section aspect ratio (i.e., test section width/melt depth) to the greatest extent possible to more accurately mock up prototypic conditions. To this end, the project prepared two design documents [3,4] that were submitted to the PRG for review. On this basis, the design was finalized, the apparatus was fabricated and assembled, and the experiment was conducted on September 25, 2008. Specifications for CCI-5 are provided in Table 1-1. The initial corium composition and concrete types were the same as those of CCI-3, but the dimensions and design of the test section were different. In particular, CCI-3 was conducted with a test section that featured two-ablating sidewalls with an initial basemat cross-section of 50 cm x 50 cm, whereas the CCI-5 test section featured one ablating concrete sidewall, an opposing MgO refractory sidewall, and a concrete basemat that was initially 50 cm x 79 cm in cross-sectional area. The input power for CCI-5 during the dry ablation phase was specified to be 145 kW, which was based on the requirement of providing an initial 'prototypic' heat flux of ~160 kW/m^2 across all melt surfaces that were not in contact with insulating sidewall material. This is the same surface heat flux requirement used to specify the total input power for tests CCI-2 through CCI-4. The initial melt depth for CCI-5 was set at 25 cm, which is the same as that used in previous tests. Since the surface area of the CCI-5 basemat was larger than that of previous tests, the initial melt mass to achieve this depth was increased considerably to 590 kg. With these specifications, CCI-5 could be considered a repeat of CCI-3, but with the aspect ratio increased to the greatest extent possible using: i) available hardware and ii) an inert wall that provided a symmetry boundary condition on one side of the test section.

The objective of this data report is to provide the thermalhydraulic results from this test. To this end, a summary description of the test apparatus is provided first, followed by descriptions of the test operating procedure and key experiment results.

2.0 FACILITY DESCRIPTION

The overall facility design and operating procedures for CCI-5 were similar to those used in the previous four tests [1-2]. However, at the 3rd PRG meeting for MCCI-2, the MB directed the project to increase the test section aspect ratio to the greatest extent possible. Given the test section overall planar dimensions, the approach for reaching this objective was to increase the aspect ratio to the highest possible value to more accurately mock up conditions at plant scale by incorporating one inert MgO sidewall into the overall design. This step created a symmetry (i.e., ~ adiabatic) boundary condition on one side of the test section which, in theory, doubled the aspect ratio for a given basemat width. With the symmetry boundary condition, the test simulated erosion in a 50 cm x 158 cm test section. Additional details regarding this modification are provided in the balance of this section, along with a general description of the overall facility for CCI-5. Specifications for the experiment were provided previously in Table 1-1.

Table 1-1. Specifications for CCI-5.

Parameter	Specification
Corium	100 % oxidized PWR with 15 wt % siliceous concrete
Concrete type	Siliceous concrete (CEA-type)
Initial basemat dimension	50 cm x 79 cm
Initial melt mass (depth[a])	590 kg (25 cm)
Test section sidewall construction	Nonelectrode wall No. 1: concrete Nonelectrode wall No. 2: MgO protected by UO_2 pellet layer. Electrode walls: MgO protected by UO_2 pellet layers.
Lateral and axial ablation limits	40 and 42.5 cm, respectively
System operating pressure	Atmospheric
Melt formation technique (timescale)	Chemical reaction (~30 seconds)
Initial melt temperature	1950 ºC
Melt heating technique	Direct Electrical (Joule) Heating
Power input prior to water addition	Constant power at 145 kW
Criteria for water addition	1) 6.0 hours of operation with DEH input, 2) lateral ablation reaches 35 cm, or 3) axial ablation reaches 37.5 cm
Inlet water temperature	20 ºC
Inlet water flow rate	2 liters/second
Sustained water depth over melt	50 ± 5 cm
Power input after water addition	Constant voltage
Test termination criteria	1) T_{melt} < concrete solidus, 2) concrete ablation is arrested, 3) maximum lateral/axial ablation limit is reached, or 4) 1.5 hours operation with water present in the cavity.

2.1 Test Apparatus

The CCI facility consisted of a test apparatus, a power supply for Direct Electrical Heating (DEH) of the corium, a water supply system, two steam condensation (quench) tanks, a ventilation system to complete filtration and exhaust the off-gases, and a data acquisition system. A schematic illustration of the facility for CCI-5 is provided in Figure 2-1. The apparatus consisted of three rectilinear sidewall sections and a lid. The overall structure was 3.4 m tall. The two upper sidewall sections had a square internal cross sectional area of 50 cm x 50 cm.

The test section for containment of the core melt was located at the bottom of the apparatus. A top view of this component is shown in Figure 2-2, while cross-sectional views of the electrode and non-electrode sidewalls are provided in Figures 2-3 and 2-4, respectively. The thickness of the new non-electrode sidewall was the same as the existing MgO electrode walls (i.e., 25 cm), and it was also protected with a crushed UO_2 pellet liner. This approach had been found to provide an inert (i.e., non-ablative) and highly insulated wall surface. As shown in Figure 2-4, the underside of the test section transition plate was exposed due to the addition of the thin MgO sidewall. To provide thermal protection, the plate was lined with Al_2O_3 insulation and a tungsten heat shield. A similar heat shield design was also used to protect the inner surface of the ACE/MCCI test apparatus lid. [5] The thickness of the concrete sidewall was the same as that used in the CCI-3 test. [1]

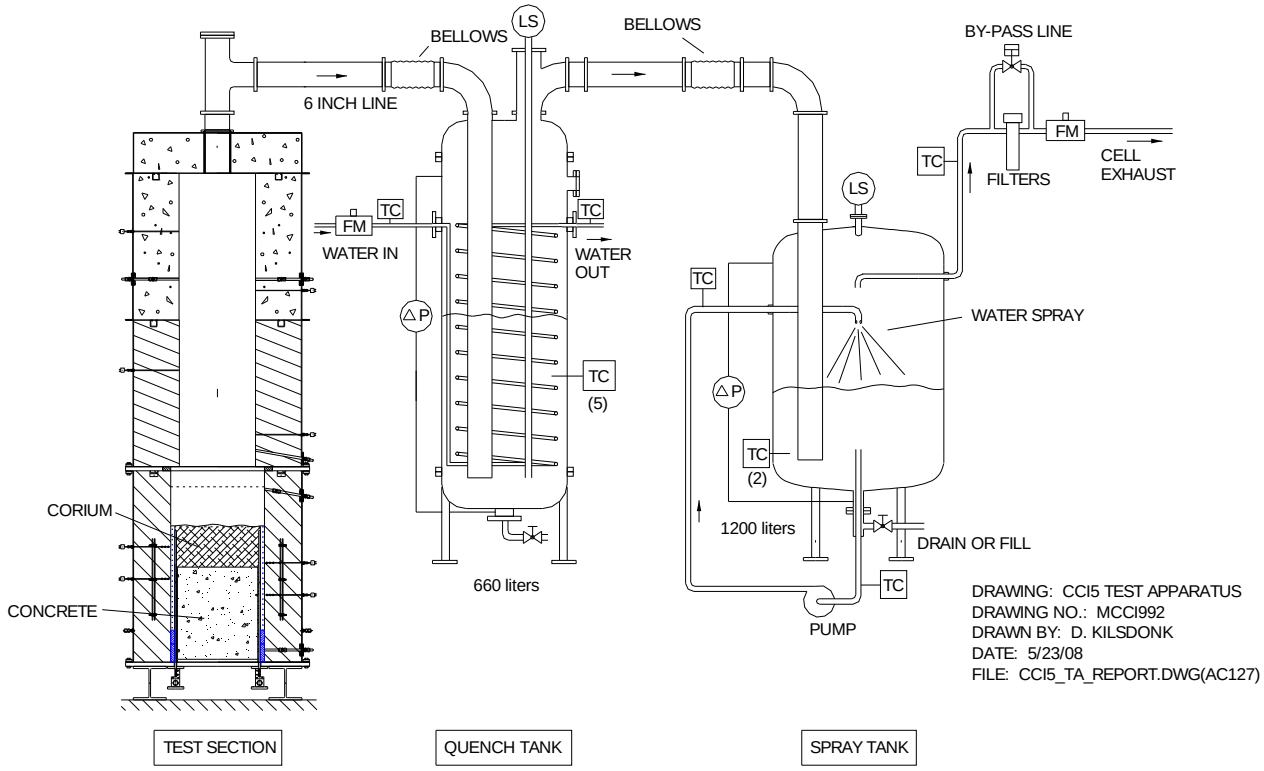

Figure 2-1. Schematic of CCI Test Facility.

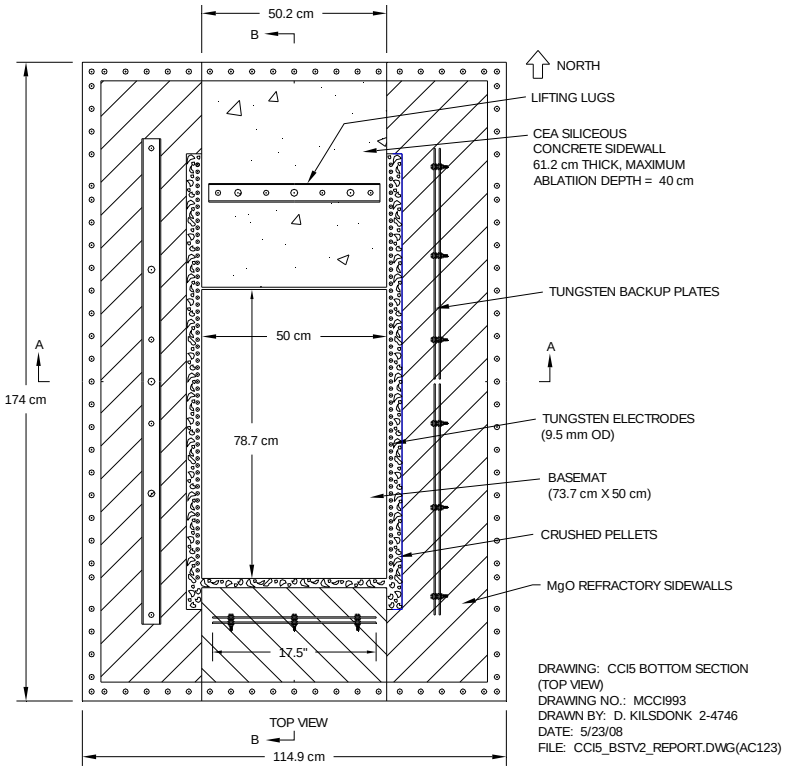

Figure 2-2. Top View of Lower Test Section.

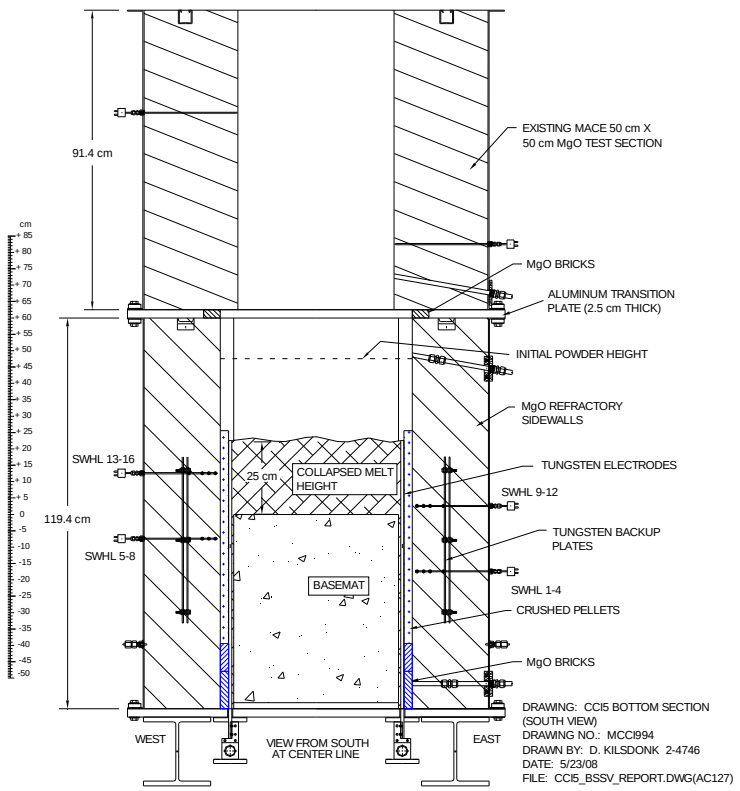

Figure 2-3. Side View of Lower Test Section Showing Inert MgO Sidewall Sections.

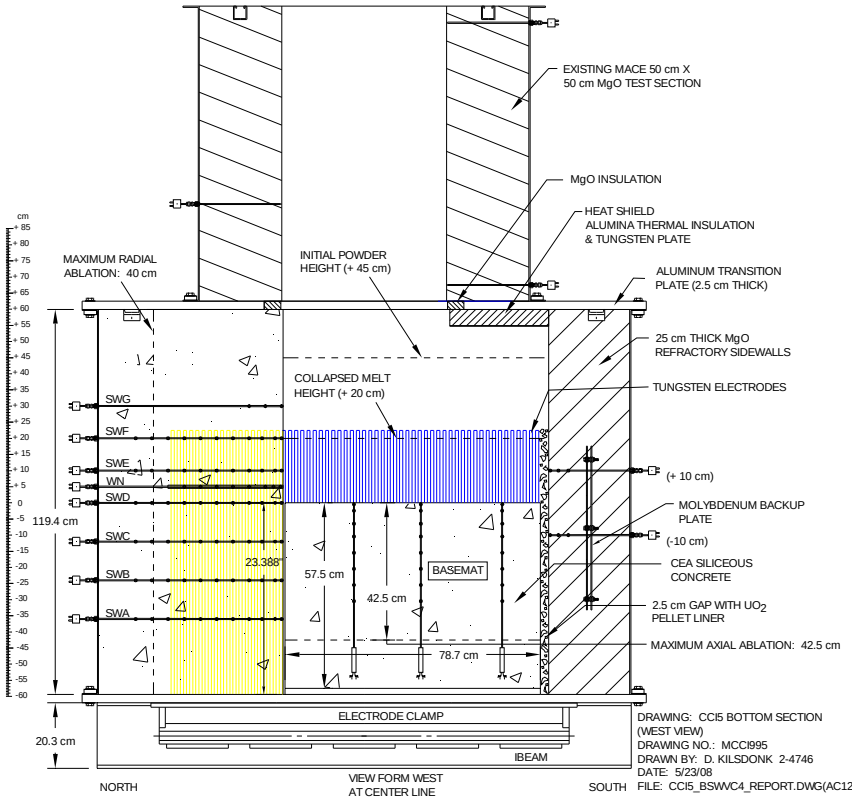

Figure 2-4. Side View of Lower Test Section Showing Concrete Sidewall.

The selected sidewall dimensions increased the basemat width from 50 cm in CCI-3 to 79 cm for the current design. Taking credit for the symmetry boundary condition, then the aspect (width/melt depth) ratio was increased from (25 cm/25 cm =) 1.0 in test CCI-3 to (79 cm/25 cm =) 3.2 for CCI-5, given the initial melt depth of 25 cm for CCI-5 (see Table 1-1). Note that the safety plan for the CCI tests assumed that a minimum thickness of 15 cm was maintained for all concrete components to ensure final containment of the melt. On this basis, up to 40 cm of lateral ablation could be accommodated in the concrete sidewall. Conversely, up to 42.5 cm of axial ablation could be accommodated given the initial basemat thickness of 57.5 cm.

As shown in Figures 2-2 and 2-3, the concrete and MgO sidewalls were contained within a flanged steel forms that were used to secure the lower section to the balance of the existing test section components with the aluminum transition plate. The flanges allowed the lower sidewalls to be disassembled to reveal the solidified corium following the test. As previously noted, a layer of crushed UO_2 pellets was used to protect the interior surface of the MgO sidewalls against thermo-chemical attack by the corium. Molybdenum and tungsten plates were embedded in the sidewalls to stop erosion in case the UO_2 pellet layer failed to provide adequate protection. Multi-junction Type C thermocouple assemblies were cast within the sidewalls so that the time-dependent heat loss from the melt could be calculated from the local temperature gradient and the thermal conductivity of the MgOThe melt was produced through an exothermic chemical reaction yielding the target melt mass over a timescale of ~ 30 seconds. After the chemical reaction, DEH simulating decay heat was applied through two banks of tungsten electrodes. As shown in Figures 2-2 and 2-3, the electrodes lined the interior surfaces of the two opposing MgO sidewalls. The electrodes were 9.5 cm in diameter and aligned in a row with a pitch of 1.9 cm. They were attached by copper clamps and water-cooled buss bars to a 560 kW AC power supply. As shown in Figure 2-2, the electrodes spanned a total width of 120 cm on each sidewall of the lower section. At the start of the experiment, the electrical current was drawn through the center, 79 cm-wide section of electrodes that were in direct contact with the melt. As the test progressed and the concrete sidewall was eroded, additional electrodes were exposed to the corium. Current was drawn through these newly exposed heating elements, thereby maintaining a uniform internal heat pattern in the melt over the course of the experiment. With the overall electrode span of 120 cm, the entire 40 cm of lateral sidewall erosion could be accommodated while ensuring that the entire melt cross-sectional area was in contact with the electrodes.

After the melt was formed, ablation of the concrete basemat and sidewall would eventually commence. As shown in Figure 2-1, a large (15 cm diameter) gas line was used to vent the helium cover gas and the various gas species arising from the core-concrete interaction (i.e., CO, CO_2, H_2O, and H_2) into adjacent tanks that were partially filled with water. In the initial phase of the experiment when the cavity remained dry, the tanks served to cool the off-gases and filter aerosols generated from the core-concrete interaction.

After a specified period of core-concrete interaction, the cavity was to be flooded using an instrumented water supply system (Figure 2-5). The water entered the test section through two weirs located in the opposing (non-electrode) sidewalls of the top test section. Steam and concrete decomposition gases passed from the test section through the 15 cm vent line into an instrumented quench tank (Figure 2-6) that was equipped with a cooling coil to remove heat from steam condensation, thereby maintaining a subcooled state. If the condensate level in the

tank rose to a level of 560 l, spillover into an adjacent overflow tank would occur. The quench tank and the interconnecting piping were insulated to minimize heat losses.

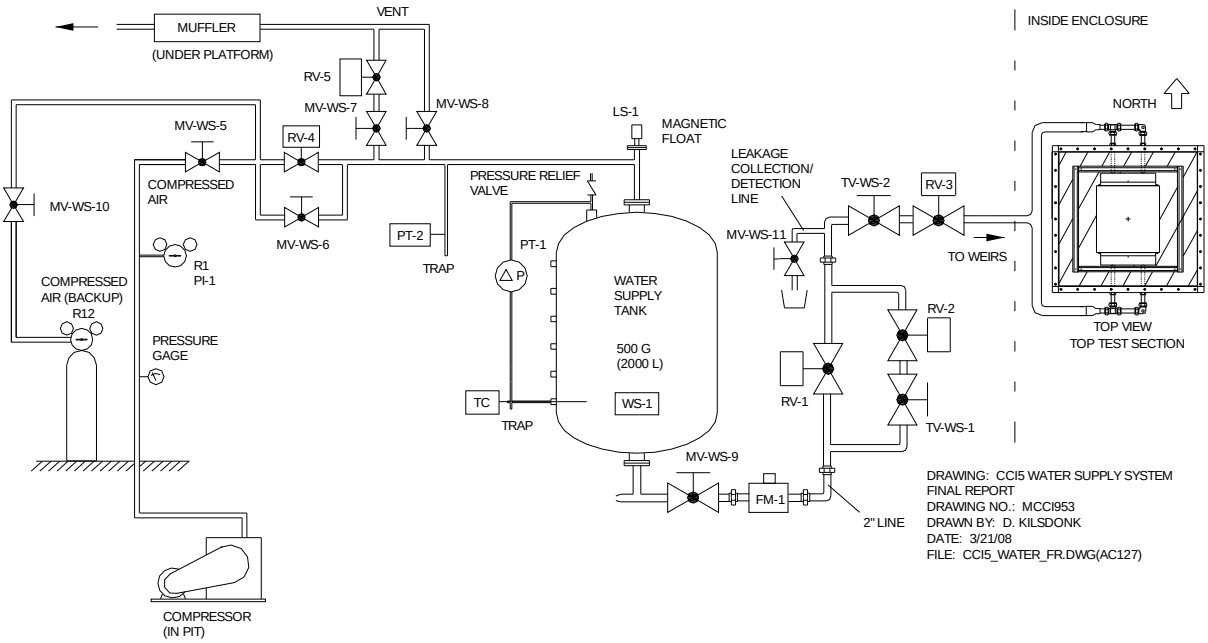

Figure 2-5. Test Section Water Supply System.

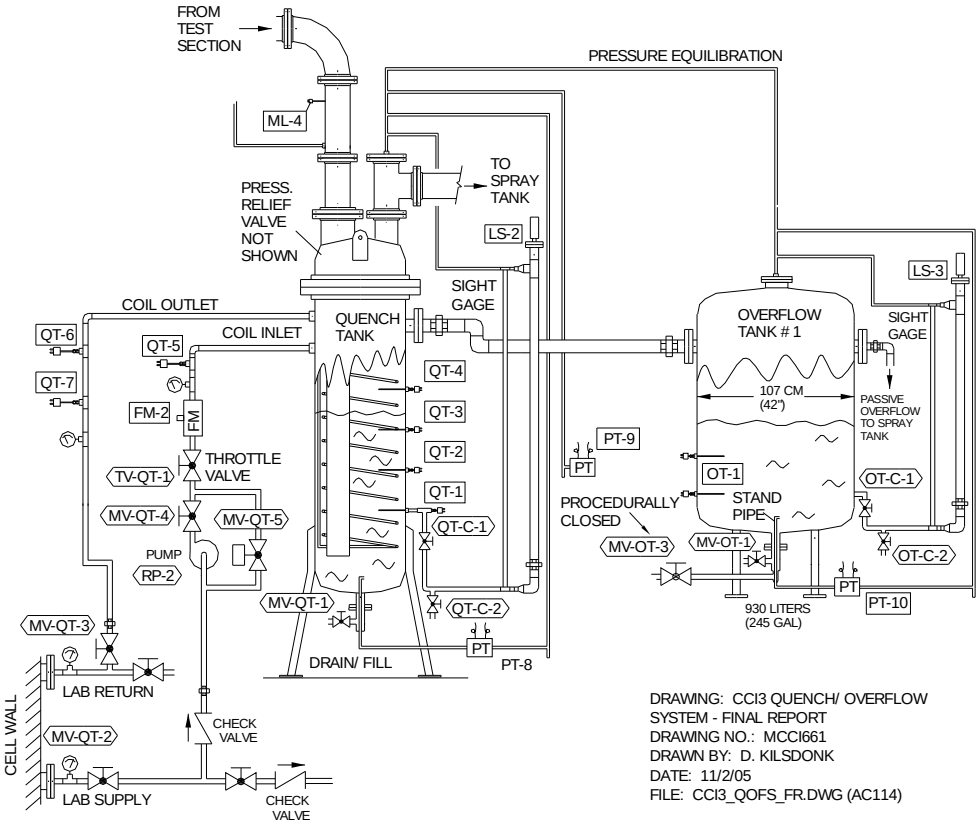

Figure 2-6. Quench and Overflow Tanks.

A secondary spray tank was connected to the quench tank by a 15 cm diameter vent line (Figure 2-7). In situations when the steam generation rate overwhelmed the primary quench tank, the secondary spray tank served to condense the remaining steam. The spray tank and interconnecting piping were also insulated to minimize heat losses.

An off gas system (Figure 2-8) filtered noncondensable concrete decomposition gases as well as test section covergas exiting the spray tank before venting the gas stream to the cell atmosphere. The gas stream first passed through a flow separator and filter bank to remove any remaining particulate. The flow then passed through the final off gas flowmeter to the cell atmosphere. The filters were equipped with a passive counter-weighted check valve set to open at a nominal differential pressure of 7 kPa. The bypass valve was provided to ensure that a vent path for the test section was always available in the event that the filters become plugged during the experiment.

After a specified time with water present in the cavity, the crust formed at the melt-water interface was to be broken with an insertable crust lance (Figure 2-9) to obtain data on the crust breach cooling mechanism. The lance was made from 2.54 cm diameter, 304 stainless steel rod with a pointed tip. The lance contained an electrical isolation hub so that there was no need to terminate power input to the melt during the crust loading procedure. As shown in Figure 2-9, the driving force for the lance was simply a 450 kg dead weight that was remotely lowered with the crane during the test.

Finally, the test section was also equipped with an instrumented pressure relief system to prevent over-pressurization and possible failure of the test section (Figures 2-10 and 2-11). The system consisted of a 15 cm diameter vent line from the test section to an auxiliary tank that was initially filled with 400 l of water. This tank was open to the atmosphere. The pressure relief line included a passive, counter-weighted check valve set to open at a pressure of nominally 68 kPad. A rupture diaphragm (68 ± 13.4 kPad) upstream from the check valve prevented any flow through the line unless the pressure in the test section exceeded the design value of 68 kPad. The line was also equipped with a vacuum breaker valve to prevent water hammer from occurring from steam condensation should the relief valve open and then reseat after introduction into the test section. The initial tank water inventory was provided to cool gases from the test section and to remove aerosols before the noncondensable gases were passed into the cell atmosphere. Instruments were provided to measure water depth and temperature so that the steam condensation rate could be determined if the relief system activated after water addition into the test section.

2.2 Instrumentation and Data Acquisition

The CCI facility was instrumented to monitor and guide experiment operation and to log data for subsequent evaluation. Principal parameters that were monitored during the course of the test included the power supply voltage, current, and gross input power to the melt; melt temperature and temperatures within the concrete basemat and sidewall; crust lance position and applied load; supply water flow rate; water volume and temperature within the test apparatus, and water volume and temperature within the quench system tanks. Other key data recorded by

the DAS included temperatures within test section structural sidewalls, off gas temperature and flow rate, and pressures at various locations within the system.

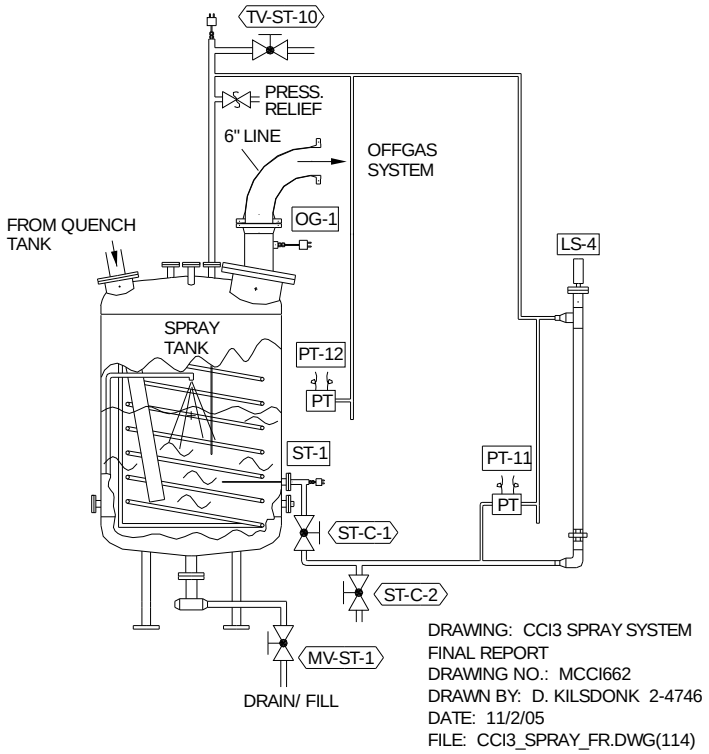

Figure 2-7. Spray Tank.

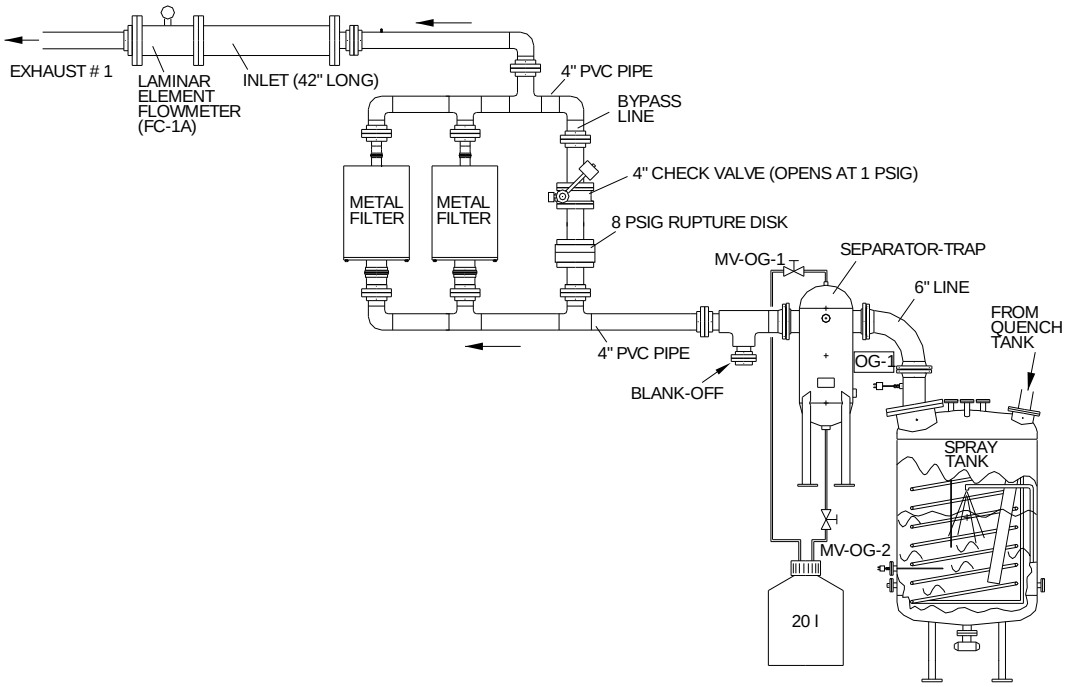

Figure 2-8. Off Gas System.

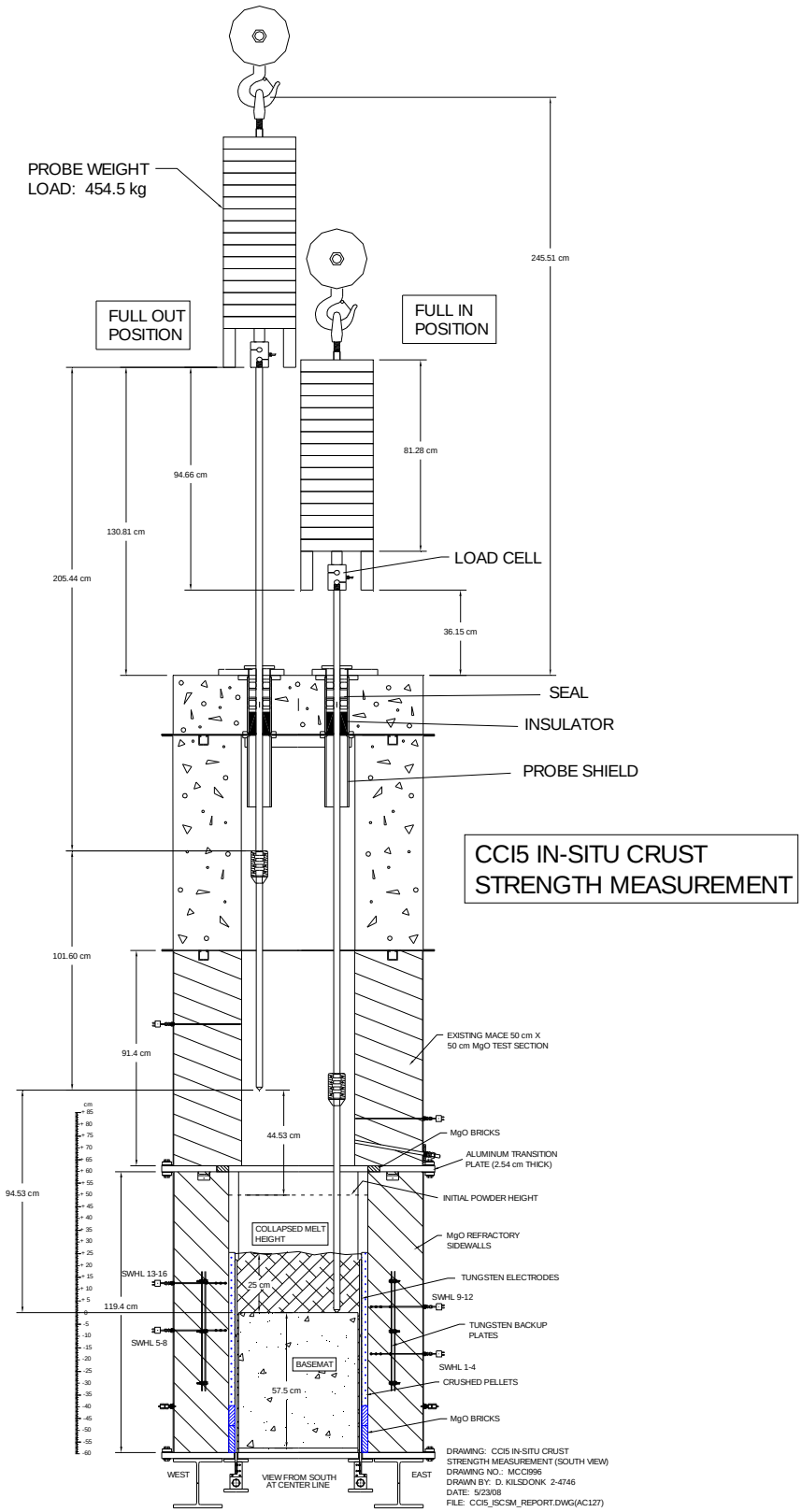

Figure 2-9. Illustration of CCI-5 Crust Lance Assembly Mounted in Test Section.

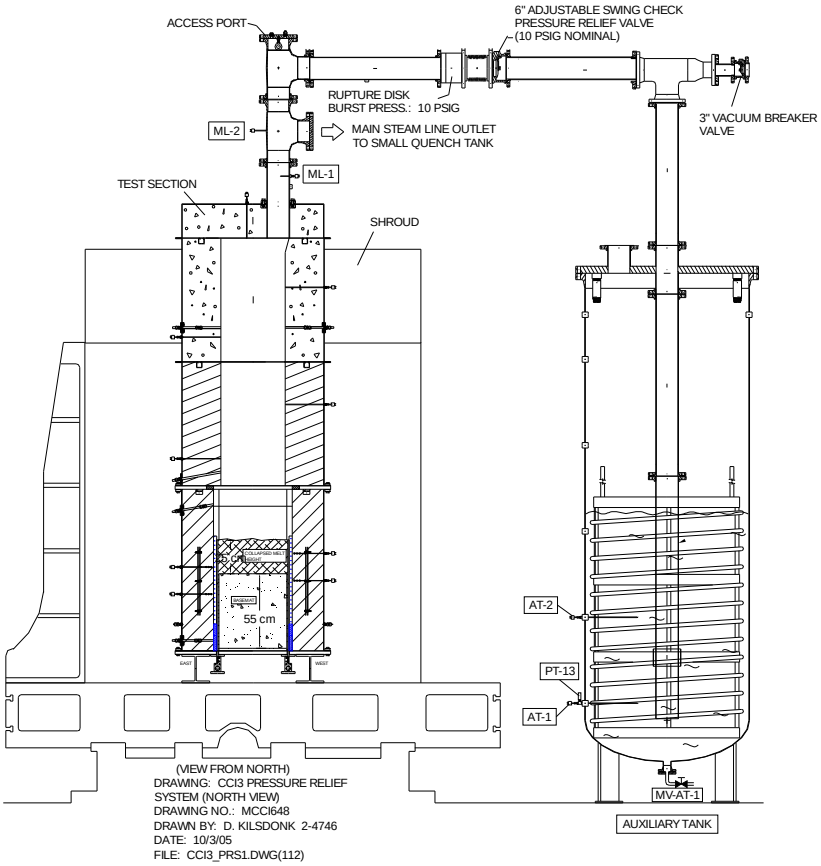

Figure 2-10. Test Section Pressure Relief System.

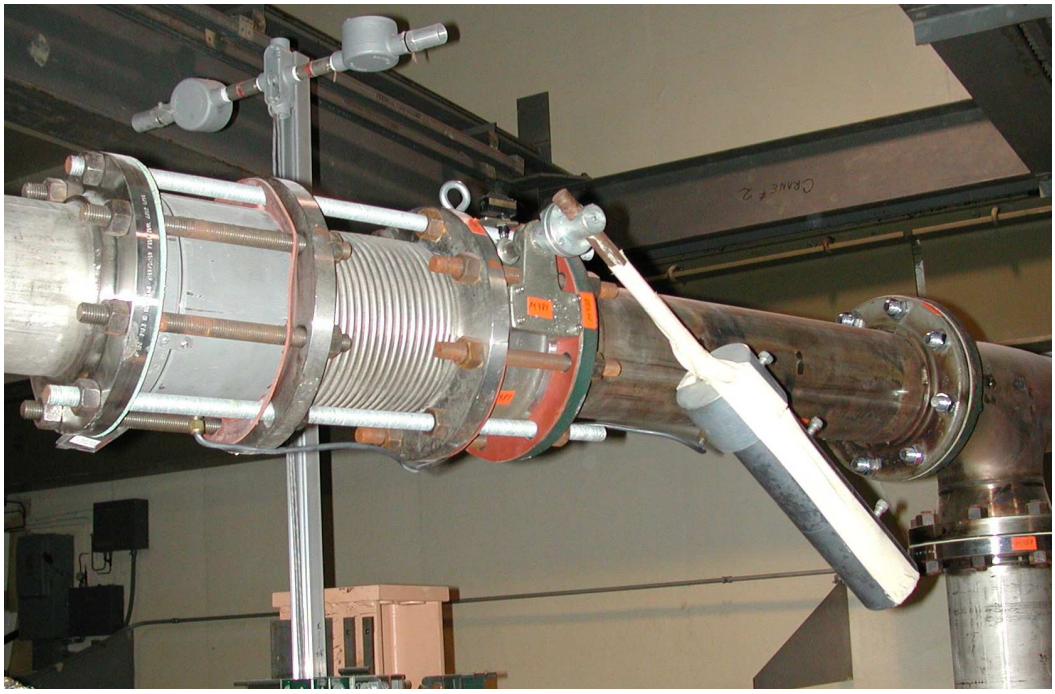

Figure 2-11. Photograph of Rupture Disk and Counter-Weighted Check Valve Assembly.

Detailed plan and elevation views of the basemat thermocouple layout are provided in Figures 2-12 and 2-13, respectively, while the concrete sidewall instrumentation locations are shown in Figures 2-4 and 2-14. Both the basemat and sidewall were instrumented with multi-junction Type K thermocouple assemblies to determine the 2-D ablation profile as a function of time. In addition, Type C thermocouple assemblies in tungsten thermowells protruded upwards from the basemat and laterally inwards from the concrete sidewall in several locations. The purpose of these instruments was to provide data on the axial and lateral melt temperature distribution as a function of time. Note that the thermocouple junction locations were repositioned to provide melt temperature and ablation front location data over the increased range of lateral and axial concrete ablation that was designed into this experiment. The concrete instrumentation layout was similar to CCI-3, with the exception that additional thermocouples were added on both sides of the concrete sidewall centerline at several axial elevations to provide additional data on the radial ablation progression; locations are detailed in Figure 2-14.

Other significant test instrumentation included a stationary (lid mounted) video camera for observing physical characteristics of the core-concrete interaction. In addition, a two-color optical pyrometer was added to measure the debris upper surface temperature during periods in which aerosol production did not optically occlude the view of the surface.

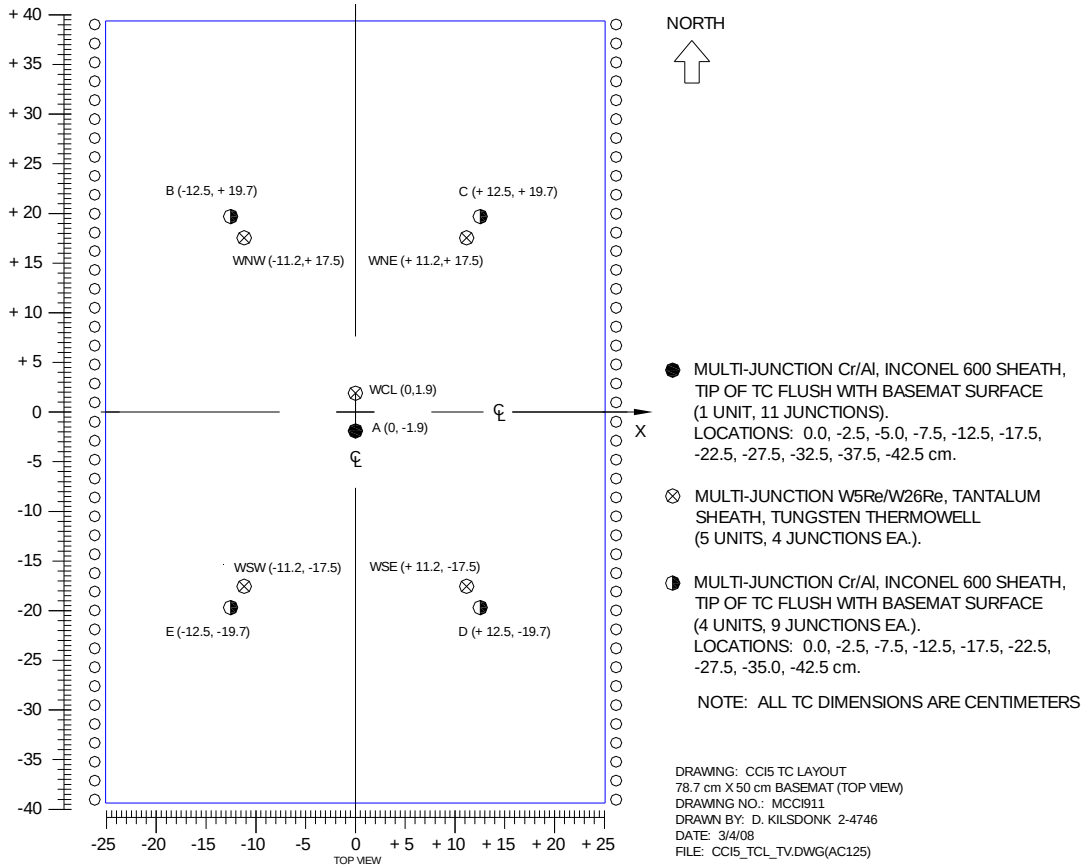

Figure 2-12. Plan View of Basemat Instrumentation Layout (dimensions are in cm).

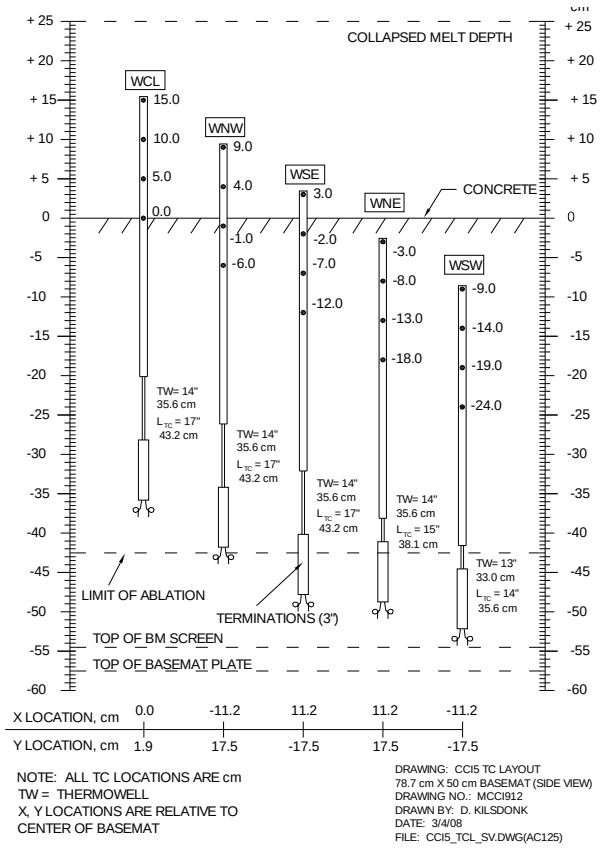

Figure 2-13. Elevation View of Basemat Type C Thermocouple Locations.

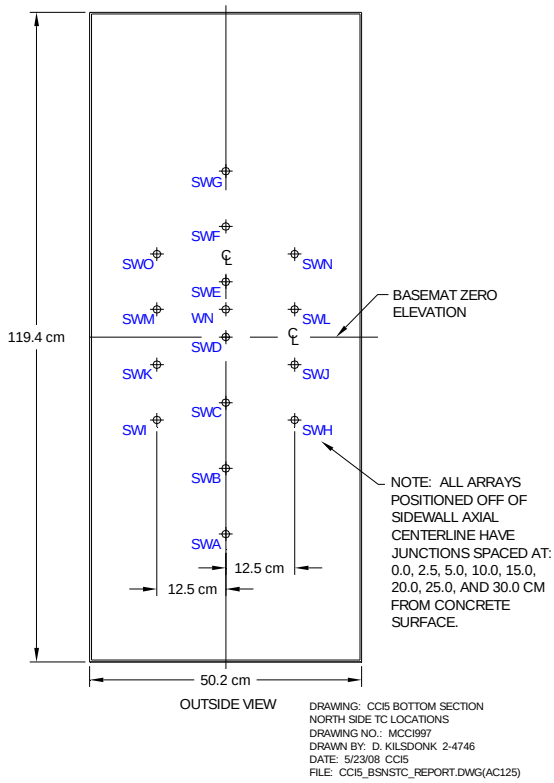

Figure 2-14. Exterior View of Concrete Sidewall Form Showing Instrument Locations.

All data acquisition and process control tasks were managed by a PC executing LabVIEW 8.4 under Windows XP. Sensor output terminals were connected inside the test cell to model HP E1345A 16-channel multiplexers that were integrated into a mainframe chassis in groups of eight. An illustration of the DAS setup is provided in Figure 2-15. The multiplexers directed signals to an HP E1326B 5 ½ digit multimeter incorporated into each chassis. Three independent 128 channel systems were used for a total capacity of 384 channels.

Signal noise was reduced by the digitizer through integration over a single power line cycle (16.7 ms). The digitized sensor readings were routed from the test cell to the PC in the control room via two HP-IB extenders. The extenders allowed the ASCII data from the HP to be sent through the cell wall over a BNC cable. The extender within the control room then communicated with a GPIB card within the PC. This configuration also permitted remote control of the multimeter through LabVIEW.

Integration of the signal over the period of a power line cycle limited the speed with which the multiplexer could scan the channel list. The minimum time for the digitizer to scan the channel list was ~1.7 s (i.e., 16.7 ms • 100 channels/chassis for this test). Though the three systems operated independently, implying the ability to update all 300 channels in roughly two seconds, the actual time required for the update was about 5.5 s.

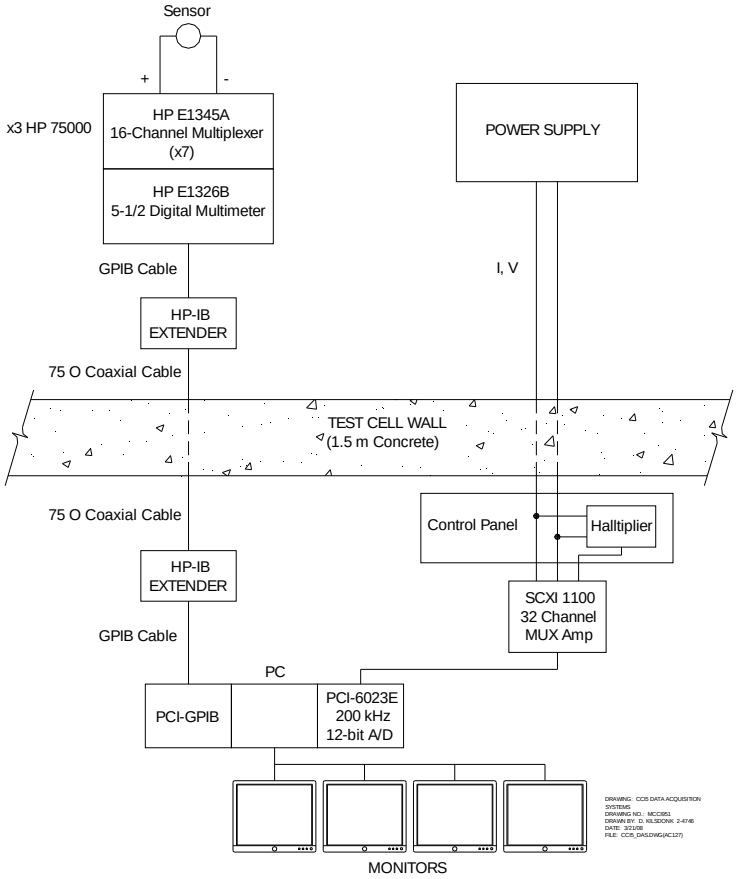

Figure 2-15. CCI Data Acquisition and Control Systems.

2.3 Corium Composition

As shown in Table 1-1, the corium oxide phase composition for CCI-5 was specified to contain 15 wt % calcined siliceous concrete as an initial constituent. As part of the developmental work for the SSWICS-6 and CCI-3 experiments, a specific thermite was developed to produce this particular melt composition. The thermite reaction was of the form:

$$1.22U_3O_8 + 3.3Zr + 0.978Si + 2.282SiO_2 + 0.05Mg + 0.69CaO + 0.055Al + 2.165CrO_3 \rightarrow$$

$$3.66UO_2 + 3.3ZrO_2 + 3.26SiO_2 + 0.05MgO + 0.69CaO + 0.11Al_2O_3 + 2.165Cr;$$

$$Q = -228.17 \text{ kJ/mole } (1.721 \text{ MJ/kg});$$

$$T_{adiabatic} = 2504 \text{ °C}; T_{actual} \sim 1950 \text{ °C}$$

The composition of the melt produced from this reaction is summarized in Table 2-1, while the detailed pre- and post-reaction compositions are provided in Table 2-2. Note that the pre- and post-reaction compositions shown in these tables do not include the additional mass of crushed UO_2 pellets that were used to line the test section MgO sidewalls. Experience had shown that this material did not participate in the initial exothermic chemical reaction, and remained essentially intact as a protective layer during the ensuing core-concrete interaction. The actual mass of UO_2 that dissolved into the melt over the course of the experiment was determined as part of the posttest examination activities.

The thermite powders were packed into the test section in a large, 1.7 mil aluminized Saran bag that was pre-installed over the basemat to prevent water absorption by CrO_3 and concrete oxides (principally CaO and SiO_2), since these constituents are hygroscopic. As an additional measure to prevent moisture infiltration into the thermite from the concrete, the basemat and sidewalls were completely covered with continuous sheets of Saran film before thermite loading.

2.4 Concrete Composition

As shown in Table 1-1, the composition of the CCI-5 concrete basemat and sidewalls is specified to be of the siliceous type. The engineering composition for this particular concrete is shown in Table 2-3. The sand and aggregate for the mix were supplied by CEA as an in-kind contribution to the program. The chemical composition of this concrete is shown in Table 2-3. The composition was determined[1] based on chemical analysis of the archive sample that was produced when the components for this test were poured.

To prevent downward migration and possible escape of concrete decomposition gases during the course of the experiment, the electrode penetrations through the bottom support plate were sealed using O-rings. As described in the next section, the test section was leak checked at 83 kPa differential pressure as part of pretest operations to verify a low leak rate. On this basis, essentially all concrete decomposition gases migrated upwards through the melt pool during the experiment, as opposed to partial loss through the bottom support plate of the apparatus. Reinforcing rod was eliminated so that it did not mask or delay the attainment of a fully oxidized

[1]Chemical analysis carried out by the Construction Technologies Laboratories (CTL Group) in Skokie, Illinois.

melt. In previous tests, the concrete surfaces were protected by a layer 3 mm thick layer of ZrO_2 felt insulation to prevent thermal shock of the concrete basemat and sidewalls during the initial exothermic chemical reaction. However, for CCI-5 this insulation was omitted in order to minimize the time to onset of concrete ablation after the thermite burn was completed.

The density of the siliceous concrete was ~ 2382 kg/m^3, which was calculated based on the measured mass and volume of the CCI-5 concrete archive sample.

Table 2-1. Post-Reaction Bulk Composition for CCI-5 Thermite.

Constituent	Wt%
UO_2	56.32
ZrO_2	23.13
Calcined Concrete	14.14[a]
Cr	6.41

[a]Calcined siliceous concrete, consisting of 79.0/0.9/15.6/4.5 wt% SiO_2/MgO/CaO/Al_2O_3

Table 2-2. Detailed Pre- and Post-Reaction Compositions for CCI-5 Thermite.

Constituent	Reactant		Product	
	Wt %	Mass, kg	Wt %	Mass, kg
U_3O_8	58.70	346.33	-	-
UO_2	-	-	56.32	332.29
Zr	17.16	101.24	-	-
ZrO_2	-	-	23.13	136.47
Si	1.57	9.26	-	-
SiO_2	7.84	46.26	11.17	65.90
Mg	0.07	0.41	-	-
MgO	-	-	0.12	0.70
Al	0.09	0.53	-	-
Al_2O_3	-	-	0.64	3.78
CaO	2.21	13.04	2.21	13.04
CrO_3	12.36	72.93	-	-
Cr	-	-	6.41	37.82
Total	100.00	590.00	100.00	590.00

Table 2-3. Engineering Composition of CCI-5 Siliceous Concrete Basemat and Sidewall.

Constituent	wt %	Size Distribution
Aggregate	47.4	5-8 mm: 16.6 wt % 8-11 mm: 20.4 wt% 11-16 mm: 10.4 wt%
Sand	30.6	0-2 mm: 12.2 wt % 2-4 mm: 18.4 wt %
Type 1 Cement	15.3	N/A
Tap Water	6.7	N/A

Table 2-4. Chemical Composition of Siliceous Concrete.

Oxide	Wt%
SiO_2	58.27
Al_2O_3	3.51
Fe_2O_3	1.33
CaO	20.20
MgO	0.92
SO_3	0.45
Na_2O	0.49
K_20	0.80
TiO_2	0.15
P_2O_5	0.07
Mn_2O_3	0.05
SrO	0.03
CO_2	9.50
H_2O, Free	1.90
H_2O, Bound	2.88
Total	100.54

3.0 TEST PROCEDURES

3.1 Pretest Operations

Assembly of the apparatus began by installing the tungsten electrodes (126 total; 63 per side) into machined copper electrode clamps. The electrode clamps were then attached to the bottom of the 2.54 cm thick aluminum support plate which served as the foundation for the entire apparatus. With the electrode clamps installed, the support plate was moved into position on the ZPR-9 reactor bed. The concrete basemat was then placed atop the support plate. The basemat was then completely covered with a continuous sheet of 1.7 mil aluminized Saran film to prevent moisture contamination of the thermite powders from the basemat once the powders were loaded into the test section. The lower test section concrete and MgO sidewalls were then set in place. The concrete sidewall was also covered with aluminized Saran before placement to prevent moisture contamination of the thermite once the powders were loaded. The lower section flange bolts and clamping bars were then installed and torqued according to an approved procedure.

In parallel with test section assembly, the thermite powders were mixed in preparation for corium loading. As a precursor for initiating mixing, a gas sample test[a] was conducted to verify that the initial level of volatile impurities in a sample prepared from the CCI-5 thermite constituents was sufficiently low to preclude excessive gas release during the burn. The results of this test indicated moisture content within acceptable limits. On this basis, mixing was initiated.

[a]The gas sample test procedure consisted of igniting a representative sample of the thermite in a closed vessel. The amount of noncondensable gas produced was determined from the ideal gas law; the composition of the evolved gases was determined using gas mass spectroscopy.

Once the lower section was assembled, preparations for loading of the corium charge began. A single, large 1.7 mil aluminized Saran bag was preinstalled over the basemat. During loading, the 590 kg thermite charge was placed within this single bag in order to minimize the amount of bagging material present in the thermite. As the powders were placed in the test section, the basemat melt temperature thermocouples were monitored to detect any localized heating in the corium powders. If heating was observed, the cell was to be evacuated immediately. As the thermite was placed, the gap between the tungsten electrodes and MgO sidewalls was filled with crushed UO_2 pellets. A temporary sheet metal form was also designed that allowed a uniform 2.5 cm thick layer of crushed pellets to be installed between the corium powders and the non-heated MgO sidewall. The crushed pellets served as a protective layer against excessive chemical/thermal attack by the corium during the test. Once loading was completed, two sparkler igniters were placed a few centimeters below the top of the powders near the center of the test section, and then the bag was folded and sealed.

Once loading was completed, a removable train containing a 1.0 kg bagged sample of thermite was installed over the powder bed; an illustration is provided in Figure 3-1. The sample train was removed weekly and the sample weighed to monitor the moisture pickup by the thermite during the period between loading and test initiation. Note from Figure 3-1 that the top portion of the train also contained a 4.5 kg canister of desiccant. The desiccant was provided to maintain the plenum gas as dry as possible during pretest operations. As an additional measure to prevent moisture accumulation in the powder bed, the lower test section was continuously purged with argon (2 slpm) from the time loading was completed until the test was initiated.

After installation of the sample train, the remainder of the test apparatus was assembled. This included installation of the transition plate, two upper sidewall sections, and finally the enclosure lid. Peripheral instrumentation was then installed on the lid and sidewalls of the test section. The main steamline run from the test section to the primary quench tank was completed, as well as the pressure relief line from the test section to the auxiliary tank. (The main steamline was closed off from the test section using an insertable blank-off plate throughout pretest operations to preclude moisture migration from the quench tank into the test section).

After assembly was completed, extensive system checkout procedures were performed to ensure that the facility was in proper working order. This included a proof test of the test section at 83 kPad, which was 20 % in excess of the pressure relief system activation pressure of 68 kPad. The pressurization gas for this test was argon. An insertable blind flange was installed upstream of the rupture disk in the pressure relief line to isolate this system. During the test, the apparatus was gradually pressurized to the proof pressure of 83 kPad. After a 1 minute hold at this pressure, the system was isolated to determine the leak rate. The leak rate of the CCI-5 test section was found to be 3.0 kPa/min (13 slpm) at a nominal pressure of 55 kPad, which was significantly below the acceptable leak rate of the fully assembled test section (i.e., < 2 % of the expected peak gas/vapor generation rate during the test).

Pretest preparations for CCI-5 culminated with a final full system checkout that involved remotely running all equipment with the power supply in operation across a water cooled dummy load. Once the full system check was completed, final system preparations were carried out. These efforts included: (i) hookup of the power supply to the tungsten electrodes through water

cooled buss bars, (ii) installation of the final piping connection between the water supply tank and the test section, and (iii) removal of the sample train from within the test section. Following connection of the power supply to the electrode clamps, the key for the power supply lockout located in the cell, as well as the key for the interlock located on the control room console, were assigned to a custodian who kept the keys in their possession until the test was initiated. This step was taken to preclude inadvertent activation of the power supply.

Over the five week time interval spanning pretest operations, the moisture content of the removable sample of bagged thermite increased gradually from 0.187 wt % to 0.225 wt %. The final moisture content was within the maximum permissible level of 0.3 wt %. On this basis, final approval was granted to proceed with the execution of Test CCI-5.

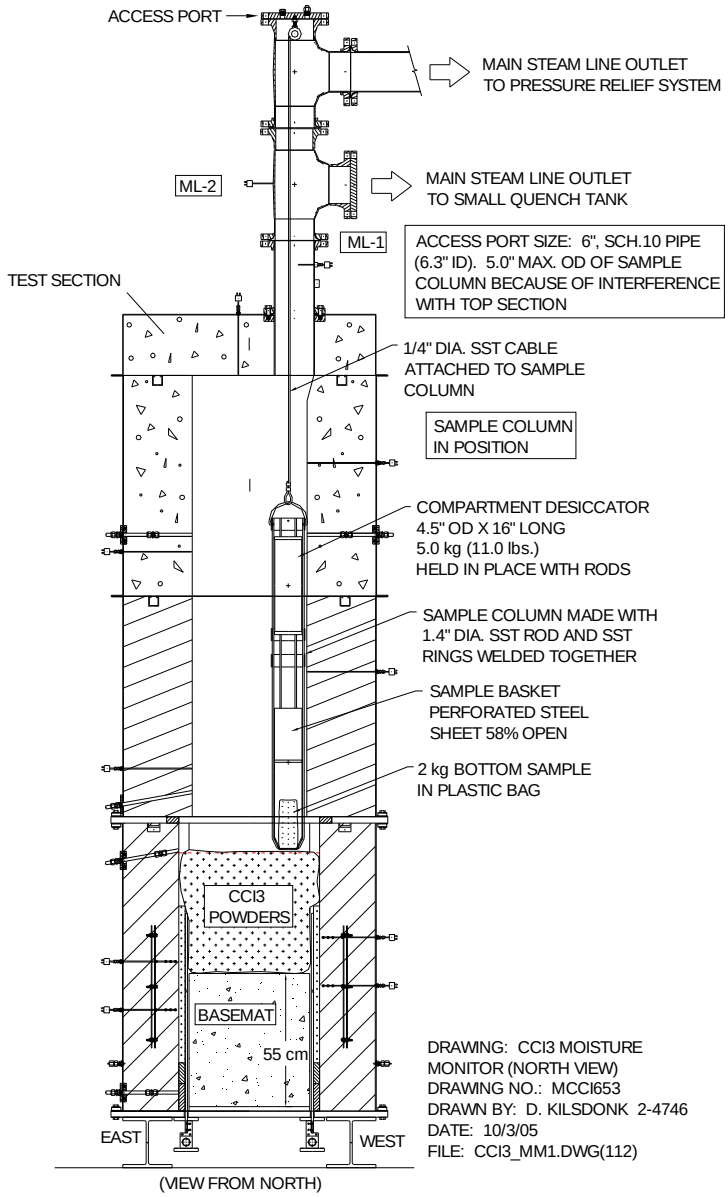

Figure 3-1. Illustration of Thermite Sample Train Installed in Test Section.

3.2 Test Operations

The planned test operating procedure is described first, followed by a brief summary of the actual operating procedure.

As shown in Table 1-1, target power for the dry core-concrete interaction phase of the test was 145 kW.[b] After melt formation, the input power would be brought up to 145 kW and held there for the balance of dry cavity operations. Onset of basemat ablation would define time t = 0 for the experiment. After ablation began, the interaction would be permitted to proceed for 6.0 hours, or until the ablation depth reached 35 cm laterally or 37.5 cm axially. After one of these two criteria was met, the cavity would then be flooded. However, if a crust was present at the melt upper surface, the crust lance would be used to fail the crust prior to flooding so that the water would be able to contact the underlying melt. Following water addition, the power supply operation would be switched from constant power at 145 kW to a constant voltage operating mode. (With constant voltage, the input power density would remain relatively constant if a significant quench front developed). Forty five minutes after water addition, or after the debris cooling rate had been reduced to a relatively low level, the crust would be failed with the lance to obtain data on the transient crust breach cooling mechanism. After breach, power supply operation would continue for an additional 45 minutes, yielding a total operating period of 90 minutes with water present in the cavity, or until the ablation limit of 40 cm was reached laterally or 42.5 cm axially. At this point, the input power would be turned off and the test terminated.

CCI-5 was performed on 25 September 2008. On the evening prior to the experiment, the apparatus was inerted with a slow bleed of helium into the test section. On the day of the experiment, the apparatus was brought up to operating conditions, a final walk through inspection was performed by operating personnel, the thermite igniter was hooked up, and finally the power supply was energized before the containment was evacuated and sealed. Data acquisition was initiated at 5:00 pm. Coolant and cover gas flows were brought up to design conditions, and the cell ventilation system was closed and sealed per test procedures.

The event sequence for CCI-5 is provided in Table 3-1. In the discussion that follows, time t = 0 corresponds to the onset of basemat ablation. The criterion used to define the onset of concrete ablation at a given location was that the local temperature reached the siliceous concrete liquidus temperature of 1250 °C. [5]

As shown in Table 3-1, data acquisition began at -6.0 minutes relative to initial melt contact with the concrete basemat. As shown in Figure 3-2, power was applied to the nichrome wire/sparkler located at the top of the powder charge at -1.2 minutes. Based on video camera data from the test section and plenum gas temperature readings inside the test section, thermite ignition was announced and logged in the control room at -0.9 minutes. Based on readings from thermocouples located near the top of the concrete, the burn front reached the bottom of the powder bed in ~ 40 seconds (i.e., at -0.3 minutes), which was within the planning basis for the experiment. The readings from selected melt temperature thermocouples are shown in Figure 3-3 over the first few minutes of the interaction. As is evident from this collection of data, peak

[b]The 145 kW power level for CCI-5 is based on the requirement of providing an initial 'prototypic' heat flux of ~ 160 kW/m^2 across all melt surfaces that are not in contact with insulating sidewall material.

melt temperatures near the center of the melt in the first 30 seconds of the interaction were in the range of 1930 to 1970 °C, with the average value being ~ 1950 °C.

Table 3-1. CCI-5 Event Sequence (times relative to onset of cavity ablation).

Time (Minutes)	Event
-6.0	DAS started.
-1.2	Power applied to thermite igniter wire.
-0.9	Thermite burn initiated; view of melt surface occluded by aerosol within 5 seconds.
-0.3	Thermite burn completed (burn time ~ 40 seconds); melt temperature ~1950 °C
0.0	Onset of ablation detected at all five basemat and all five sidewall TC array locations initially contacted by melt; average time for onset is 0.0 minutes, which defined time t = 0 for the experiment. Standard deviation in time spread is 0.14 minutes. Hereafter, there were local spatial variations, but on average axial ablation proceeds slowly but steadily at ~ 3 cm/hour.
1.9	Target DEH input power of 145 kW reached.
3.5-49.0	Melt surface view effectively blocked by aerosols generated by the CCI.
1.4-10.2	Test section pressure steadily increases from 1.14 to 1.62 Bar at which point test section pressure relief system activated.
40.7	Tap change from 56 to 112 Volt range on the power supply.
49.0-54.0	Aerosols in plenum gradually cleared to reveal the interaction. Melt surface was crust free and highly agitated by sparging gases. Melt surface continued to heat up until the view was lost due to excessive light intensity (through a No. 4 filter). View of surface not recovered until ~ 178 minutes.
44.0-76.0	Bulk melt temperature measurements were scattered, but average value rises from ~ 1710 to ~1780 °C over this interval, while melt surface temperature rises from 850 to 1767 °C at the same time.
158.0	Sidewall ablation suddenly increases and remains fairly steady over the balance of the experiment. Average rate is ~ 10 cm/hour.
171.3-199.0	Test section pressure relief system activates, causing test section pressure to drop gradually from 1.7 to 1.28 Bar over this time interval before settling out.
178.0-280.0	Melt surface video showed predominately a molten surface, but crust segments periodically formed on sidewalls, broke, and were mixed in with melt.
259-271.4	Pyrometer measured steady surface temperature decline from 1513 °C to 1250 °C, before rebounding suddenly back to 1515 °C. During this time, crust grew to cover surface except for a small pocket in NW corner. At 269 minutes, melt began to flow over the crust. At 269.2 minutes, large crust segments gradually broke off and were mixed into the bulk, and by 269.5 most of surface was crust-free.
257.7	Crust lance inserted to break crust; minimal force was required to puncture the material.
275.4	South MgO sidewall surface temperature reached 1230 °C at the + 10 cm elevation. Decision made to terminate the test on the basis of excessive sidewall heatup.
280.8	Input power to melt terminated. Average input power over the time interval from 0 to 280.8 minutes was 143.8 kW. Peak axial ablation depth was 22.5 cm, while peak radial ablation was 30 cm.
927.8	Data acquisition terminated.

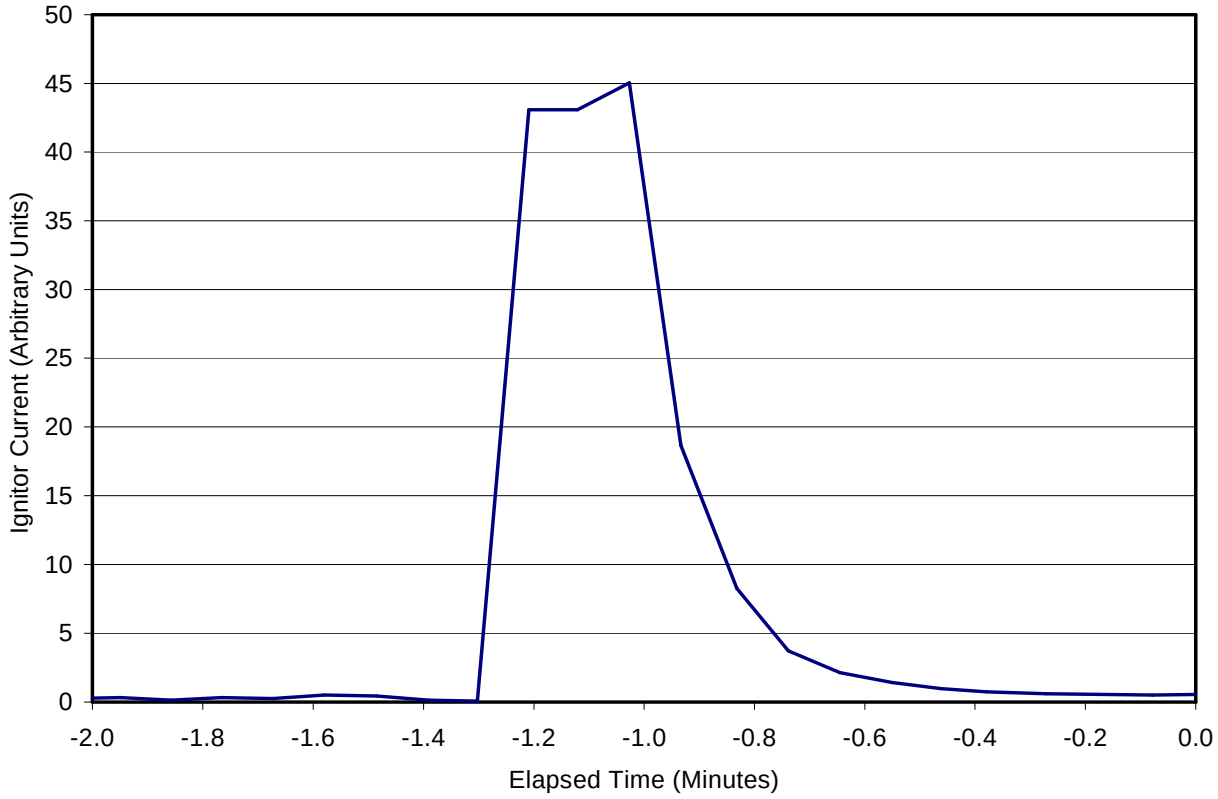

Figure 3-2. Voltage Reading Across Thermite Igniter Shunt.

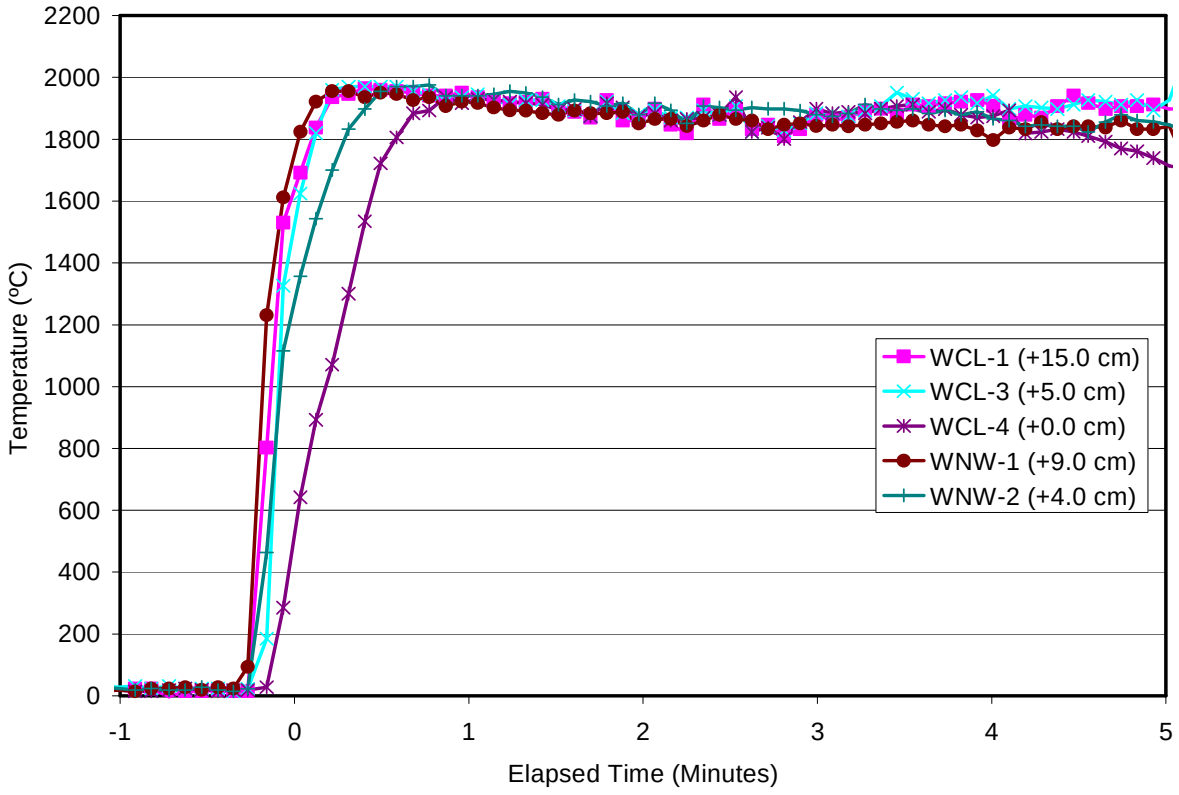

Figure 3-3. Bulk Melt Temperature Data over the First 5 Minutes of the Interaction.

Soon after the thermite burn was completed, onset of ablation was detected at all five basemat and all five sidewall thermocouple (TC) array locations initially contacted by melt; average time for ablation onset was 0.0 minutes, which defines time t = 0 for the experiment. The standard deviation in time spread for onset of ablation is 0.14 minutes. Thereafter, although there were local variations, axial ablation proceeded slowly but steadily at a rate of ~ 3 cm/hour, while onset of radial ablation was delayed until later in the experiment sequence.

At completion of the burn, a power supply current ramp up to the target power of 145 kW was initiated. This power level was reached at 1.9 minutes, where it was maintained for the balance of the test. A power supply voltage tap change was made at 40.7 minutes to accommodate the increased voltage required to maintain constant power input as the melt resistance increased (due to incorporation of concrete slag into the melt). Over the time interval from 1.4 to 10.2 minutes, the pressure in the test section steadily increased. The test data, as well as posttest examinations, indicated that this occurred due to plugging of the final off-gas flowmeter by aerosols that were entrained through the system during the thermite burn. The test section pressure is shown in Figure 3-4, while the quench and spray tank pressures are shown in Figure 3-5. In addition, a photograph of the aerosol that plugged the inlet to the gas flowmeter is shown in Figure 3-6. As indicated in Figure 3-4, the pressure in the test section gradually increased from 1.14 to 1.62 Bar over the time interval from 1.4 to 10.2 minutes, at which time the pressure suddenly decreased to 1.36 Bar. This sudden reduction was most likely caused by activation of the rupture disk in the test section pressure relieve system; the rupture disk was rated for 68 ± 13 kPad. The data also indicates that the counter-weighted check valve (Figures 2-10 and 2-11) subsequently reset, causing the pressure in the test section to gradually rise again. The pressure hovered in the range of 1.36 to 1.7 Bar until 171.3 minutes, at which point the check valve appears to have reopened, and remained that way during the balance of the test. This occurrence was most likely due to a large increase in noncondensable gas flow associated with the onset of sidewall ablation at 158 minutes (Table 3-1), after which point the sidewall ablation rate remained fairly steady at ~ 10 cm/hour. The fact that the pressure relief line remained open after 171 minutes was verified by the sustained heatup of the water inventory in the auxiliary tank past this time; see Figure 3-7. This response also indicated that there was little flow bypass through the pressure relief system in the time interval following initial rupture disk failure (at 10.2 minutes) up to the time that the relief line reopened (at 171 minutes).

As the experiment progressed, the lower test section MgO sidewalls continued to heat up due to convection from the melt. The most intense thermal loading occurred on the south MgO sidewall opposite from the concrete sidewall undergoing ablation. The thermal response in this wall at the + 10.0 cm elevation is shown in Figure 3-8. The temperature near the surface in this wall reached 1230 °C at 275.4 minutes. The decision was then made to terminate the test on the basis of excessive sidewall heatup. Input power to the melt was subsequently terminated at 280.8 minutes. Peak axial ablation depth was 22.5 cm at this time, while the peak radial ablation was 30.0 cm. The cavity was not flooded due to the concern that, with the plugged offgas system, the resultant steam spike could lead to gross failure of the test section. Data logging continued overnight, and the DAS was subsequently turned off at 927.8 minutes.

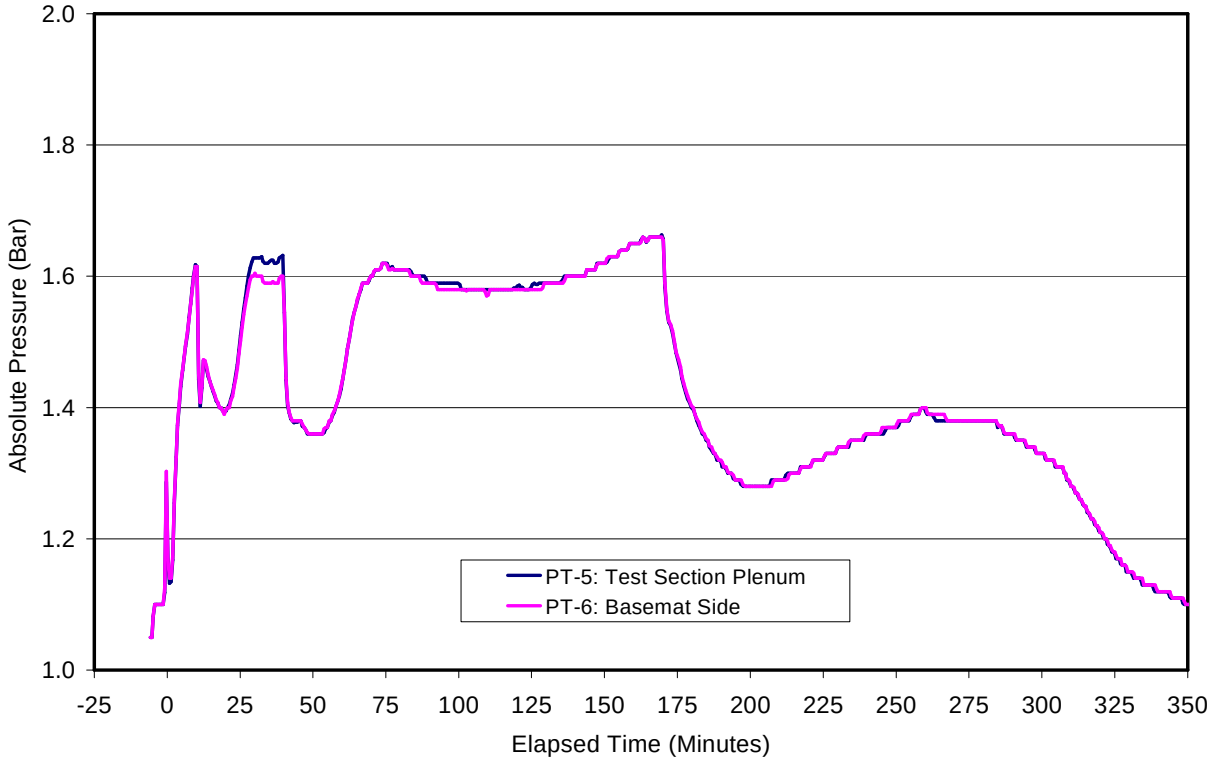

Figure 3-4. Test Section Pressure Response.

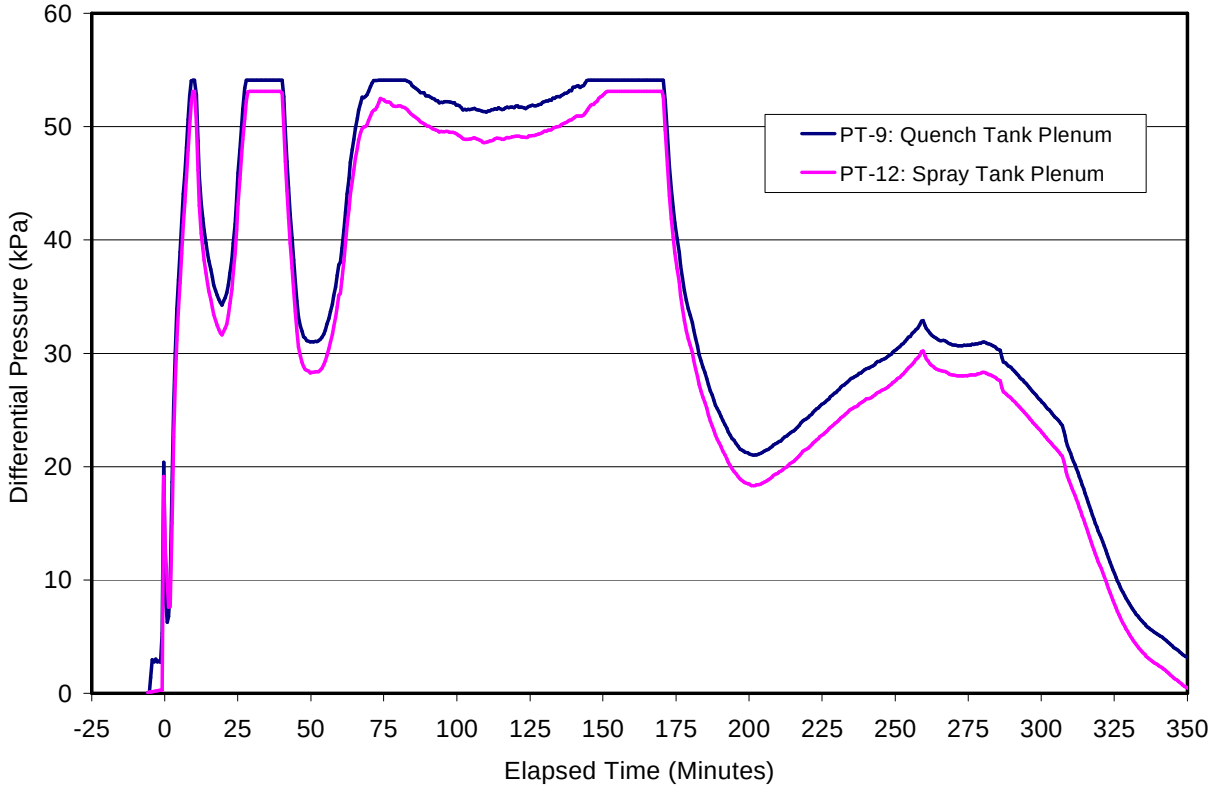

Figure 3-5. Quench System Tank Differential Pressure Responses (the range of these units is 0-35 kPad, and they clip at ~ 55 kPad).

Figure 3-6. Photo of Aerosol Plugging of Offgas Flowmeter Inlet (pipe ID is 10 cm).

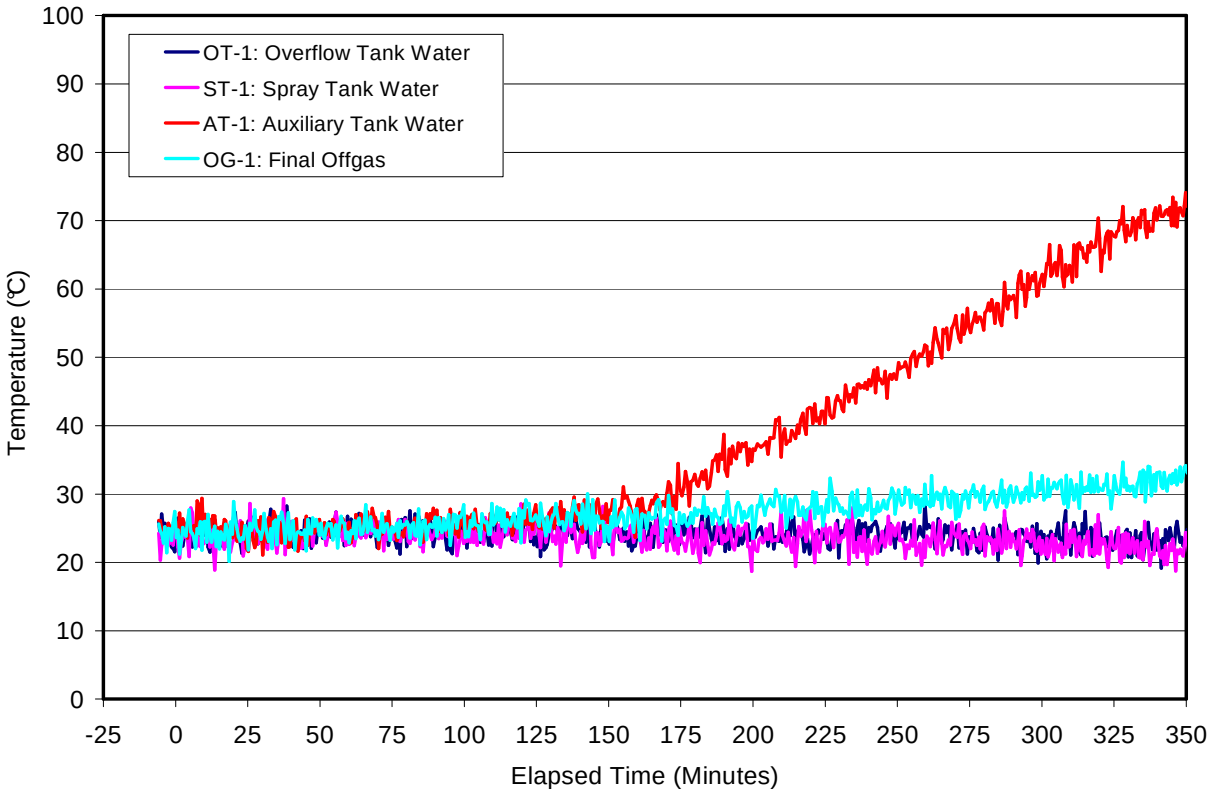

Figure 3-7. Miscellaneous Temperatures in Quench and Off-Gas Systems.

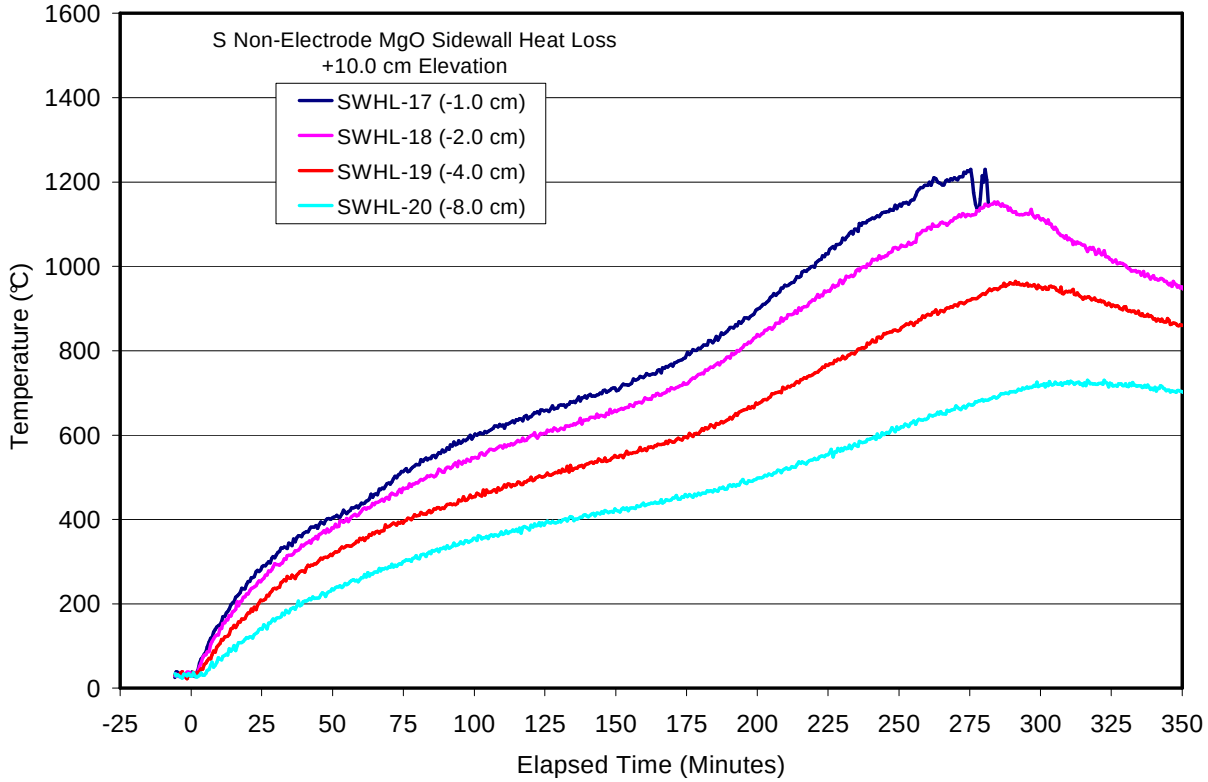

Figure 3-8. Thermal Response in South MgO Sidewall at the +10 cm Elevation.

During the course of the interaction, the lid video camera provided some information on melt pool phenomenology. Over the first 49 minutes, the view of the melt surface was effectively blocked by aerosols generated from the core-concrete interaction. At ~ 49 minutes, aerosols in the plenum gradually cleared to reveal the interaction. The surface was observed to be crust free, and was highly agitated by sparging gases. The melt continued to heat up to the point where the view was lost due to high light intensity (through a No. 4 filter) at ~ 54 minutes. The view was effectively lost until ~ 178 minutes. At this time, the melt had cooled to the point where surface features could again be distinguished. This view revealed a predominately molten surface, with crust segments periodically forming on sidewalls, breaking off, and mixing back into the melt. From 259 to 271 minutes, the melt pyrometer measured a steady surface temperature decline from 1513 °C to 1250 °C, before rebounding suddenly back to 1515 °C. During this time interval crust material grew steadily out from the sidewalls to the point where the entire surface was covered, except for a small pocket in the northwest corner. At 269 minutes, melt began to flow over the crust. At 269.2 minutes, large crust segments gradually broke off and were mixed into the bulk, and by 269.5 minutes most of surface was crust-free. This re-sorption of crust material occurred simultaneously with the sudden increase in surface temperature from 1250 °C to 1515 °C that was recorded by the optical pyrometer.

4.0 RESULTS

A summary of key thermalhydraulic results from CCI-5 is provided in this section. A complete list of instruments used in the test is provided in Appendix A, while plots of all data logged from these instruments are provided in Appendix B.

4.1 Electric Power

The DEH power for CCI-5 is shown in Figure 4-1; the corresponding voltage and current traces are provided in Appendix B (see Figures B-50 and B-51, respectively). At completion of the thermite burn, the power supply voltage was steadily increased until the input power reached the target level of 145 kW at 1.9 minutes. Thereafter, input power was held constant at ~ 145 kW over the balance of dry cavity operations. A voltage tap change was made at 40.7 minutes in order to maintain constant power as the load resistance presented by the melt increased during the course of the test. Power input was terminated at 280.7 minutes on the basis of excessive heatup in the south MgO sidewall. Average input power over the time interval from 0 to 280.8 minutes was 143.8 kW.

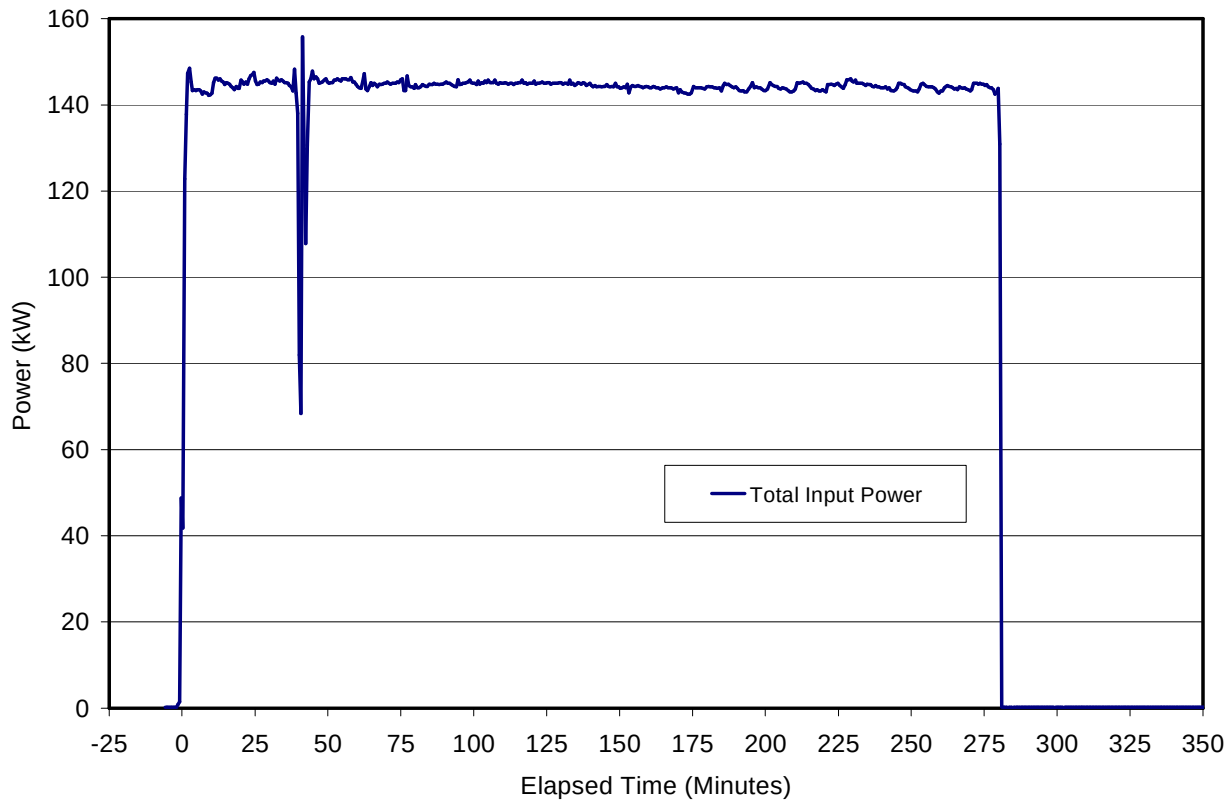

Figure 4-1. DEH Input Power.

4.2 Melt Temperatures

As described in Section 2.0, a total of twenty eight W5%Re/W26%Re (Type C) thermocouple junctions were used to monitor bulk melt temperatures at various axial and lateral locations in CCI-5. In addition, a two-color optical pyrometer was used to measure melt surface

temperature. The data from all these instruments are shown collectively in Figure 4-2. To improve the readability, two actions have been taken: i) the data have been averaged or 30 second time intervals, and ii) only data preceding the first off-scale reading by the thermocouples are shown. Data plots for each individual instrument are provided in Appendix B.

Examination of Figure 4-2 indicates that the melt temperature declined from a high of ~1950 ˚C measured soon after initial melt contact with the concrete surfaces, to ~1630 ˚C at the time input power was terminated at 280 minutes. Over the last few hours of the interaction, melt temperatures were fairly uniform across the extent of the interaction, generally clustering within a band of approximately ± 50 ˚C of the average at any given time.

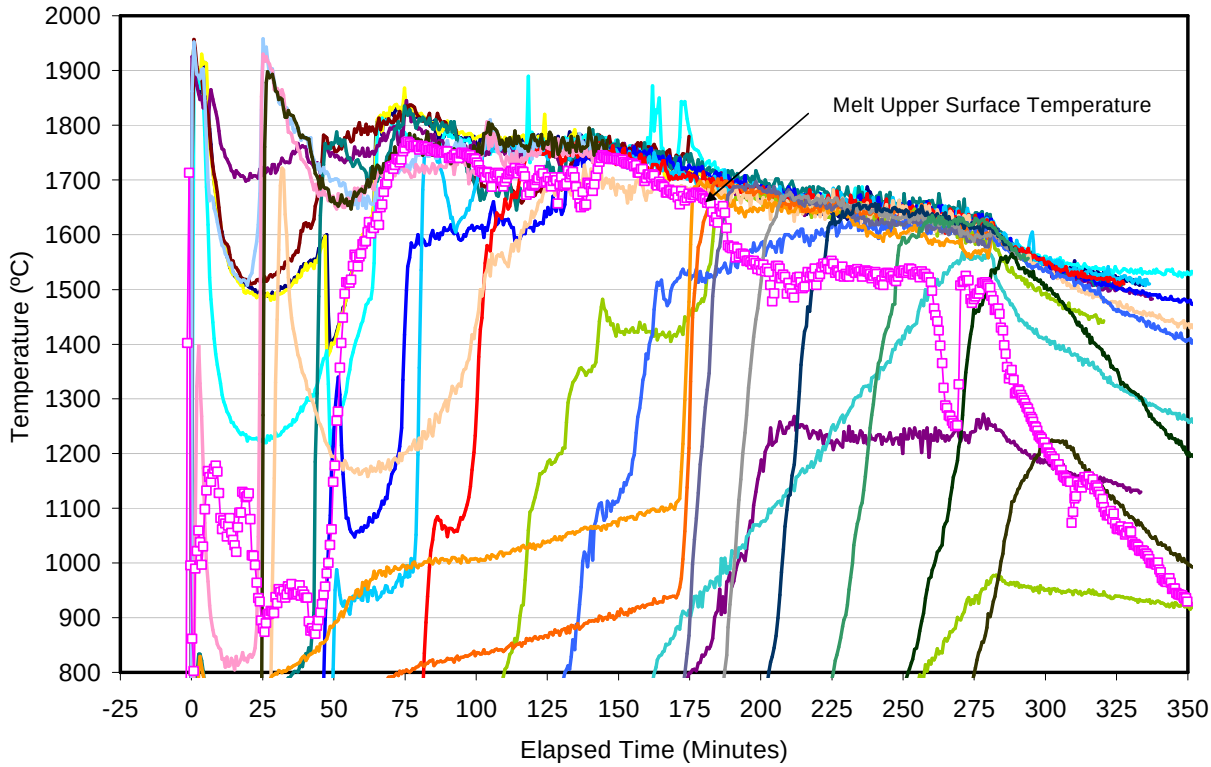

Figure 4-2. Melt Temperatures Measured During CCI-5.

4.3 Concrete Basemat and Sidewall Ablation Rates

As described in Section 2.0, the basemat was instrumented with five multi-junction Type K thermocouple arrays to monitor the axial progression of the ablation front, while the concrete sidewall was instrumented with fifteen arrays to monitor the lateral ablation front progression at eleven different elevations. When a thermocouple reached the siliceous concrete liquidus temperature of 1250 ºC [5], the melt was considered to be in contact with the thermocouple at the junction location.

Figure 4-3 provides the axial ablation depth versus time based on the signal responses from the Type K basemat arrays, while Figure 4-4 provides the analogous plot of the lateral ablation depth in the North concrete wall. The ablation progression for test CCI-3, which was conducted with the same concrete type and at the same power level but with two ablating concrete sidewalls [6], is also shown in the figures for comparison. Examination of the data

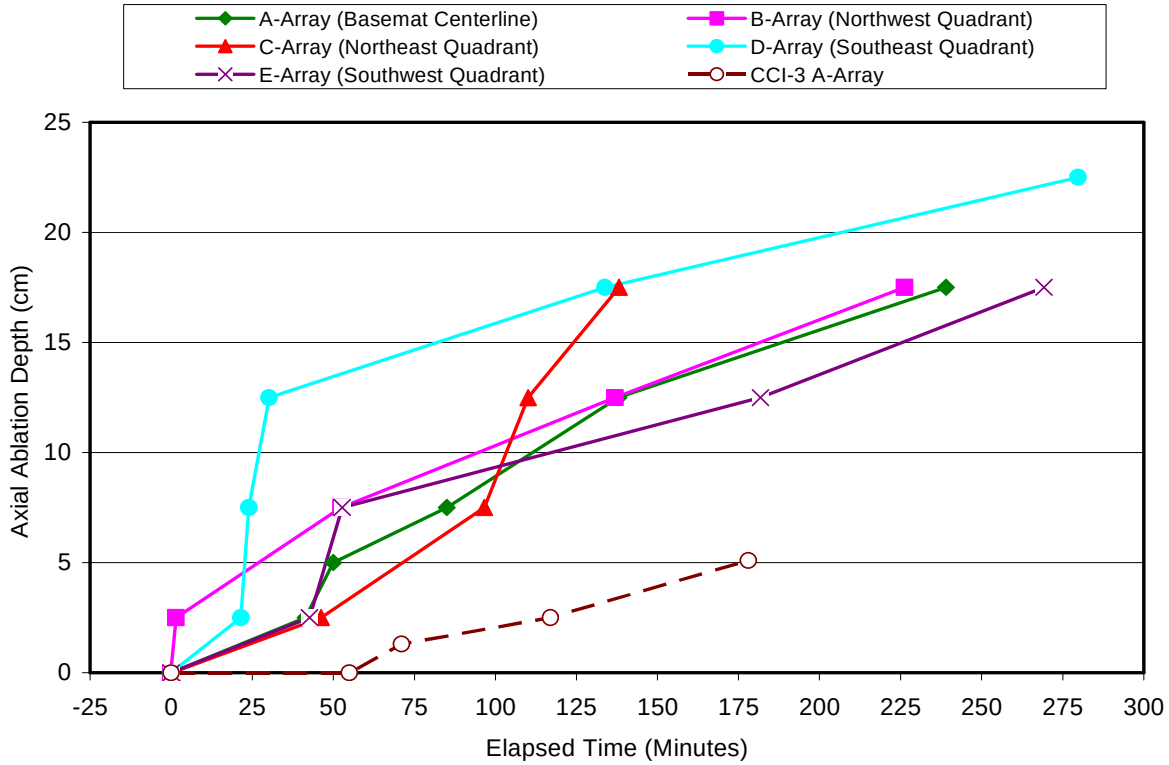

Figure 4-3. Basemat Axial Ablation Front Location.

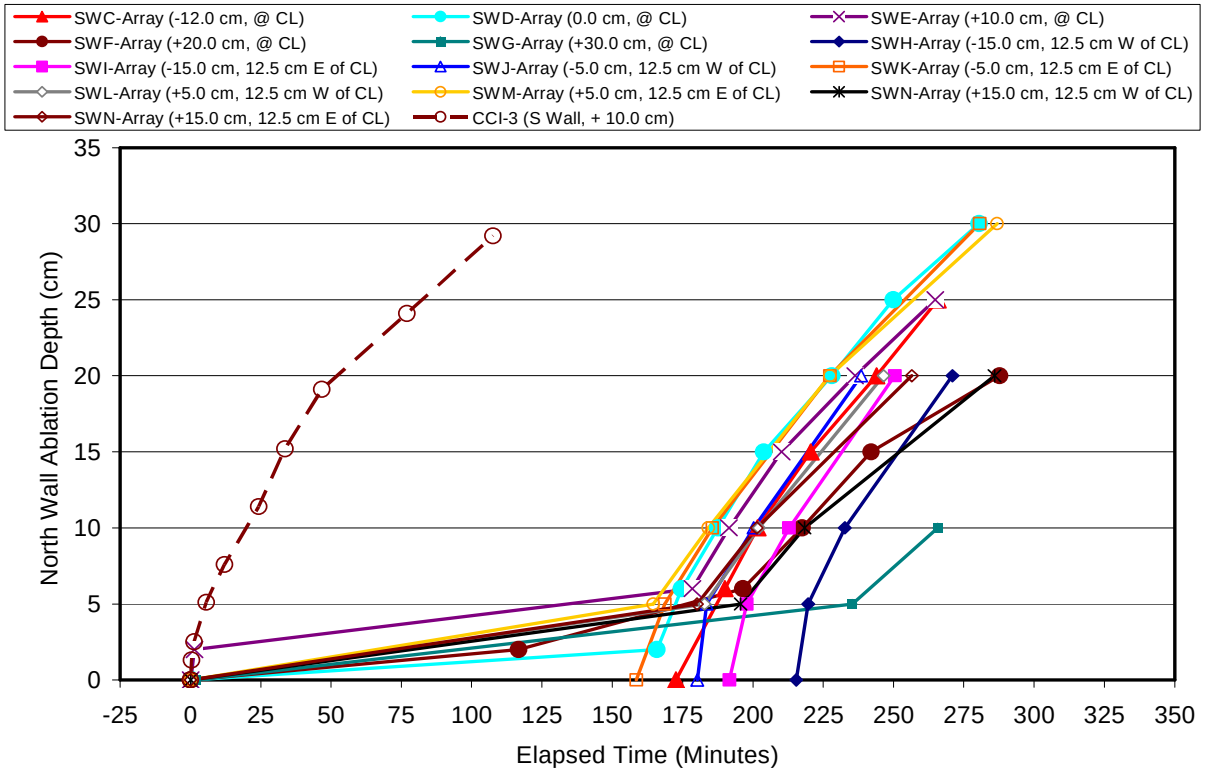

Figure 4-4. North Sidewall Lateral Ablation Front Location.

indicates that axial erosion began almost immediately after contact with the basemat, and proceeded fairly steadily at a rate of ~ 3 cm/hour after the initial transient had passed. Conversely, onset of significant sidewall ablation was delayed until ~ 158 minutes. At this time, lateral ablation proceeded in a uniform fashion at a rate of ~ 10 cm/hour. At the time the test was terminated at 280 minutes, the peak axial ablation depth was 22.5 cm, while the peak radial depth was 30 cm. Additional information on the posttest cavity erosion profile is provided in the next subsection.

4.4 Posttest Debris Examination and Chemical Analysis Results

Following the test, the apparatus was carefully disassembled to document the posttest debris configuration. A picture showing a view into the cavity after removal of the test section lid is provided in Figure 4-5(a), while a view of the debris upper surface after removal of the middle section transition plate is provide in Figure 4-5(b). A side view of the lower section after removal of the MgO sidewalls is provided in Figure 4-6, while Figures 4-7 and 4-8 provide two different views of the solidified corium over the basemat after removal from the test section bottom plate. Figure 4-9 provides the analogous photographs of the corium remaining on the North concrete sidewall. Finally, renderings of the posttest debris configuration are provided in Figure 4-10. In general, the posttest examinations revealed that, in contrast to tests with limestone/common sand concrete, melt foaming was not a major issue and as a result the vast majority of the corium was left as a uniform layer atop the basemat. The morphology of the solidified corium for CCI-5 was somewhat different in comparison to the other CCI tests where the cavity was flooded late in the experiment sequence. In particular, for CCI-5, the solidified corium was dominated by a dense, monolithic, homogenous oxide layer over the basemat with very little porosity and few cracks. This morphology can be contrasted with the other tests in which there was generally a substantial layer of porous material (5-10 cm thick) overlying monolithic material which had more cracks in comparison to the CCI-5 corium mass.

Consistent with the thermocouple measurements shown in Figures 4-3 through 4-4, the posttest examinations indicate that the overall cavity erosion was slightly skewed radially by the end of the experiment. As the debris was removed, samples were collected for chemical analysis by ICP/AES. Sample locations are shown in Figure 4-10. Key results from the analysis of five of these samples are provided in Table 4-1. The compositions shown in the table have been simplified in the terms of core, structural, and concrete (CaO, SiO_2, MgO, Al_2O_3) oxides; raw data are provided in Appendix C. Also provided in the table is an estimate of the end-of-test average melt composition that was formulated by taking the melt composition at the start of the test minus material splatter in the upper regions of the test section (50.44 kg; see Figure 4-10(a)), oxidizing all the remaining metals, and then incorporating 275.2 kg[2] of slag from the decomposition of 321.1 kg of concrete that is estimated to have been eroded during the test.

Samples from the dense oxide layer (i.e., Nos. 5, 7, 8, and 9) do not indicate a significant dependency of the composition on axial or radial position within the layer. This observation is consistent with the melt temperature thermocouple measurements in the latter phase of the experiment that indicated that the melt pool was well mixed. The composition of the porous

[2]Slag mass estimated based on the eroded concrete mass of 321.1 kg after the loss of 14.28 wt % of H_2O and CO_2 gases upon decomposition; see initial concrete composition shown in Table 2-4.

oxide layer on top the dense oxide was highly enriched in concrete oxides relative to the dense oxide. Overall, the samples contain slightly more concrete content than would be expected based on the estimated end of test composition. The discrepancy could arise thorough an underestimate of the mass of splatter material removed from the melt zone at the start of the experiment, which is possible since a substantial amount of material was deposited on the MgO sidewalls in the lower section (see Figure 3-33). However, segregating the initially deposited material from that subsequently deposited by melt voiding as the test progressed was not practical.

Table 4-1. Chemical Analysis Results for Samples Collected from CCI-5 Posttest Debris (data are in wt %).

Oxide	**5 Dense Oxide at Axial Centerline and by North Wall**	**7 Dense Oxide Near Core-Concrete Interface at Center of Test Section**	**8 Dense Oxide Near Axial Centerline at Center of Test Section**	**9 Dense Oxide Near Top at Center of Test Section**	**10 Porous Oxide at Center of Test Section**	**Estimated End-of-Test Composition**
UO_2	34.04	33.71	33.39	31.16	25.67	36.59
ZrO_2	12.27	10.14	12.32	12.53	12.70	15.02
Cr_2O_3	0.23	0.15	0.23	0.31	0.37	6.06
concrete	53.46	56.00	54.07	55.99	61.25	42.33
Total	100.00	100.00	100.00	100.00	100.00	100.00

(a) **(b)**

Figure 4-5. Top Views of the Test Section (a) After Lid Removal, and (b) After Removal of Top Section, Middle Section, and Test Section Transition Plate.

Figure 4-6. Side View of Lower Section (from west) After Removal of MgO Sidewalls.

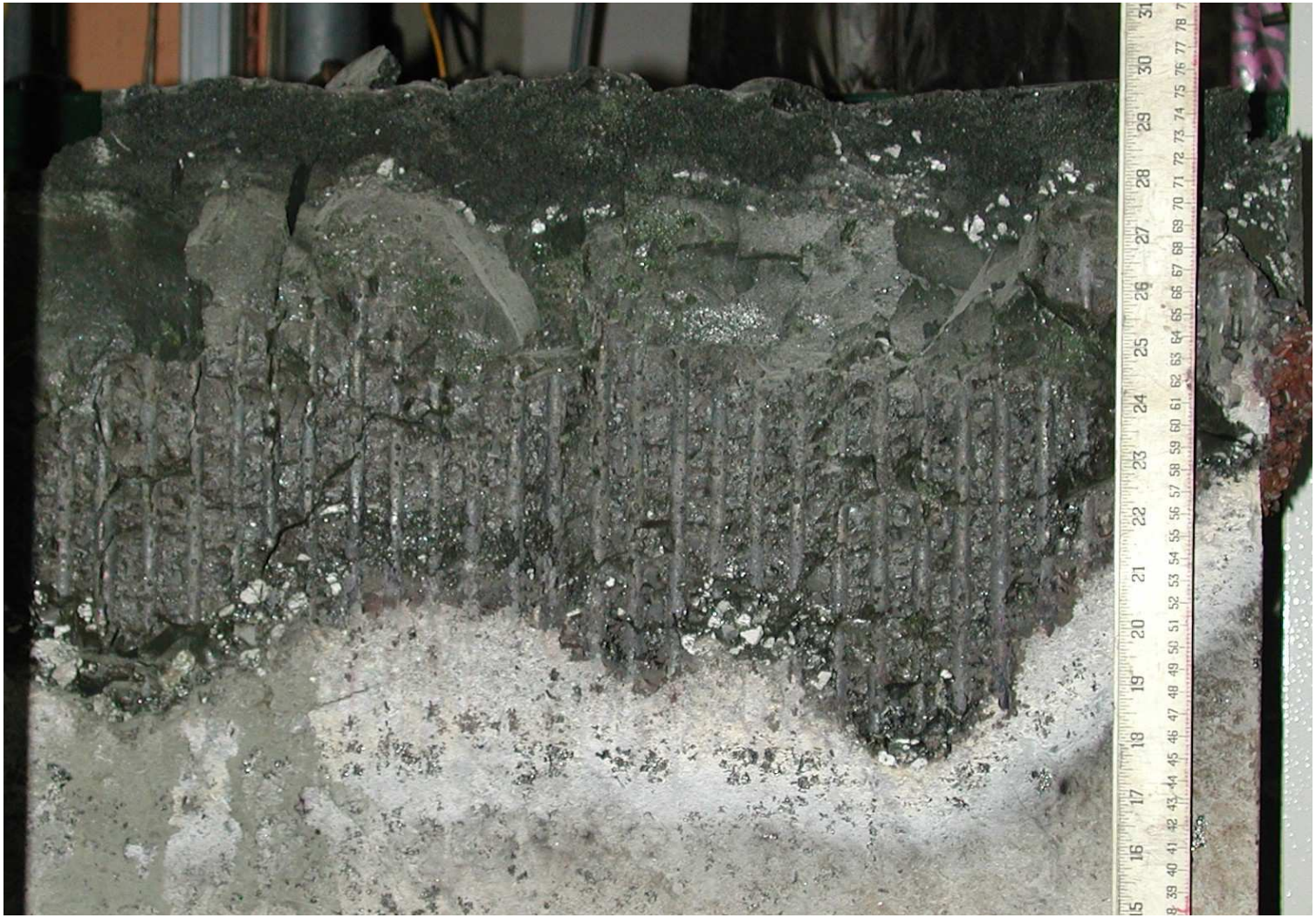

Figure 4-7. View from the West of the Solidified Corium over the Basemat. (The sintered UO_2 pellets that protected the south MgO sidewall are visible on the far right of the photograph).

Figure 4-8. View from the North of the Solidified Corium over the Basemat.

(a) **(b)**

Figure 4-9. (a) Perspective and (b) Close-up Photographs of Corium on the North Concrete Sidewall.

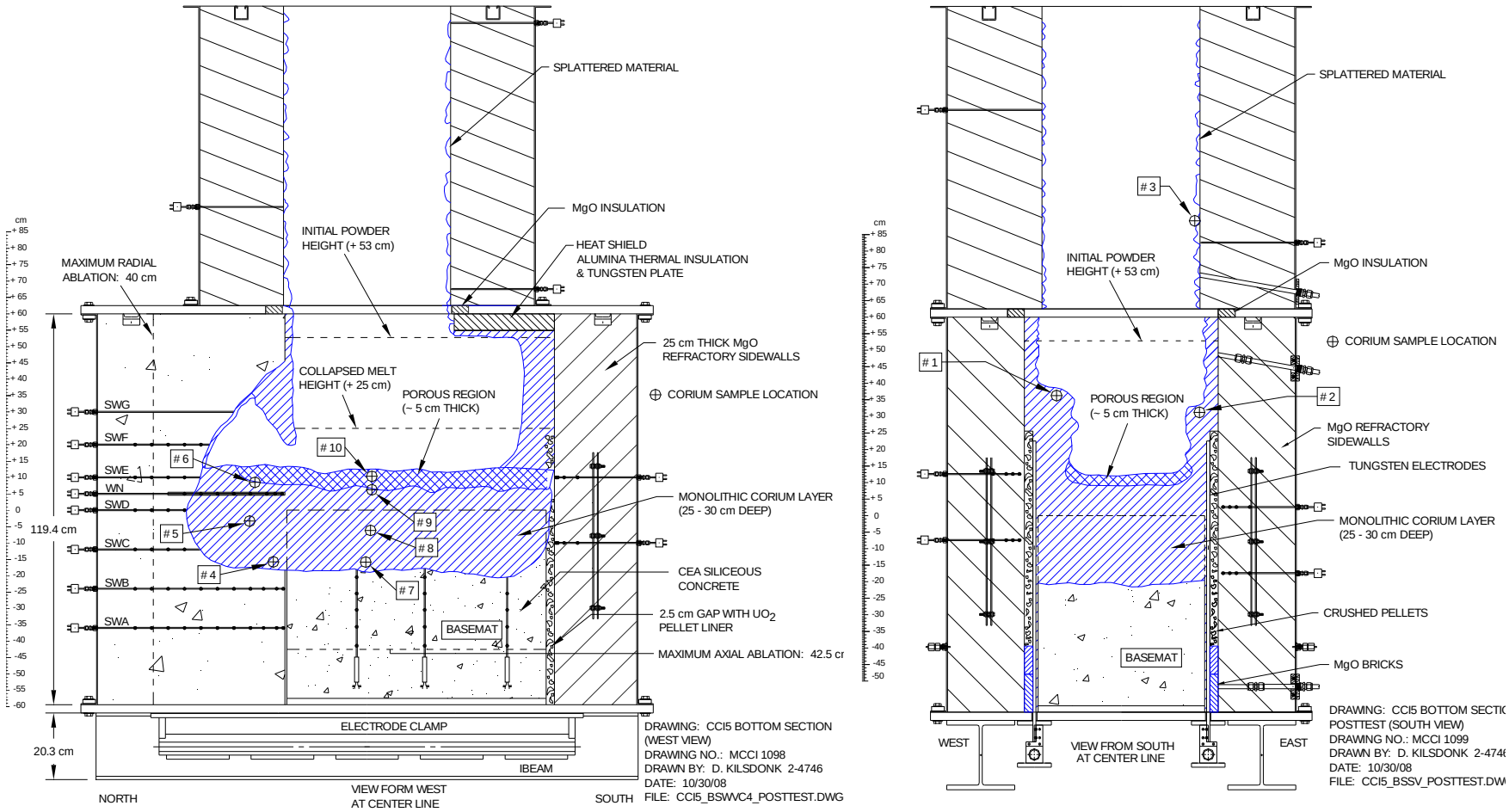

(a) **(b)**

Figure 4-10. Posttest Debris Renderings as Viewed from the (a) West and (b) South.

5.0 REFERENCES

1. M. T. Farmer, S. Lomperski, D. J. Kilsdonk, and R. W. Aeschlimann, "OECD MCCI Project 2-D Core Concrete Interaction (CCI) Tests: Final Report," OECD/MCCI-2005-TR05, January 2, 2006.

2. M. T. Farmer, R. W. Aeschlimann, D. J. Kilsdonk, and, S. Lomperski, "2-D Core Concrete Interaction (CCI) Tests CCI-4 Final Report," Rev.0, OECD/MCCI-2007-TR06, November, 2007.

3. M. T. Farmer, D. J. Kilsdonk, S. Lomperski, and R. W. Aeschlimann, "Draft Specifications and Design for OECD/MCCI-2 Program CCI-5 Test," whitepaper, Rev. 0, October 26, 2007.

4. M. T. Farmer, D. J. Kilsdonk, S. Lomperski, and R. W. Aeschlimann, "Draft Specifications and Design for OECD/MCCI-2 Program CCI-5 Test," whitepaper, Rev. 1, November 20, 2007.

5. D. H. Thompson, M. T. Farmer, J. K. Fink, D. R. Armstrong, and B. W. Spencer, "ACE Phase C Final Report: Volume I-MCCI Thermalhydraulic Results," EPRI/ACE-TR-C42, September, 1997.

6. M. T. Farmer, S. Lomperski, D. J. Kilsdonk, R. W. Aeschlimann, and S. Basu, "2-D Core Concrete Interaction (CCI) Tests: CCI-3 Test Data Report-Thermalhydraulic Results," Rev. 0, OECD/MCCI-2005-TR04, October 15, 2005

APPENDIX A
Data Acquisition System Channel Assignments

This Appendix provides the channel assignments for the three independent DAS systems that were used to record the data for CCI-5. For convenience, these three 128 channel systems were referred to the "Basemat", "Power," and "Quench" systems by operating personnel. The channel assignment lists for each of these three systems are provided in Tables A-1 through A-3. The data recorded on each of these channels is provided in Appendix B.

Table A-1. "Concrete" DAS Channel Assignments for CCI-5.

Channel	Variable	Sensor	Location	Elevation	Range/Limit	Accuracy
00	T	Diode Sensor	TC compensation Channels B01-B49		130 C	
01	T	TC Type C	Concrete Basemat 0.0 cm, +1.9 cm WCL-1	+15.0 cm	2320 C	± 1%
02	T	TC Type C	Concrete Basemat 0.0 cm, +1.9 cm WCL-2	+10.0 cm	2320 C	± 1%
03	T	TC Type C	Concrete Basemat 0.0 cm, +1.9 cm WCL-3	+5.0 cm	2320 C	± 1%
04	T	TC Type C	Concrete Basemat 0.0 cm, +1.9 cm WCL-4	0.0 cm	2320 C	± 1%
05	T	TC Type C	Concrete Basemat -11.2 cm, +17.5 cm WNW-1	+9.0 cm	2320 C	± 1%
06	T	TC Type C	Concrete Basemat -11.2 cm, +17.5 cm WNW-2	+4.0 cm	2320 C	± 1%
07	T	TC Type C	Concrete Basemat -11.2 cm, +17.5 cm WNW-3	-1.0 cm	2320 C	± 1%
08	T	TC Type C	Concrete Basemat -11.2 cm, +17.5 cm WNW-4	-6.0 cm	2320 C	± 1%
09	T	TC Type C	Concrete Basemat +11.2 cm, +17.5 cm WNE-1	-3.0 cm	2320 C	± 1%
10	T	TC Type C	Concrete Basemat +11.2 cm, +17.5 cm WNE-2	-8.0 cm	2320 C	± 1%
11	T	TC Type C	Concrete Basemat +11.2 cm, +17.5 cm WNE-3	-13.0 cm	2320 C	± 1%
12	T	TC Type C	Concrete Basemat +11.2 cm, +17.5 cm WNE-4	-18.0 cm	2320 C	± 1%
13	T	TC Type C	Concrete Basemat +11.2 cm, -17.5 cm WSE-1	+3.0 cm	2320 C	± 1%
14	T	TC Type C	Concrete Basemat +11.2 cm, -17.5 cm WSE-2	-2.0 cm	2320 C	± 1%
15	T	TC Type C	Concrete Basemat +11.2 cm, -17.5 cm WSE-3	-7.0 cm	2320 C	± 1%
16	T	TC Type C	Concrete Basemat +11.2 cm, -17.5 cm WSE-4	-12.0 cm	2320 C	± 1%
17	T	TC Type C	Concrete Basemat -11.2 cm, -17.5 cm WSW-1	-9.0 cm	2320 C	± 1%
18	T	TC Type C	Concrete Basemat -11.2 cm, -17.5 cm WSW-2	-14.0 cm	2320 C	± 1%
19	T	TC Type C	Concrete Basemat -11.2 cm, -17.5 cm WSW-3	-19.0 cm	2320 C	± 1%
20	T	TC Type C	Concrete Basemat -11.2 cm, -17.5 cm WSW-4	-24.0 cm	2320 C	± 1%
21	T	TC Type C	N Concrete Sidewall, 0.0 cm deep, centerline WN-1	+5.0 cm	2320 C	± 1%
22	T	TC Type C	N Concrete Sidewall, 2.5 cm deep, centerline WN-2	+5.0 cm	2320 C	± 1%
23	T	TC Type C	N Concrete Sidewall, 5.0 cm deep, centerline WN-3	+5.0 cm	2320 C	± 1%
24	T	TC Type C	N Concrete Sidewall, 10.0 cm deep, centerline WN-4	+5.0 cm	2320 C	± 1%
25	T	TC Type K	N Concrete Sidewall, 35.0 cm deep, centerline SWA-9	-36.0 cm	1400 C	± 0.75%
26	T	TC Type K	N Concrete Sidewall 40.0 cm deep, centerline SWA-10	-36.0 cm	1400 C	± 0.75%

27	T	TC Type K	N Concrete Sidewall 45.0 cm deep, centerline SWA-11	-36.0 cm	1400 C	± 0.75%
28	T	TC Type C	N Concrete Sidewall, 15.0 cm deep, centerline WN-5	+5.0 cm	2320 C	± 1%
29	T	TC Type K	Concrete Basemat 0.0 cm, -1.9 cm A-1	0.0 cm	1400 C	± 0.75%
30	T	TC Type K	Concrete Basemat 0.0 cm, -1.9 cm A-2	-2.5 cm	1400 C	± 0.75%
31	T	TC Type K	Concrete Basemat 0.0 cm, -1.9 cm A-3	-5.0 cm	1400 C	± 0.75%
32	T	TC Type K	Concrete Basemat 0.0 cm, -1.9 cm A-4	-7.5 cm	1400 C	± 0.75%
33	T	TC Type K	Concrete Basemat 0.0 cm, -1.9 cm A-5	-12.5 cm	1400 C	± 0.75%
34	T	TC Type K	Concrete Basemat 0.0 cm, -1.9 cm A-6	-17.5 cm	1400 C	± 0.75%
35	T	TC Type K	Concrete Basemat 0.0 cm, -1.9 cm A-7	-22.5 cm	1400 C	± 0.75%
36	T	TC Type K	Concrete Basemat 0.0 cm, -1.9 cm A-8	-27.5 cm	1400 C	± 0.75%
37	T	TC Type K	Concrete Basemat 0.0 cm, -1.9 cm A-9	-32.5 cm	1400 C	± 0.75%
38	T	TC Type K	Concrete Basemat 0.0 cm, -1.9 cm A-10	-37.5 cm	1400 C	± 0.75%
39	T	TC Type K	Concrete Basemat 0.0 cm, -1.9 cm A-11	-42.5 cm	1400 C	± 0.75%
40	T	TC Type K	Concrete Basemat –12.5 cm, +19.7 cm B-1	0.0 cm	1400 C	± 0.75%
41	T	TC Type K	Concrete Basemat –12.5 cm, +19.7 cm B-2	-2.5 cm	1400 C	± 0.75%
42	T	TC Type K	Concrete Basemat –12.5 cm, +19.7 cm B-3	-7.5 cm	1400 C	± 0.75%
43	T	TC Type K	Concrete Basemat –12.5 cm, +19.7 cm B-4	-12.5 cm	1400 C	± 0.75%
44	T	TC Type K	Concrete Basemat –12.5 cm, +19.7 cm B-5	-17.5 cm	1400 C	± 0.75%
45	T	TC Type K	Concrete Basemat –12.5 cm, +19.7 cm B-6	-22.5 cm	1400 C	± 0.75%
46	T	TC Type K	Concrete Basemat –12.5 cm, +19.7 cm B-7	-27.5 cm	1400 C	± 0.75%
47	T	TC Type K	Concrete Basemat –12.5 cm, +19.7 cm B-8	-35.0 cm	1400 C	± 0.75%
48	T	TC Type K	Concrete Basemat –12.5 cm, +19.7 cm B-9	-42.5 cm	1400 C	± 0.75%
49	T	TC Type C	N Concrete Sidewall, 20.0 cm deep, centerline WN-6	+5.0 cm	2320 C	± 1%
50	T	Diode Sensor	TC compensation Channels B51-B99		130 C	
51	T	TC Type K	Concrete Basemat +12.5 cm, +19.7 cm C-1	0.0 cm	1400 C	± 0.75%
52	T	TC Type K	Concrete Basemat +12.5 cm, +19.7 cm C-2	-2.5 cm	1400 C	± 0.75%
53	T	TC Type K	Concrete Basemat +12.5 cm, +19.7 cm C-3	-7.5 cm	1400 C	± 0.75%
54	T	TC Type K	Concrete Basemat +12.5 cm, +19.7 cm C-4	-12.5 cm	1400 C	± 0.75%
55	T	TC Type K	Concrete Basemat +12.5 cm, +19.7 cm C-5	-17.5 cm	1400 C	± 0.75%

56	T	TC Type K	Concrete Basemat +12.5 cm, +19.7 cm C-6	-22.5 cm	1400 C	± 0.75%
57	T	TC Type K	Concrete Basemat +12.5 cm, +19.7 cm C-7	-27.5 cm	1400 C	± 0.75%
58	T	TC Type K	Concrete Basemat +12.5 cm, +19.7 cm C-8	-35.0 cm	1400 C	± 0.75%
59	T	TC Type K	Concrete Basemat +12.5 cm, +19.7 cm C-9	-42.5 cm	1400 C	± 0.75%
60	T	TC Type C	N Concrete Sidewall, 25.0 cm deep, centerline WN-7	+5.0 cm	2320 C	± 1%
61	T	TC Type K	Concrete Basemat +12.5 cm, -19.7 cm D-1	0.0 cm	1400 C	± 0.75%
62	T	TC Type K	Concrete Basemat +12.5 cm, -19.7 cm D-2	-2.5 cm	1400 C	± 0.75%
63	T	TC Type K	Concrete Basemat +12.5 cm, -19.7 cm D-3	-7.5 cm	1400 C	± 0.75%
64	T	TC Type K	Concrete Basemat +12.5 cm, -19.7 cm D-4	-12.5 cm	1400 C	± 0.75%
65	T	TC Type K	Concrete Basemat +12.5 cm, -19.7 cm D-5	-17.5 cm	1400 C	± 0.75%
66	T	TC Type K	Concrete Basemat +12.5 cm, -19.7 cm D-6	-22.5 cm	1400 C	± 0.75%
67	T	TC Type K	Concrete Basemat +12.5 cm, -19.7 cm D-7	-27.5 cm	1400 C	± 0.75%
68	T	TC Type K	Concrete Basemat +12.5 cm, -19.7 cm D-8	-35.0 cm	1400 C	± 0.75%
69	T	TC Type K	Concrete Basemat +12.5 cm, -19.7 cm D-9	-42.5 cm	1400 C	± 0.75%
70	T	TC Type C	N Concrete Sidewall, 30.0 cm deep, centerline WN-8	+5.0 cm	2320 C	± 1%
71	T	TC Type K	Concrete Basemat -12.5 cm, -19.7 cm E-1	0.0 cm	1400 C	± 0.75%
72	T	TC Type K	Concrete Basemat -12.5 cm, -19.7 cm E-2	-2.5 cm	1400 C	± 0.75%
73	T	TC Type K	Concrete Basemat -12.5 cm, -19.7 cm E-3	-7.5 cm	1400 C	± 0.75%
74	T	TC Type K	Concrete Basemat -12.5 cm, -19.7 cm E-4	-12.5 cm	1400 C	± 0.75%
75	T	TC Type K	Concrete Basemat -12.5 cm, -19.7 cm E-5	-17.5 cm	1400 C	± 0.75%
76	T	TC Type K	Concrete Basemat -12.5 cm, -19.7 cm E-6	-22.5 cm	1400 C	± 0.75%
77	T	TC Type K	Concrete Basemat -12.5 cm, -19.7 cm E-7	-27.5 cm	1400 C	± 0.75%
78	T	TC Type K	Concrete Basemat -12.5 cm, -19.7 cm E-8	-35.0 cm	1400 C	± 0.75%
79	T	TC Type K	Concrete Basemat -12.5 cm, -19.7 cm E-9	-42.5 cm	1400 C	± 0.75%
80	Reserve					
81	T	TC Type K	N Concrete Sidewall 0.0 cm deep, centerline SWA-1	-36.0 cm	1400 C	± 0.75%
82	T	TC Type K	N Concrete Sidewall 2.0 cm deep, centerline SWA-2	-36.0 cm	1400 C	± 0.75%
83	T	TC Type K	N Concrete Sidewall 6.0 cm deep, centerline SWA-3	-36.0 cm	1400 C	± 0.75%
84	T	TC Type K	N Concrete Sidewall 10.0 cm deep, centerline SWA-4	-36.0 cm	1400 C	± 0.75%

85	T	TC Type K	N Concrete Sidewall 15.0 cm deep, centerline SWA-5	-36.0 cm	1400 C	± 0.75%
86	T	TC Type K	N Concrete Sidewall 20.0 cm deep, centerline SWA-6	-36.0 cm	1400 C	± 0.75%
87	T	TC Type K	N Concrete Sidewall 25.0 cm deep, centerline SWA-7	-36.0 cm	1400 C	± 0.75%
88	T	TC Type K	N Concrete Sidewall 30.0 cm deep, centerline SWA-8	-36.0 cm	1400 C	± 0.75%
89	T	TC Type K	N Concrete Sidewall 0.0 cm deep, centerline SWB-1	-24.0 cm	1400 C	± 0.75%
90	T	TC Type K	N Concrete Sidewall 2.0 cm deep, centerline SWB-2	-24.0 cm	1400 C	± 0.75%
91	T	TC Type K	N Concrete Sidewall 6.0 cm deep, centerline SWB-3	-24.0 cm	1400 C	± 0.75%
92	T	TC Type K	N Concrete Sidewall 10.0 cm deep, centerline SWB-4	-24.0 cm	1400 C	± 0.75%
93	T	TC Type K	N Concrete Sidewall 15.0 cm deep, centerline SWB-5	-24.0 cm	1400 C	± 0.75%
94	T	TC Type K	N Concrete Sidewall 20.0 cm deep, centerline SWB-6	-24.0 cm	1400 C	± 0.75%
95	T	TC Type K	N Concrete Sidewall 25.0 cm deep, centerline SWB-7	-24.0 cm	1400 C	± 0.75%
96	T	TC Type K	N Concrete Sidewall 30.0 cm deep, centerline SWB-8	-24.0 cm	1400 C	± 0.75%
97	T	TC Type K	N Concrete Sidewall 0.0 cm deep, centerline SWC-1	-12.0 cm	1400 C	± 0.75%
98	T	TC Type K	N Concrete Sidewall 2.0 cm deep, centerline SWC-2	-12.0 cm	1400 C	± 0.75%
99	T	TC Type K	N Concrete Sidewall 6.0 cm deep, centerline SWC-3	-12.0 cm	1400 C	± 0.75%

Explanation of Variable Notations

T = temperature

Table A-2. "Power" DAS Channel Assignments for CCI-5.

Channel	Variable	Sensor	Location	Elevation	Range/Limit	Accuracy
00	Reserve					
01	T	TC Type K	N Concrete Sidewall 10.0 cm deep, centerline SWC-4	-12.0 cm	1400 C	± 0.75%
02	T	TC Type K	N Concrete Sidewall 15.0 cm deep, centerline SWC-5	-12.0 cm	1400 C	± 0.75%
03	T	TC Type K	N Concrete Sidewall 20.0 cm deep, centerline SWC-6	-12.0 cm	1400 C	± 0.75%
04	T	TC Type K	N Concrete Sidewall 25.0 cm deep, centerline SWC-7	-12.0 cm	1400 C	± 0.75%
05	T	TC Type K	N Concrete Sidewall 30.0 cm deep, centerline SWC-8	-12.0 cm	1400 C	± 0.75%
06	T	TC Type K	N Concrete Sidewall 35.0 cm deep, centerline SWC-9	-12.0 cm	1400 C	± 0.75%
07	T	TC Type K	N Concrete Sidewall 40.0 cm deep, centerline SWC-10	-12.0 cm	1400 C	± 0.75%
08	T	TC Type K	N Concrete Sidewall 45.0 cm deep, centerline SWC-11	-12.0 cm	1400 C	± 0.75%
09	T	TC Type K	N Concrete Sidewall 0.0 cm deep, centerline SWD-1	0.0 cm	1400 C	± 0.75%
10	T	TC Type K	N Concrete Sidewall 2.0 cm deep, centerline SWD-2	0.0 cm	1400 C	± 0.75%
11	T	TC Type K	N Concrete Sidewall 6.0 cm deep, centerline SWD-3	0.0 cm	1400 C	± 0.75%
12	T	TC Type K	N Concrete Sidewall 10.0 cm deep, centerline SWD-4	0.0 cm	1400 C	± 0.75%
13	T	TC Type K	N Concrete Sidewall 15.0 cm deep, centerline SWD-5	0.0 cm	1400 C	± 0.75%
14	T	TC Type K	N Concrete Sidewall 20.0 cm deep, centerline SWD-6	0.0 cm	1400 C	± 0.75%
15	T	TC Type K	N Concrete Sidewall 25.0 cm deep, centerline SWD-7	0.0 cm	1400 C	± 0.75%
16	T	TC Type K	N Concrete Sidewall 30.0 cm deep, centerline SWD-8	0.0 cm	1400 C	± 0.75%
17	T	TC Type K	N Concrete Sidewall 35.0 cm deep, centerline SWD-9	0.0 cm	1400 C	± 0.75%
18	T	TC Type K	N Concrete Sidewall 40.0 cm deep, centerline SWD-10	0.0 cm	1400 C	± 0.75%
19	T	TC Type K	N Concrete Sidewall 45.0 cm deep, centerline SWD-11	0.0 cm	1400 C	± 0.75%
20	T	TC Type K	N Concrete Sidewall 0.0 cm deep, centerline SWE-1	+10.0 cm	1400 C	± 0.75%
21	T	TC Type K	N Concrete Sidewall 2.0 cm deep, centerline SWE-2	+10.0 cm	1400 C	± 0.75%
22	T	TC Type K	N Concrete Sidewall 6.0 cm deep, centerline SWE-3	+10.0 cm	1400 C	± 0.75%
23	T	TC Type K	N Concrete Sidewall 10.0 cm deep, centerline SWE-4	+10.0 cm	1400 C	± 0.75%
24	T	TC Type K	N Concrete Sidewall 15.0 cm deep, centerline SWE-5	+10.0 cm	1400 C	± 0.75%
25	T	TC Type K	N Concrete Sidewall 20.0 cm deep, centerline SWE-6	+10.0 cm	1400 C	± 0.75%
26	T	TC Type K	N Concrete Sidewall 25.0 cm deep, centerline SWE-7	+10.0 cm	1400 C	± 0.75%

27	T	TC Type K	N Concrete Sidewall 30.0 cm deep, centerline SWE-8	+10.0 cm	1400 C	± 0.75%
28	T	TC Type K	N Concrete Sidewall 35.0 cm deep, centerline SWE-9	+10.0 cm	1400 C	± 0.75%
29	T	TC Type K	N Concrete Sidewall 40.0 cm deep, centerline SWE-10	+10.0 cm	1400 C	± 0.75%
30	T	TC Type K	N Concrete Sidewall 45.0 cm deep, centerline SWE-11	+10.0 cm	1400 C	± 0.75%
31	T	TC Type K	N Concrete Sidewall 0.0 cm deep, centerline SWF-1	+20.0 cm	1400 C	± 0.75%
32	T	TC Type K	N Concrete Sidewall 2.0 cm deep, centerline SWF-2	+20.0 cm	1400 C	± 0.75%
33	T	TC Type K	N Concrete Sidewall 6.0 cm deep, centerline SWF-3	+20.0 cm	1400 C	± 0.75%
34	T	TC Type K	N Concrete Sidewall 10.0 cm deep, centerline SWF-4	+20.0 cm	1400 C	± 0.75%
35	T	TC Type K	N Concrete Sidewall 15.0 cm deep, centerline SWF-5	+20.0 cm	1400 C	± 0.75%
36	T	TC Type K	N Concrete Sidewall 20.0 cm deep, centerline SWF-6	+20.0 cm	1400 C	± 0.75%
37	T	TC Type K	N Concrete Sidewall 25.0 cm deep, centerline SWF-7	+20.0 cm	1400 C	± 0.75%
38	T	TC Type K	N Concrete Sidewall 30.0 cm deep, centerline SWF-8	+20.0 cm	1400 C	± 0.75%
39	T	TC Type K	N Concrete Sidewall 35.0 cm deep, centerline SWF-9	+20.0 cm	1400 C	± 0.75%
40	T	TC Type K	N Concrete Sidewall 40.0 cm deep, centerline SWF-10	+20.0 cm	1400 C	± 0.75%
41	T	TC Type K	N Concrete Sidewall 45.0 cm deep, centerline SWF-11	+20.0 cm	1400 C	± 0.75%
42	T	TC Type K	N Concrete Sidewall 0.0 cm deep, centerline SWG-1	+30.0 cm	1400 C	± 0.75%
43	T	TC Type K	N Concrete Sidewall 5.0 cm deep, centerline SWG-2	+30.0 cm	1400 C	± 0.75%
44	T	TC Type K	N Concrete Sidewall 10.0 cm deep, centerline SWG-3	+30.0 cm	1400 C	± 0.75%
45	T	TC Type K	N Concrete Sidewall 35.0 cm deep, centerline SWB-9	-24.0 cm	1400 C	± 0.75%
46	T	TC Type K	N Concrete Sidewall 40.0 cm deep, centerline SWB-10	-24.0 cm	1400 C	± 0.75%
47	T	TC Type K	N Concrete Sidewall 45.0 cm deep, centerline SWB-11	-24.0 cm	1400 C	± 0.75%
48	Reserve					
49	Reserve					
50	T	TC Type K	N Concrete Sidewall 0.0 cm deep, 12.5 cm W of centerline, SWH-1	-15.0 cm	1400 C	± 0.75%
51	T	TC Type K	N Concrete Sidewall 5.0 cm deep, 12.5 cm W of centerline, SWH-2	-15.0 cm	1400 C	± 0.75%
52	T	TC Type K	N Concrete Sidewall 10.0 cm deep, 12.5 cm W of centerline, SWH-3	-15.0 cm	1400 C	± 0.75%
53	T	TC Type K	N Concrete Sidewall 20.0 cm deep, 12.5 cm W of centerline, SWH-4	-15.0 cm	1400 C	± 0.75%
54	T	TC Type K	N Concrete Sidewall 30.0 cm deep, 12.5 cm W of centerline, SWH-5	-15.0 cm	1400 C	± 0.75%
55	T	TC Type K	N Concrete Sidewall 40.0 cm deep, 12.5 cm W of centerline, SWH-6	-15.0 cm	1400 C	± 0.75%

56	T	TC Type K	N Concrete Sidewall 0.0 cm deep, 12.5 cm E of centerline, SWI-1	-15.0 cm	1400 C	± 0.75%
57	T	TC Type K	N Concrete Sidewall 5.0 cm deep, 12.5 cm E of centerline, SWI-2	-15.0 cm	1400 C	± 0.75%
58	T	TC Type K	N Concrete Sidewall 10.0 cm deep, 12.5 cm E of centerline, SWI-3	-15.0 cm	1400 C	± 0.75%
59	T	TC Type K	N Concrete Sidewall 20.0 cm deep, 12.5 cm E of centerline, SWI-4	-15.0 cm	1400 C	± 0.75%
60	T	TC Type K	N Concrete Sidewall 30.0 cm deep, 12.5 cm E of centerline, SWI-5	-15.0 cm	1400 C	± 0.75%
61	T	TC Type K	N Concrete Sidewall 40.0 cm deep, 12.5 cm E of centerline, SWI-6	-15.0 cm	1400 C	± 0.75%
62	T	TC Type K	N Concrete Sidewall 0.0 cm deep, 12.5 cm W of centerline, SWJ-1	-5.0 cm	1400 C	± 0.75%
63	T	TC Type K	N Concrete Sidewall 5.0 cm deep, 12.5 cm W of centerline, SWJ-2	-5.0 cm	1400 C	± 0.75%
64	T	TC Type K	N Concrete Sidewall 10.0 cm deep, 12.5 cm W of centerline, SWJ-3	-5.0 cm	1400 C	± 0.75%
65	T	TC Type K	N Concrete Sidewall 20.0 cm deep, 12.5 cm W of centerline, SWJ-4	-5.0 cm	1400 C	± 0.75%
66	T	TC Type K	N Concrete Sidewall 30.0 cm deep, 12.5 cm W of centerline, SWJ-5	-5.0 cm	1400 C	± 0.75%
67	T	TC Type K	N Concrete Sidewall 40.0 cm deep, 12.5 cm W of centerline, SWJ-6	-5.0 cm	1400 C	± 0.75%
68	T	TC Type K	N Concrete Sidewall 0.0 cm deep, 12.5 cm E of centerline, SWK-1	-5.0 cm	1400 C	± 0.75%
69	T	TC Type K	N Concrete Sidewall 5.0 cm deep, 12.5 cm E of centerline, SWK-2	-5.0 cm	1400 C	± 0.75%
70	T	TC Type K	N Concrete Sidewall 10.0 cm deep, 12.5 cm E of centerline, SWK-3	-5.0 cm	1400 C	± 0.75%
71	T	TC Type K	N Concrete Sidewall 20.0 cm deep, 12.5 cm E of centerline, SWK-4	-5.0 cm	1400 C	± 0.75%
72	T	TC Type K	N Concrete Sidewall 30.0 cm deep, 12.5 cm E of centerline, SWK-5	-5.0 cm	1400 C	± 0.75%
73	T	TC Type K	N Concrete Sidewall 40.0 cm deep, 12.5 cm E of centerline, SWK-6	-5.0 cm	1400 C	± 0.75%
74	T	TC Type K	N Concrete Sidewall 0.0 cm deep, 12.5 cm W of centerline, SWL-1	+5.0 cm	1400 C	± 0.75%
75	T	TC Type K	N Concrete Sidewall 5.0 cm deep, 12.5 cm W of centerline, SWL-2	+5.0 cm	1400 C	± 0.75%
76	T	TC Type K	N Concrete Sidewall 10.0 cm deep, 12.5 cm W of centerline, SWL-3	+5.0 cm	1400 C	± 0.75%
77	T	TC Type K	N Concrete Sidewall 20.0 cm deep, 12.5 cm W of centerline, SWL-4	+5.0 cm	1400 C	± 0.75%
78	T	TC Type K	N Concrete Sidewall 30.0 cm deep, 12.5 cm W of centerline, SWL-5	+5.0 cm	1400 C	± 0.75%
79	T	TC Type K	N Concrete Sidewall 40.0 cm deep, 12.5 cm W of centerline, SWL-6	+5.0 cm	1400 C	± 0.75%
80	T	TC Type K	N Concrete Sidewall 0.0 cm deep, 12.5 cm E of centerline, SWM-1	+5.0 cm	1400 C	± 0.75%
81	T	TC Type K	N Concrete Sidewall 5.0 cm deep, 12.5 cm E of centerline, SWM-2	+5.0 cm	1400 C	± 0.75%
82	T	TC Type K	N Concrete Sidewall 10.0 cm deep, 12.5 cm E of centerline, SWM-3	+5.0 cm	1400 C	± 0.75%
83	T	TC Type K	N Concrete Sidewall 20.0 cm deep, 12.5 cm E of centerline, SWM-4	+5.0 cm	1400 C	± 0.75%
84	T	TC Type K	N Concrete Sidewall 30.0 cm deep, 12.5 cm E of centerline, SWM-5	+5.0 cm	1400 C	± 0.75%

85	T	TC Type K	N Concrete Sidewall 40.0 cm deep, 12.5 cm E of centerline, SWM-6	+5.0 cm	1400 C	± 0.75%
86	T	TC Type K	N Concrete Sidewall 0.0 cm deep, 12.5 cm W of centerline, SWN-1	+15.0 cm	1400 C	± 0.75%
87	T	TC Type K	N Concrete Sidewall 5.0 cm deep, 12.5 cm W of centerline, SWN-2	+15.0 cm	1400 C	± 0.75%
88	T	TC Type K	N Concrete Sidewall 10.0 cm deep, 12.5 cm W of centerline, SWN-3	+15.0 cm	1400 C	± 0.75%
89	T	TC Type K	N Concrete Sidewall 20.0 cm deep, 12.5 cm W of centerline, SWN-4	+15.0 cm	1400 C	± 0.75%
90	T	TC Type K	N Concrete Sidewall 30.0 cm deep, 12.5 cm W of centerline, SWN-5	+15.0 cm	1400 C	± 0.75%
91	T	TC Type K	N Concrete Sidewall 40.0 cm deep, 12.5 cm W of centerline, SWN-6	+15.0 cm	1400 C	± 0.75%
92	T	TC Type K	N Concrete Sidewall 0.0 cm deep, 12.5 cm E of centerline, SWO-1	+15.0 cm	1400 C	± 0.75%
93	T	TC Type K	N Concrete Sidewall 5.0 cm deep, 12.5 cm E of centerline, SWO-2	+15.0 cm	1400 C	± 0.75%
94	T	TC Type K	N Concrete Sidewall 10.0 cm deep, 12.5 cm E of centerline, SWO-3	+15.0 cm	1400 C	± 0.75%
95	T	TC Type K	N Concrete Sidewall 20.0 cm deep, 12.5 cm E of centerline, SWO-4	+15.0 cm	1400 C	± 0.75%
96	T	TC Type K	N Concrete Sidewall 30.0 cm deep, 12.5 cm E of centerline, SWO-5	+15.0 cm	1400 C	± 0.75%
97	T	TC Type K	N Concrete Sidewall 40.0 cm deep, 12.5 cm E of centerline, SWO-6	+15.0 cm	1400 C	± 0.75%
98	Reserve					
99	Reserve					

Explanation of Variable Notations

T = temperature

Table A-3. "Quench" DAS Channel Assignments for CCI-5.

Channel	Variable	Sensor	Location	Level	Range/Limit	Accuracy	Notes
00	T	Diode Sensor	TC Compensation CH Q00-Q49		130 C		
01	T	TC Type C	S MgO Sidewall, Lower Section, 0.0 cm deep SWHL-17	+10.0 cm	2320 C	± 1.0%	
02	T	TC Type C	S MgO Sidewall, Lower Section, 1.0 cm deep SWHL-18	+10.0 cm	2320 C	± 1.0%	
03	T	TC Type C	S MgO Sidewall, Lower Section, 3.0 cm deep SWHL-19	+10.0 cm	2320 C	± 1.0%	
04	T	TC Type C	E MgO Sidewall, Lower Section, 1.0 cm deep SWHL-1	-17.5 cm	2320 C	± 1.0%	
05	T	TC Type C	E MgO Sidewall, Lower Section, 2.0 cm deep SWHL-2	-17.5 cm	2320 C	± 1.0%	
06	T	TC Type C	E MgO Sidewall, Lower Section, 4.0 cm deep SWHL-3	-17.5 cm	2320 C	± 1.0%	
07	T	TC Type C	E MgO Sidewall, Lower Section, 8.0 cm deep SWHL-4	-17.5 cm	2320 C	± 1.0%	
08	T	TC Type C	W MgO Sidewall, Lower Section, 1.0 cm deep SWHL-9	-7.5 cm	2320 C	± 1.0%	
09	T	TC Type C	W MgO Sidewall, Lower Section, 2.0 cm deep SWHL-10	-7.5 cm	2320 C	± 1.0%	
10	T	TC Type C	W MgO Sidewall, Lower Section, 4.0 cm deep SWHL-11	-7.5 cm	2320 C	± 1.0%	
11	T	TC Type C	W MgO Sidewall, Lower Section, 8.0 cm deep SWHL-12	-7.5 cm	2320 C	± 1.0%	
12	T	TC Type C	E MgO Sidewall, Lower Section, 1.0 cm deep SWHL-13	+2.5 cm	2320 C	± 1.0%	
13	T	TC Type C	E MgO Sidewall, Lower Section, 2.0 cm deep SWHL-14	+2.5 cm	2320 C	± 1.0%	
14	T	TC Type C	E MgO Sidewall, Lower Section, 4.0 cm deep SWHL-15	+2.5 cm	2320 C	± 1.0%	
15	T	TC Type C	E MgO Sidewall, Lower Section, 8.0 cm deep SWHL-16	+2.5 cm	2320 C	± 1.0%	
16	T	TC Type C	W MgO Sidewall, Lower Section, 1.0 cm deep SWHL-21	+12.5 cm	2320 C	± 1.0%	
17	T	TC Type C	W MgO Sidewall, Lower Section, 2.0 cm deep SWHL-22	+12.5 cm	2320 C	± 1.0%	
18	T	TC Type C	W MgO Sidewall, Lower Section, 4.0 cm deep SWHL-23	+12.5 cm	2320 C	± 1.0%	
19	T	TC Type C	W MgO Sidewall, Lower Section, 8.0 cm deep SWHL-24	+12.5 cm	2320 C	± 1.0%	
20	L	Potentiometer	Lance Position Indicator		0-125 cm		
21	T	TC Type K	Steamline internal vertical run from vessel ML-1		1400 C	± 0.75%	
22	T	TC Type K	Steamline external vertical run from vessel ML-2		1400 C	± 0.75%	
23	T	TC Type K	Steamline external lateral run from vessel ML-3		1400 C	± 0.75%	
24	T	TC Type K	Steamline external vertical run to quench tank ML-4		1400 C	± 0.75%	
25	T	TC Type K	S Middle Section Sidewall, 0.0 cm deep SWHL-25	+67.5 cm	1400 C	± 0.75%	
26						± 0.75%	

	T	TC Type K	S Middle Section Sidewall, 20.0 cm deep SWHL-26	+67.5 cm	1400 C		
27	T	TC Type K	N Top Section Sidewall, 0.0 cm deep SWHL -37	+193.0 cm	1400 C	± 0.75%	
28	FOR	Strain	Crust Force Load		0-44.6 kN		
29	T	TC Type K	Quench tank internal QT-1	21 cm	1400 C	± 0.75%	
30	T	TC Type K	Quench tank internal QT-2	55 cm	1400 C	± 0.75%	
31	T	TC Type C	S MgO Sidewall, Lower Section, 0.0 cm deep SWHL-5	-10.0 cm	2320 C	± 1.0%	
32	T	TC Type C	S MgO Sidewall, Lower Section, 1.0 cm deep SWHL-6	-10.0 cm	2320 C	± 1.0%	
33	T	TC Type C	S MgO Sidewall, Lower Section, 3.0 cm deep SWHL-7	-10.0 cm	2320 C	± 1.0%	
34	T	TC Type C	S MgO Sidewall, Lower Section, 7.0 cm deep SWHL-8	-10.0 cm	2320 C	± 1.0%	
35	T	TC Type K	Quench tank coil inlet QT-5		1400 C	± 0.75%	
36	T	TC Type K	Quench tank coil outlet QT-6		1400 C	± 0.75%	
37	T	TC Type K	Quench tank coil outlet QT-7		1400 C	± 0.75%	
38	T	TC Type K	Overflow tank internal OT-1	16 cm	1400 C	± 0.75%	
39	T	Voltage	Igniter Current		100 mV		
40	T	TC Type K	Spray tank internal ST-1	10 cm	1400 C	± 0.75%	
41	T	TC Type C	S MgO Sidewall, Lower Section, 7.0 cm deep SWHL-20	+10.0 cm	2320 C	± 1.0%	
42	T	TC Type K	N Top Section Sidewall, 2.0 cm deep SWHL-38	+193.0 cm	1400 C	± 0.75%	
43	T	TC Type K	N Middle Section Sidewall, 0.0 cm deep SWHL-29	+92.2 cm	1400 C	± 0.75%	
44	T	TC Type K	N Middle Section Sidewall, 2.0 cm deep SWHL-30	+92.2 cm	1400 C	± 0.75%	
45	T	TC Type K	W Top Section Sidewall 0.0 cm deep SWHL-39	+211.3 cm	1400 C	± 0.75%	
46	T	TC Type K	W Top Section Sidewall 2.0 cm deep SWHL-40	+211.3 cm	1400 C	± 0.75%	
47	T	TC Type K	S Middle Section Sidewall 0.0 cm deep SWHL-33	+148.8 cm	1400 C	± 0.75%	
48	T	TC Type K	S Middle Section Sidewall 2.0 cm deep SWHL-34	+148.8 cm	1400 C	± 0.75%	
49	Reserve						
50	T	Diode Sensor	TC Compensation CH Q50-Q99		130 C		
51	T	TC Type K	E Top Section Sidewall 0.0 cm deep SWHL-35	+174.7 cm	1400 C	± 0.75%	
52	T	TC Type K	E Top Section Sidewall 2.0 cm deep SWHL-36	+174.7 cm	1400 C	± 0.75%	
53	Reserve						
54			Internal, exhaust line OG-1		1400 C	± 0.75%	

	T	TC Type K					
55	T	TC Type K	Water Supply Tank Internal WS-1		1400 C	± 0.75%	
56		Optical Pyrometer	Corium Surface Temperature OP-1	242.9 cm	600-1800 C	± 4.0 C	
57	T	TC Type K	Water level probe LP-1	167/48 cm	1400 C	± 0.75%	
58	T	TC Type K	Water level probe LP-2	167/48 cm	1400 C	± 0.75%	
59	T	TC Type K	Test vessel plenum gas TS-1	223.0 cm	1400 C	± 0.75%	
60	L	Strain	Supply tank head PT-1		350-2000 l		D-6
61	P	Strain	Supply tank pressure PT-2		0-204 kPa		A-17
62	L	Strain	Test vessel head, insertion probe PT-3		63-150 l		D-3
63	L	Strain	Test vessel head, static probe PT-4		32-150 l		D-1
64	P	Strain	Test vessel plenum pressure PT-5		0-204 kPa		A-1
65	P	Strain	Basemat side pressure PT-6		0-204 kPa		A-3
66	Reserve						
67	L	Strain	Quench tank head PT-8		80-590 l		D-9
68	P	Strain	Quench/overflow tank pressure PT-9		0-35 kPad		D-2
69	L	Strain	Overflow tank head PT-10		200-900 l		D-8
70	L	Strain	Spray tank head PT-11		240-1290 l		D-5
71	P	Strain	Spray tank pressure PT-12		0-35 kPad		D-4
72	L	Magnetic Float	Supply tank volume LS-1		350-2000 l		
73	L	Magnetic Float	Quench tank volume LS-2		80-590 l		
74	L	Magnetic Float	Overflow tank volume LS-3		200-900 l		
75	L	Magnetic Float	Spray tank volume LS-4		240-1290 l		
76	F	Paddlewheel	Water supply flowrate FM-1		680 lpm		
77	F	Paddlewheel	Quench tank coil flowrate FM-2		190 lpm		
78	Reserve						
79	T	TC Type K	S Top Section Sidewall 0.0 cm deep SWHL-41	+229.6 cm	1400 C	± 0.75%	
80	T	TC Type K	S Top Section Sidewall 2.0 cm deep SWHL-42	+229.6 cm	1400 C	± 0.75%	
81	FC	Flowcontroller	Final Offgas Flowrate FC1a		0-3,000 lpm		

82		-	Calculated Water Volume in Test Section		0-150 l		
83	FC	Flowcontroller	Lid lights & camera covergas flowrate FC-2		0-200 lpm		
84	Reserve						
85		-	Calculated Total Current (Q92+Q93)		0 -10,000 A		
86		-	Calculated Total Power (Q94+Q95)		0-500 kW		
87	FC	Flowcontroller	Test vessel covergas flowrate FC-6		0-100 lpm		
88	FC	Flowcontroller	Lid camera covergas flowrate FC-7		0-350 lpm		
89	V		Pressure transducer power supply #1 voltage		0-30 V		
90	V		Pressure transducer power supply #2 voltage		0-30 V		
91	V	Voltmeter	Power supply voltage		0-200 V		
92	A	Transformer	Power supply current #2		5000 A		
93	A	Transformer	Power supply current #1		5000 A		
94	W	Hall Meter	Power supply power #2		1100 kW		
95	W	Hall Meter	Power supply power #1		1100 kW		
96	L	Strain	Auxiliary Tank Head PT-13		366-4080		D-10
97	T	TC Type K	Auxiliary Tank Internal AT-1	43 cm	1400 C	± 0.75%	
98	Reserve						
99	Reserve						

Explanation of variable notations

T = temperature P = Pressure FOR=Force L = Level V = Voltage F = Flowrate A = Current W = Power FC = Flow Controller

APPENDIX B
Test Data

This Appendix provides plots of all data recorded during Test CCI-5. The complete channel assignment list is provided in Appendix A. Time t = 0 in all plots is referenced to the time at which ablation had been initiated on the concrete basemat and sidewall. This corresponds to 6.0 minutes after onset of data acquisition; see Table 3-1. All data was logged at ~ 5.5 second time intervals during the test. The data have been averaged over 30 second intervals to improve readability.

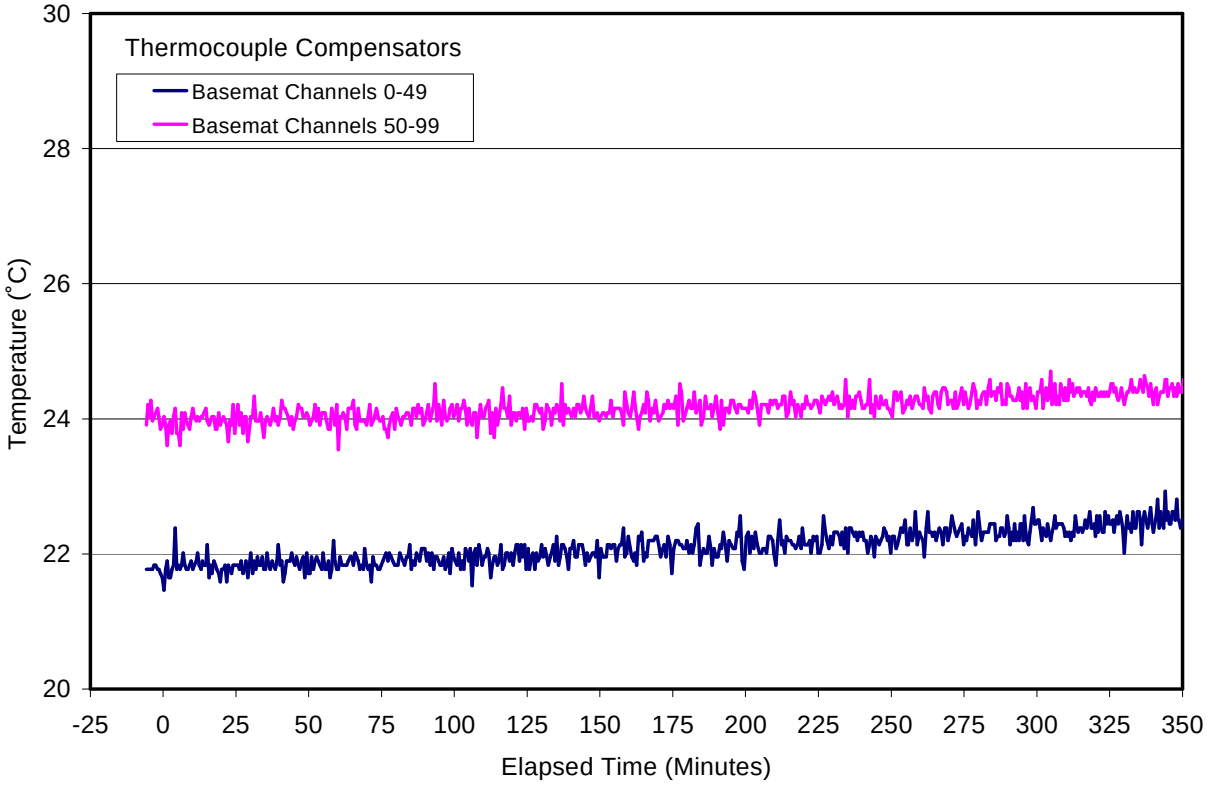

Figure B-1. Compensator Temperature, Channels B0-B49 and B50-B99.

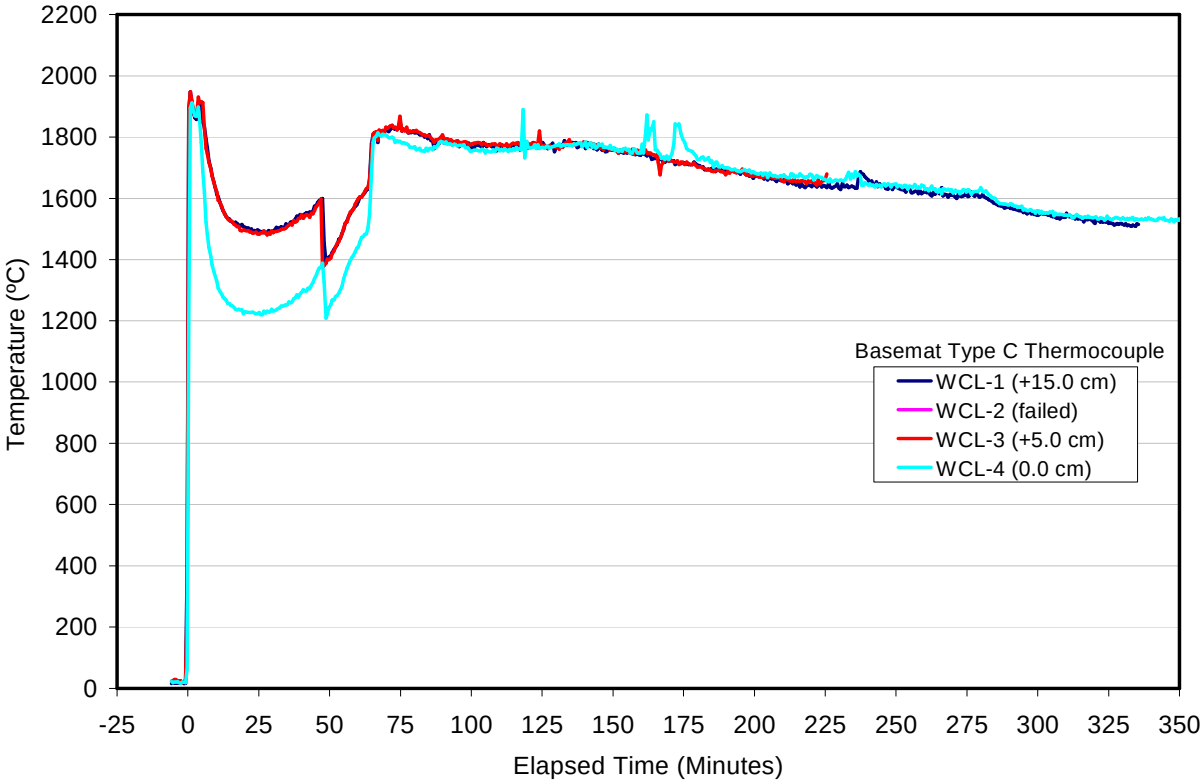

Figure B-2. Basemat Type C "WCL" Array Data.

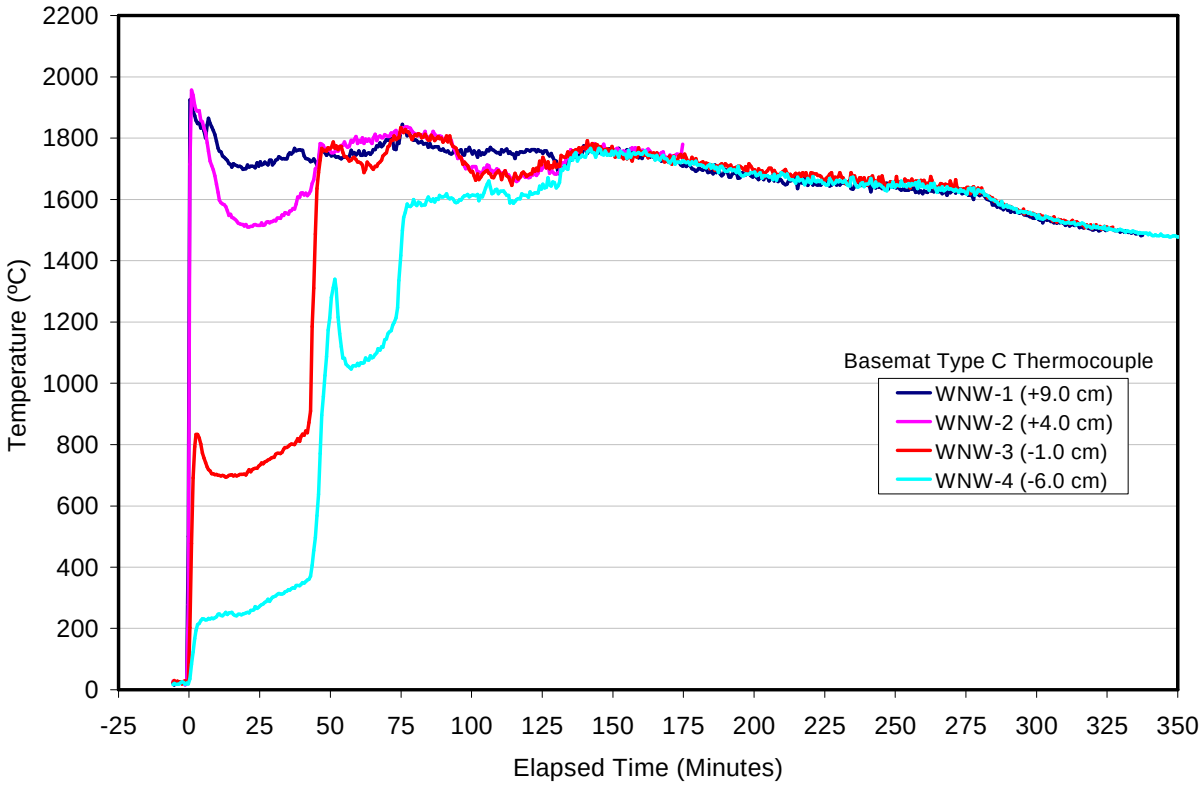

Figure B-3. Basemat Type C "WNW" Array Data.

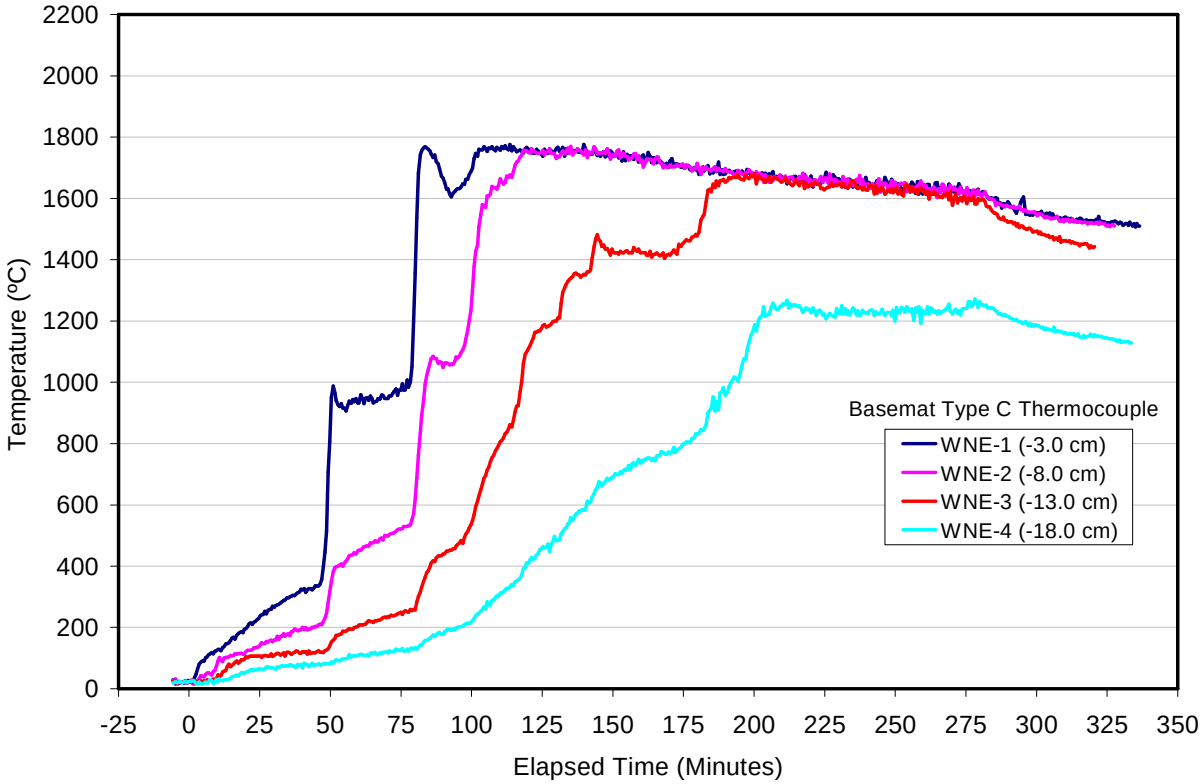

Figure B-4. Basemat Type C "WNE" Array Data.

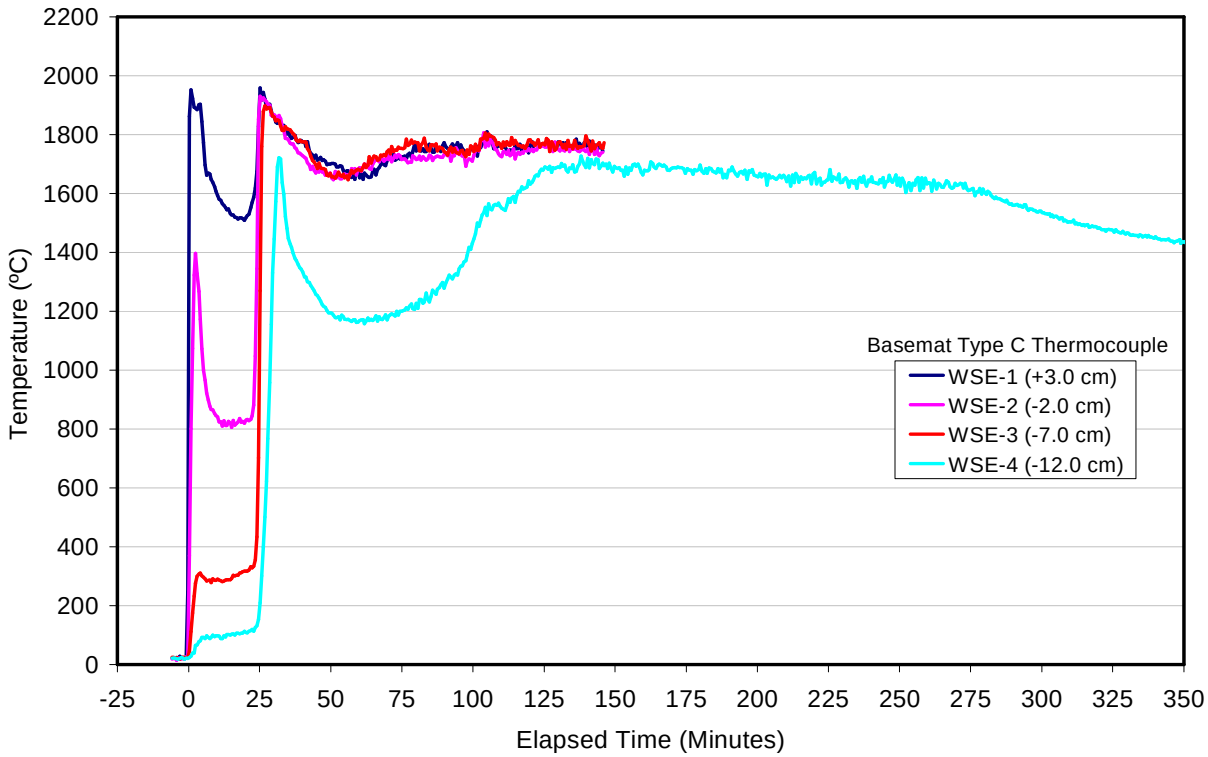

Figure B-5. Basemat Type C "WSE" Array Data.

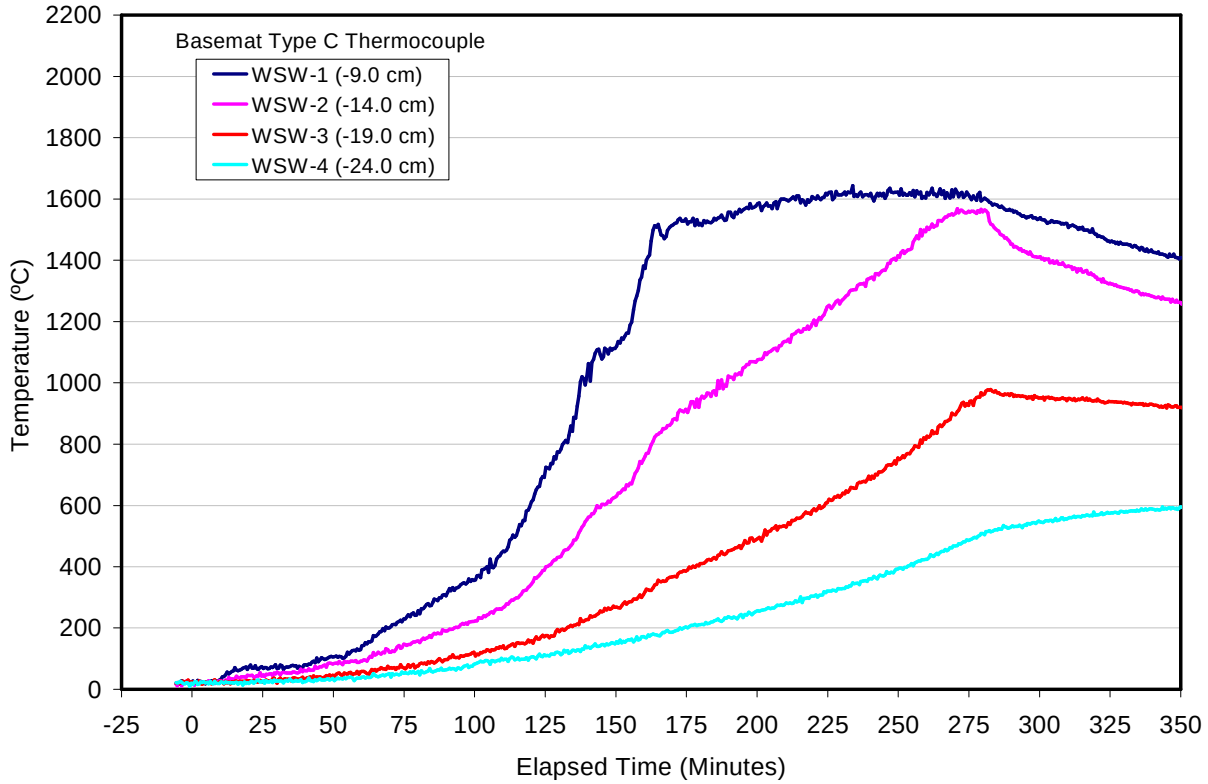

Figure B-6. Basemat Type C "WSW" Array Data.

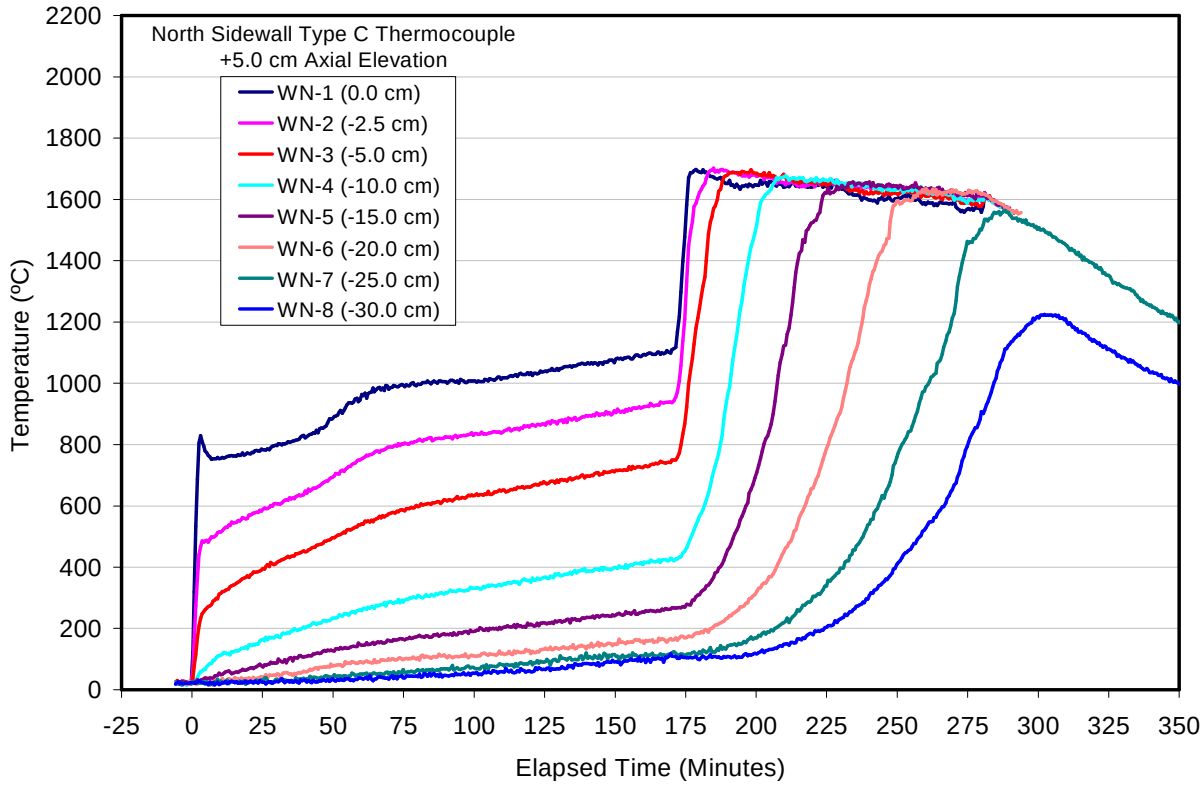

Figure B-7. North Sidewall Type C "WN" Array Data.

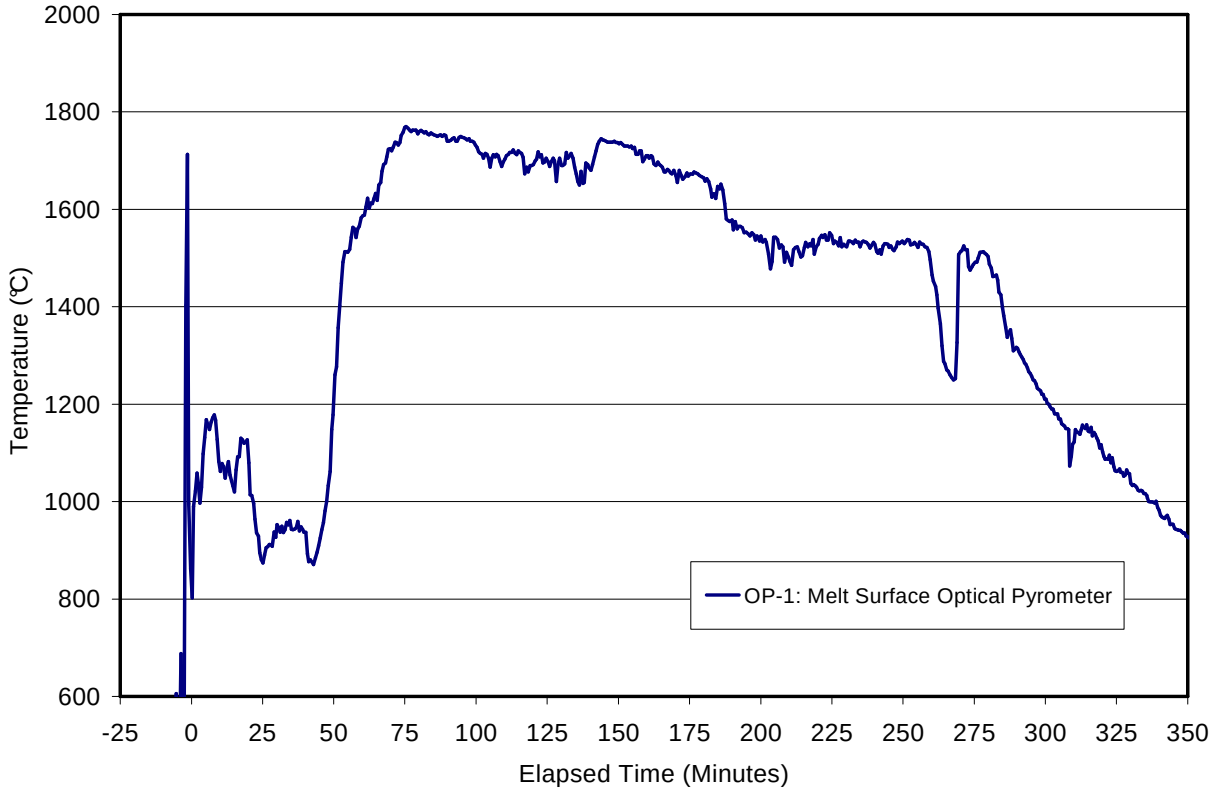

Figure B-8. Melt Surface Temperature Optical Pyrometer OP-1 Data.

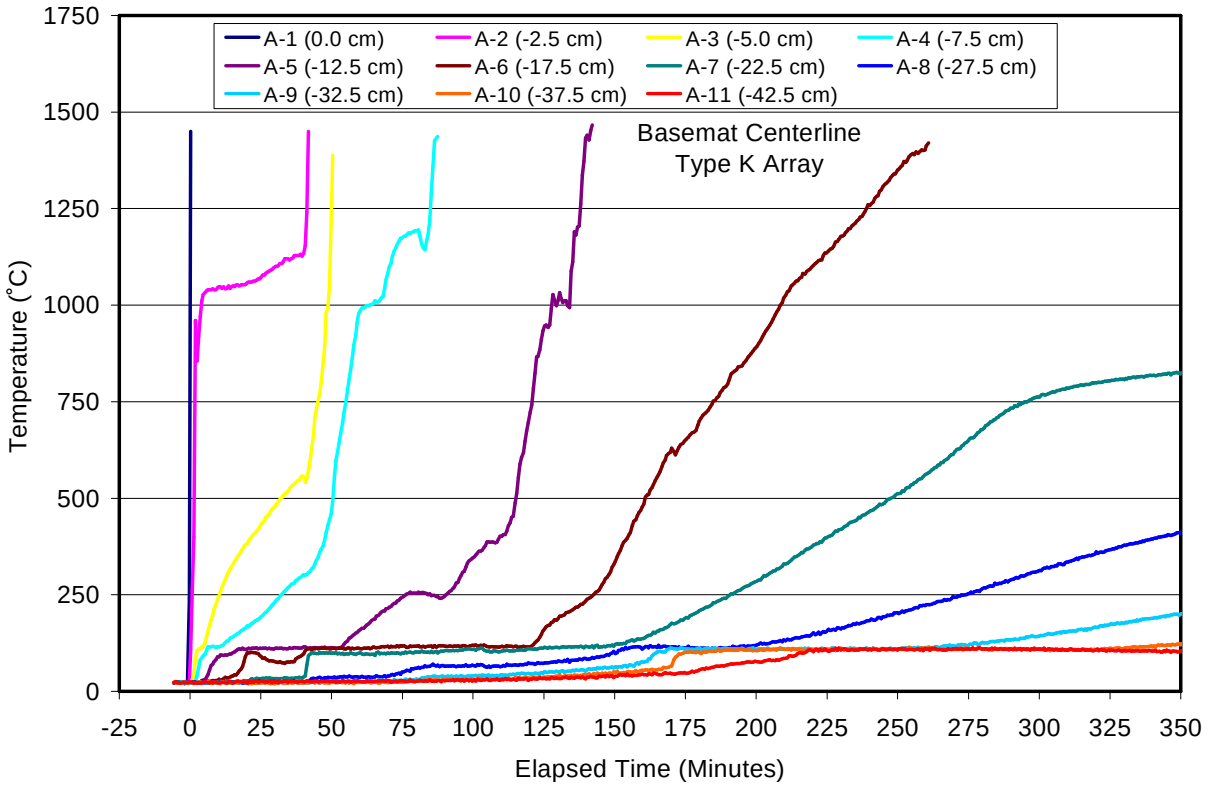

Figure B-9. Basemat Type K "A" Array Data.

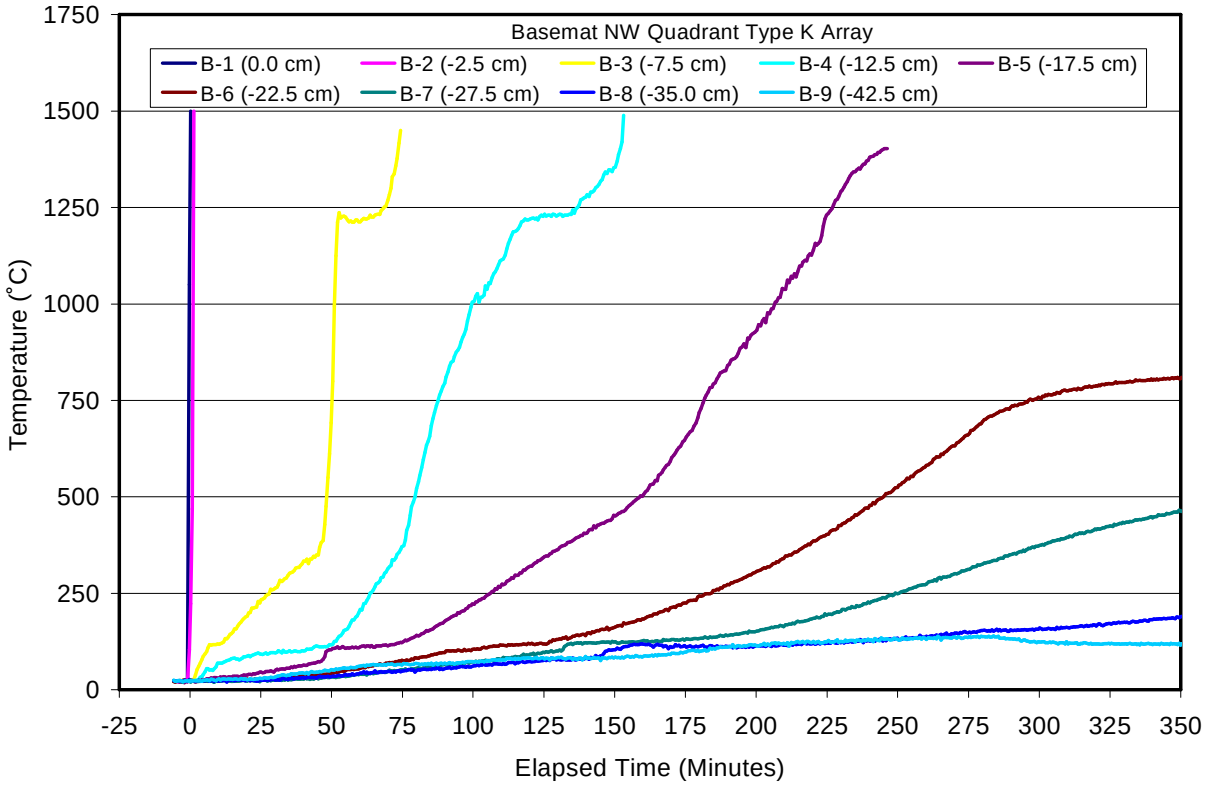

Figure B-10. Basemat Type K "B" Array Data.

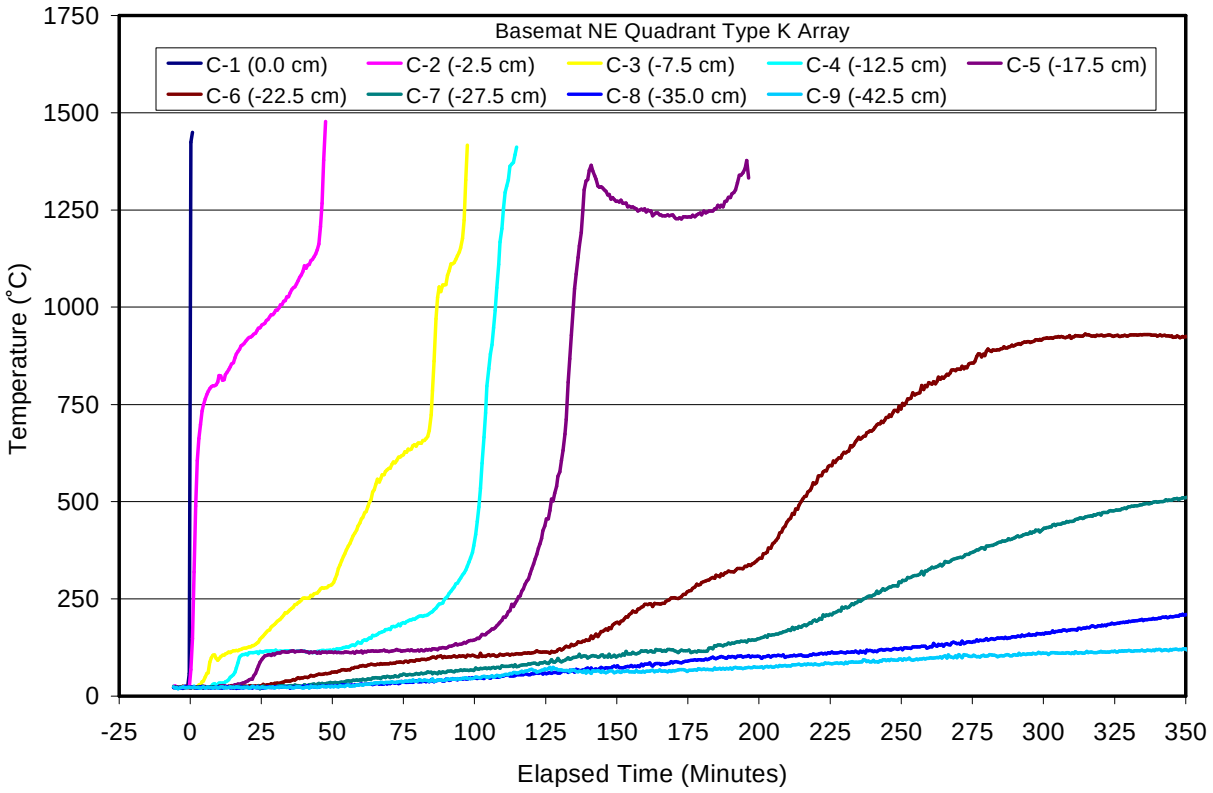

Figure B-11. Basemat Type K "C" Array Data.

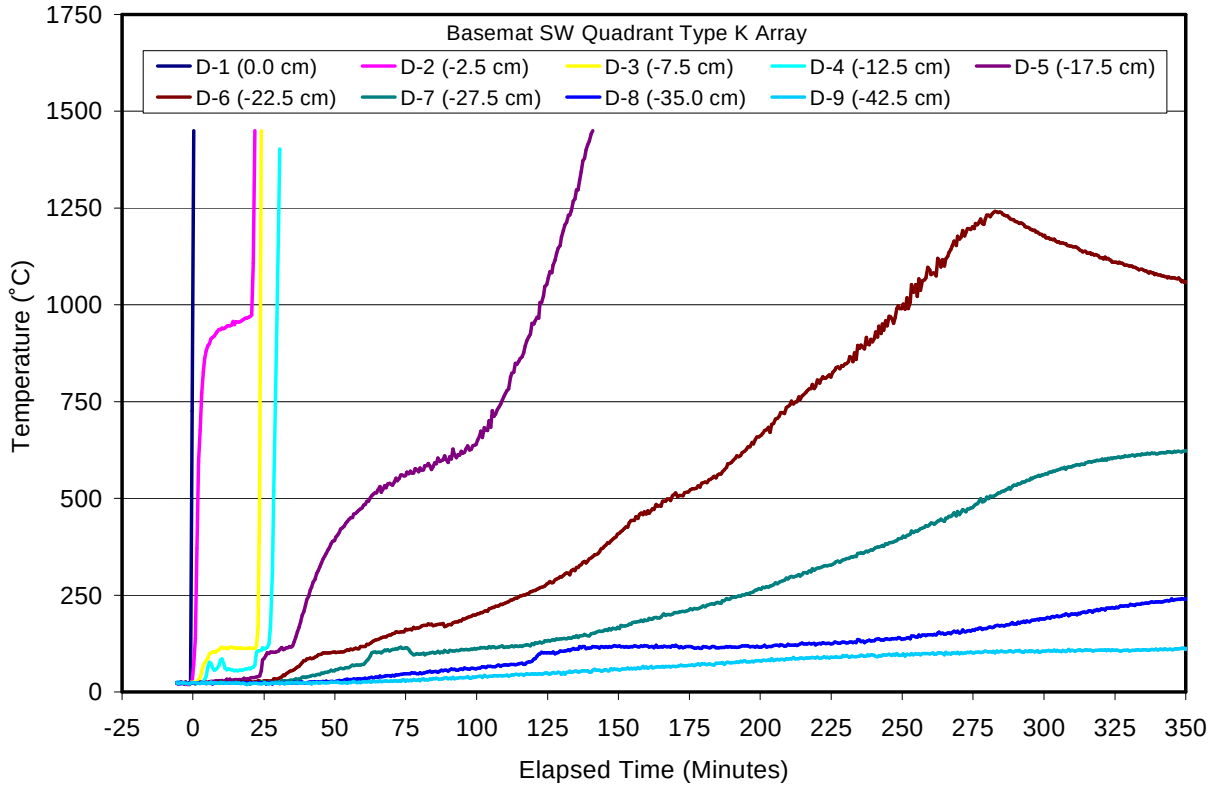

Figure B-12. Basemat Type K "D" Array Data.

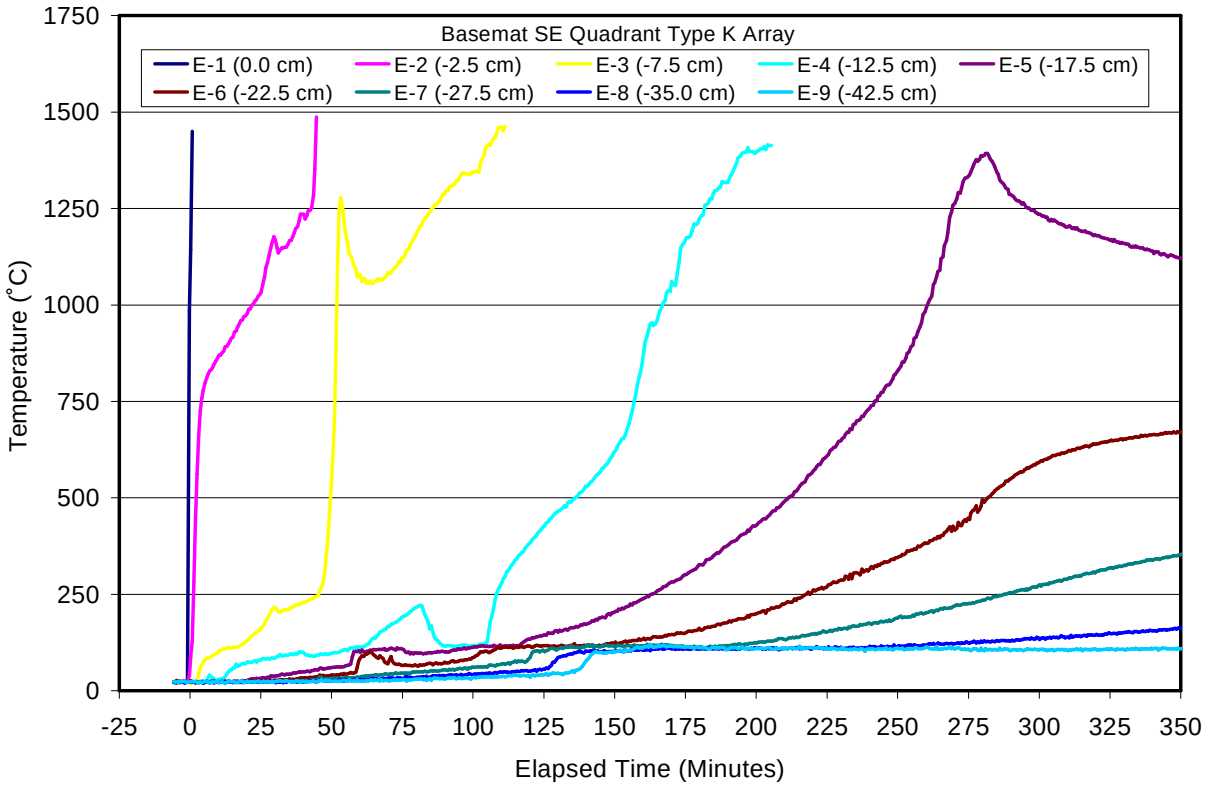

Figure B-13. Basemat Type K "E" Array Data.

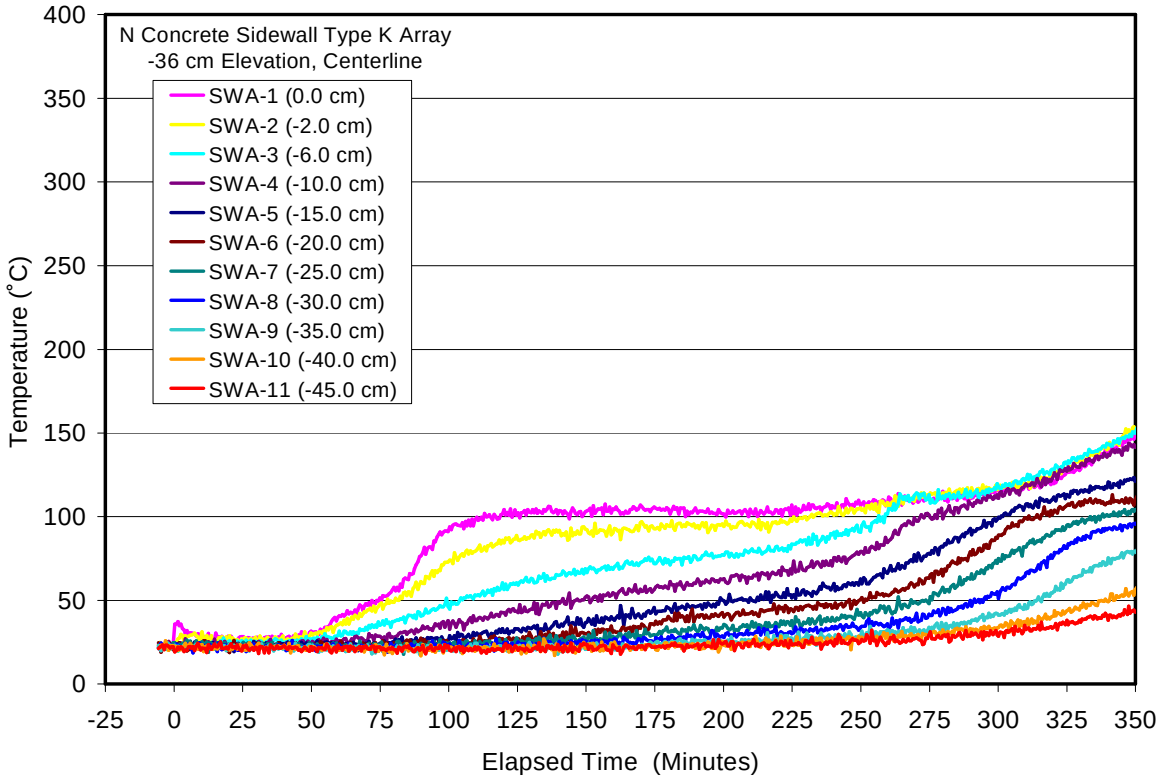

Figure B-14. North Sidewall Type K "SWA" Array Data.

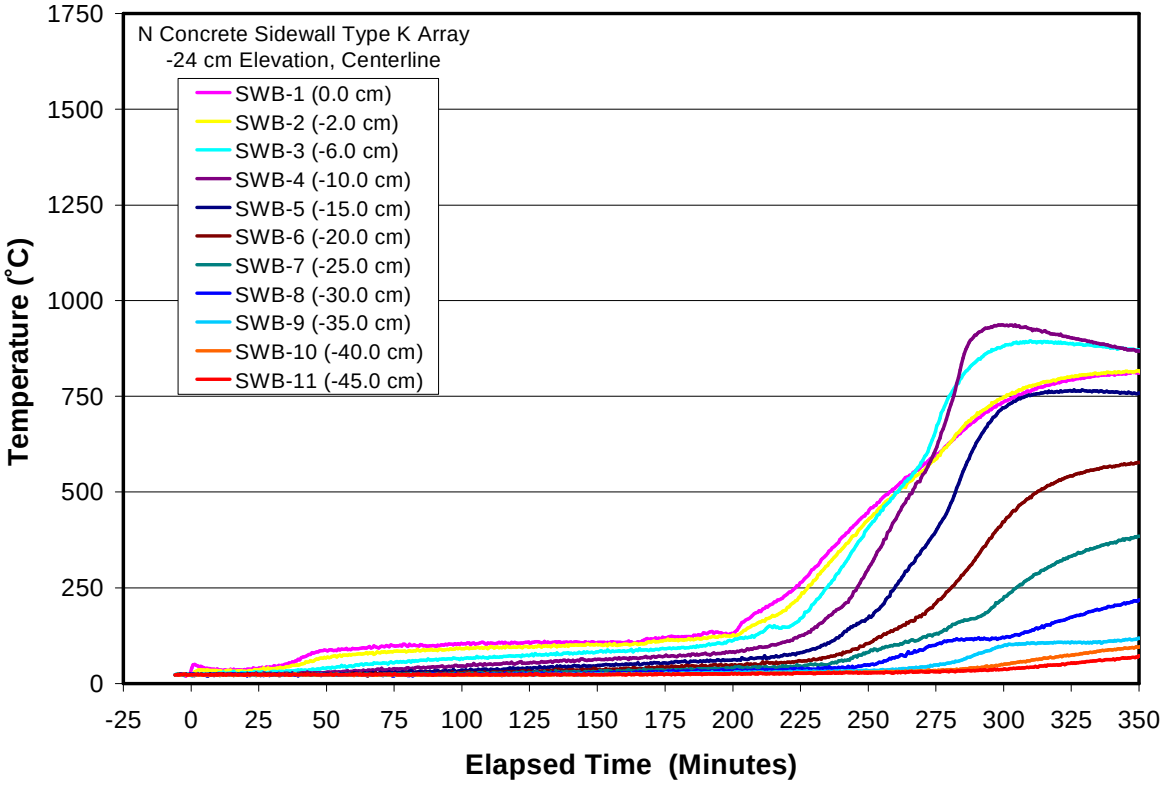

Figure B-15. North Sidewall Type K "SWB" Array Data.

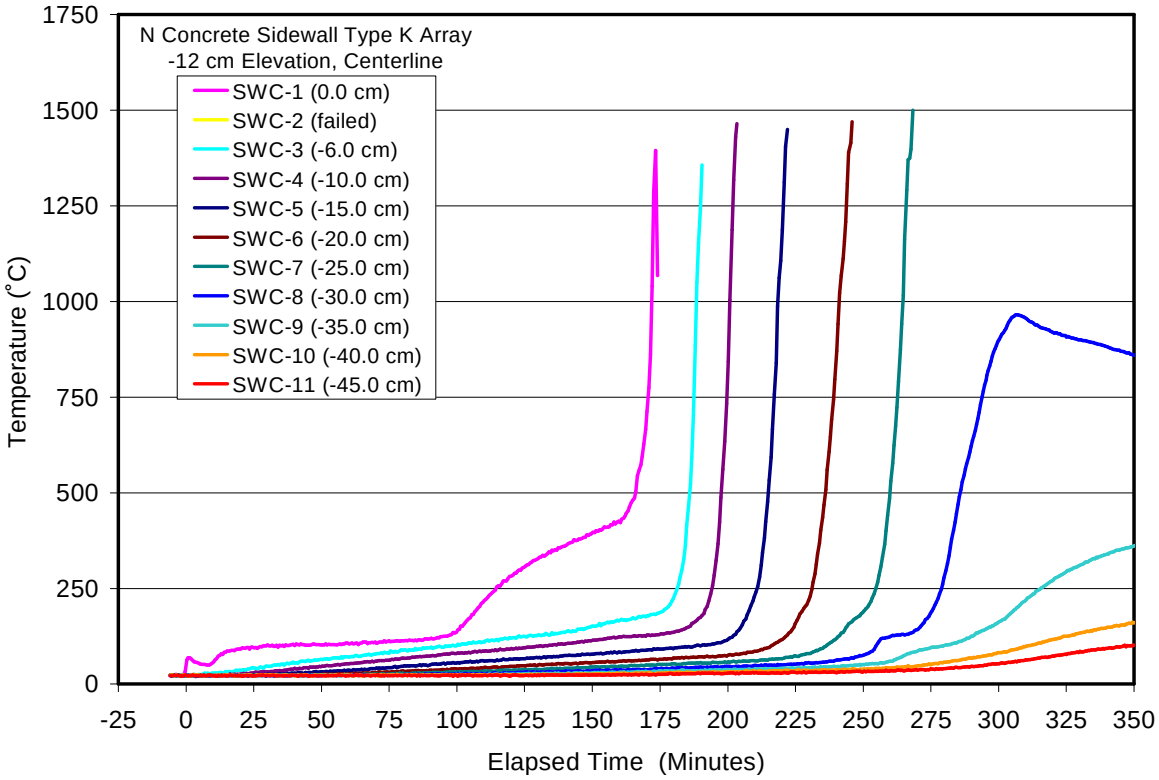

Figure B-16. North Sidewall Type K "SWC" Array Data.

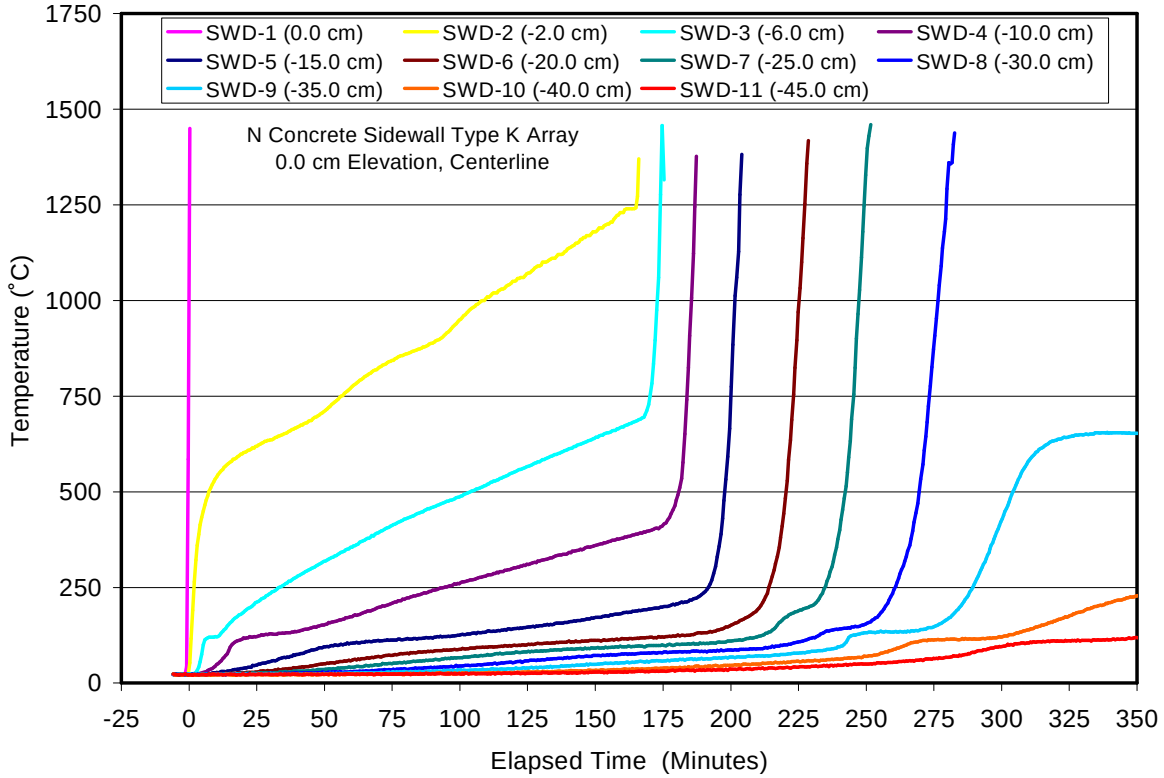

Figure B-17. North Sidewall Type K "SWD" Array Data.

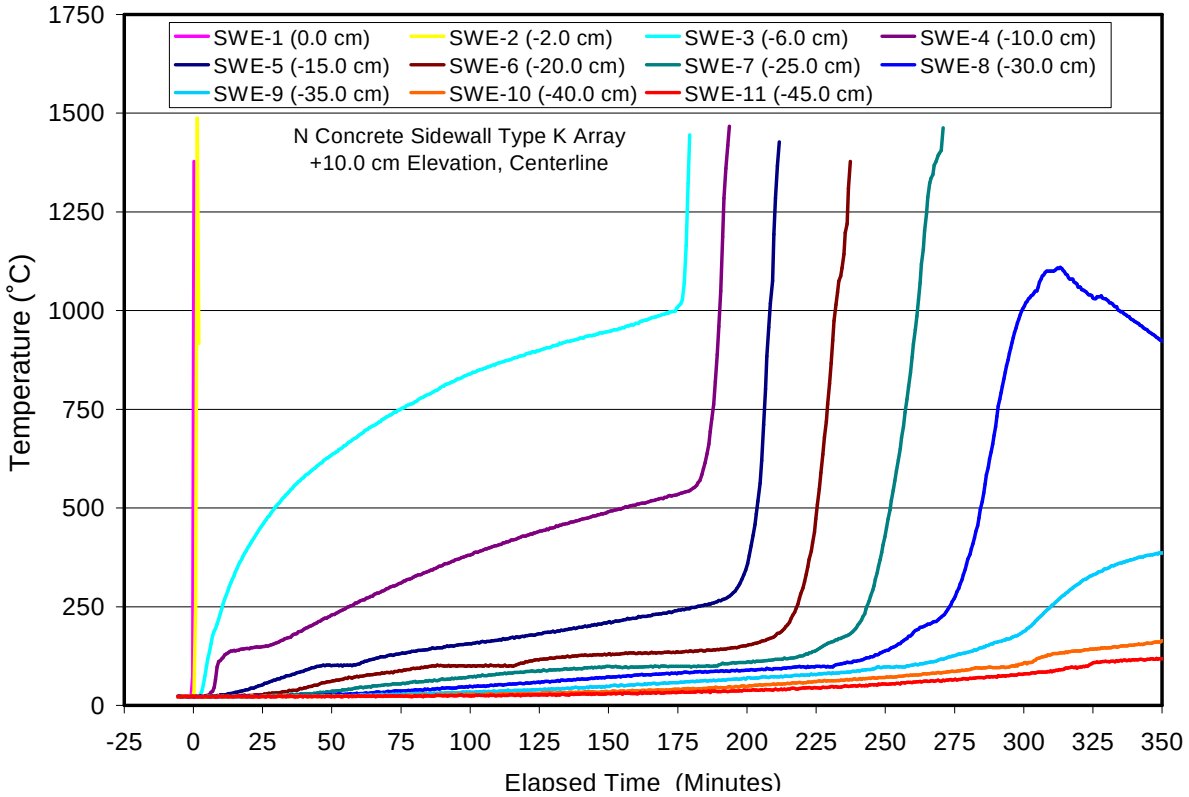

Figure B-18. North Sidewall Type K "SWE" Array Data.

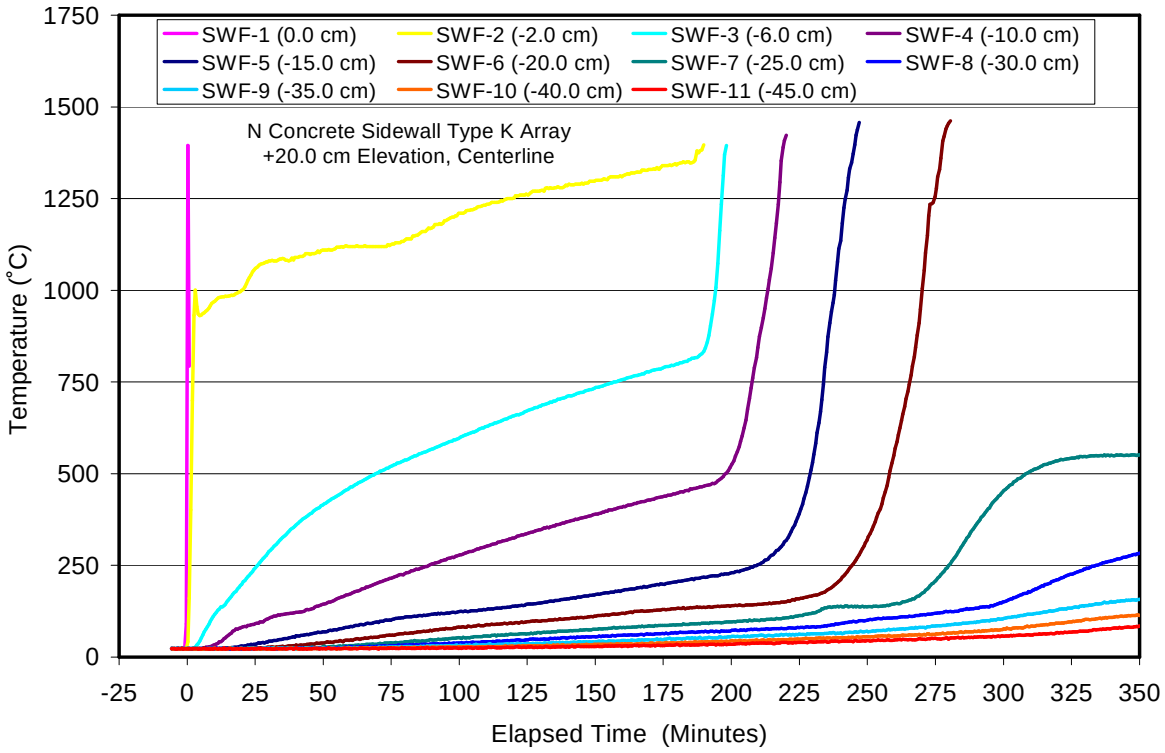

Figure B-19. North Sidewall Type K "SWF" Array Data.

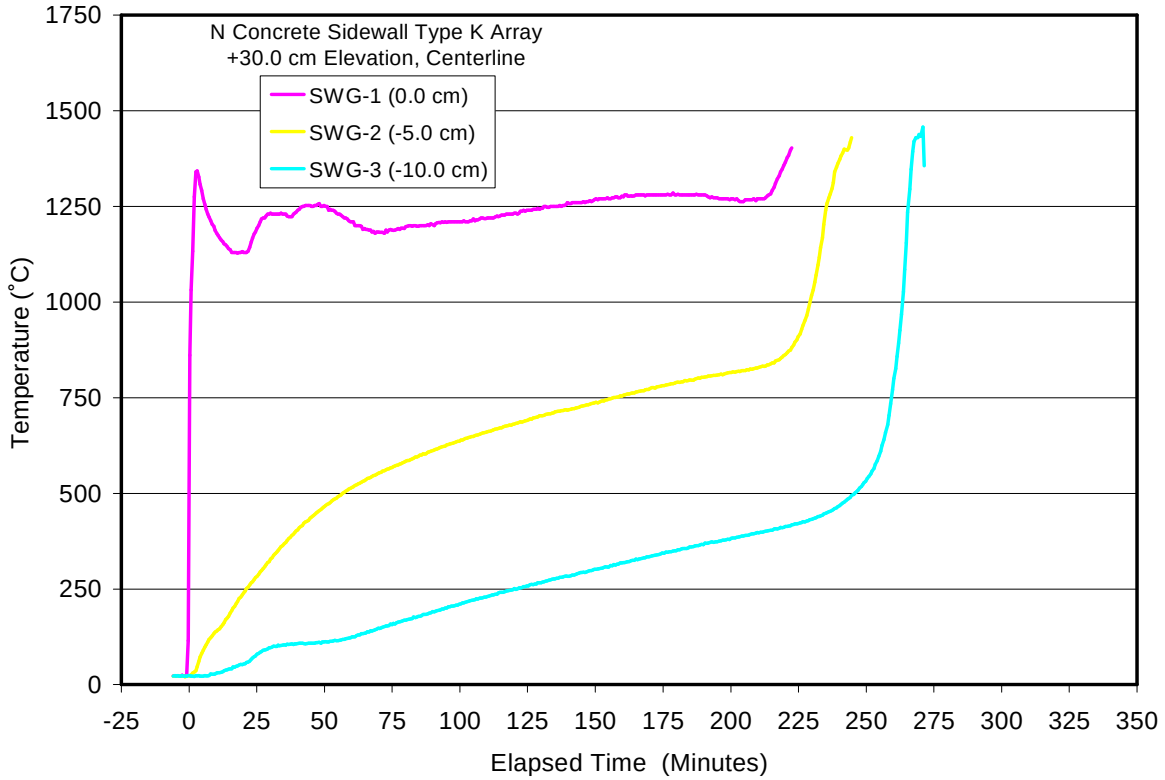

Figure B-20. North Sidewall Type K "SWG" Array Data.

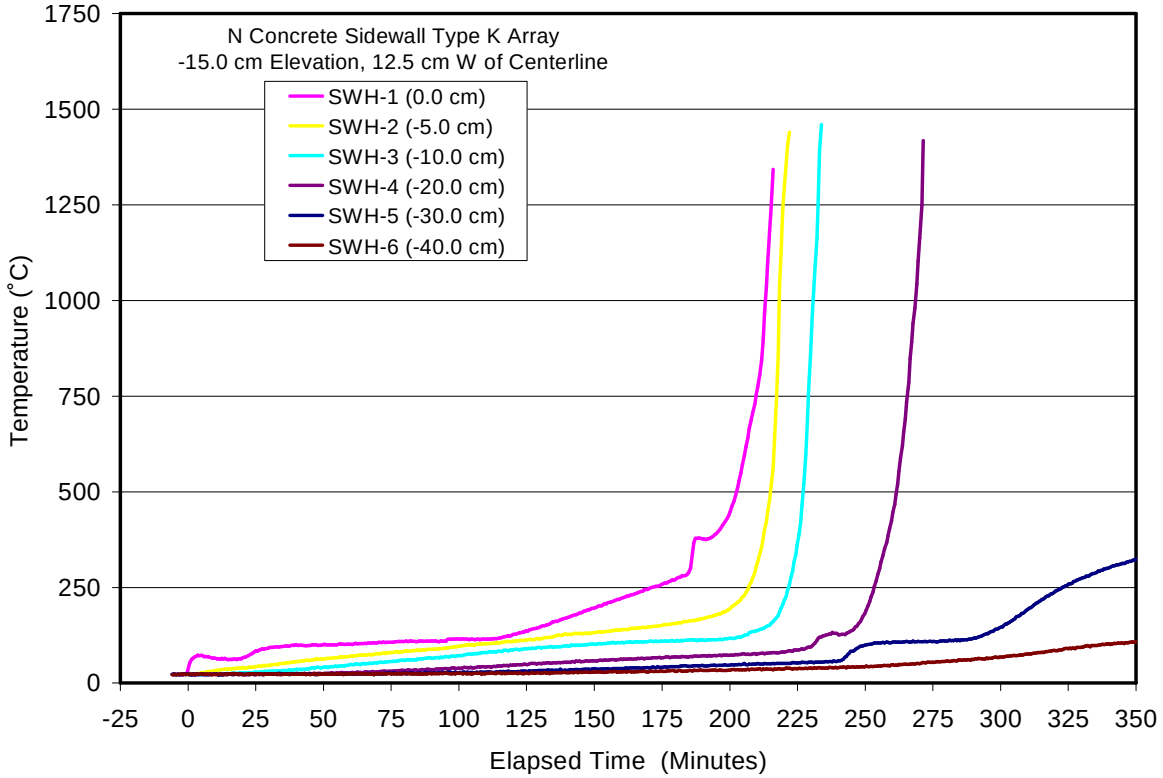

Figure B-21. North Sidewall Type K "SWH" Array Data.

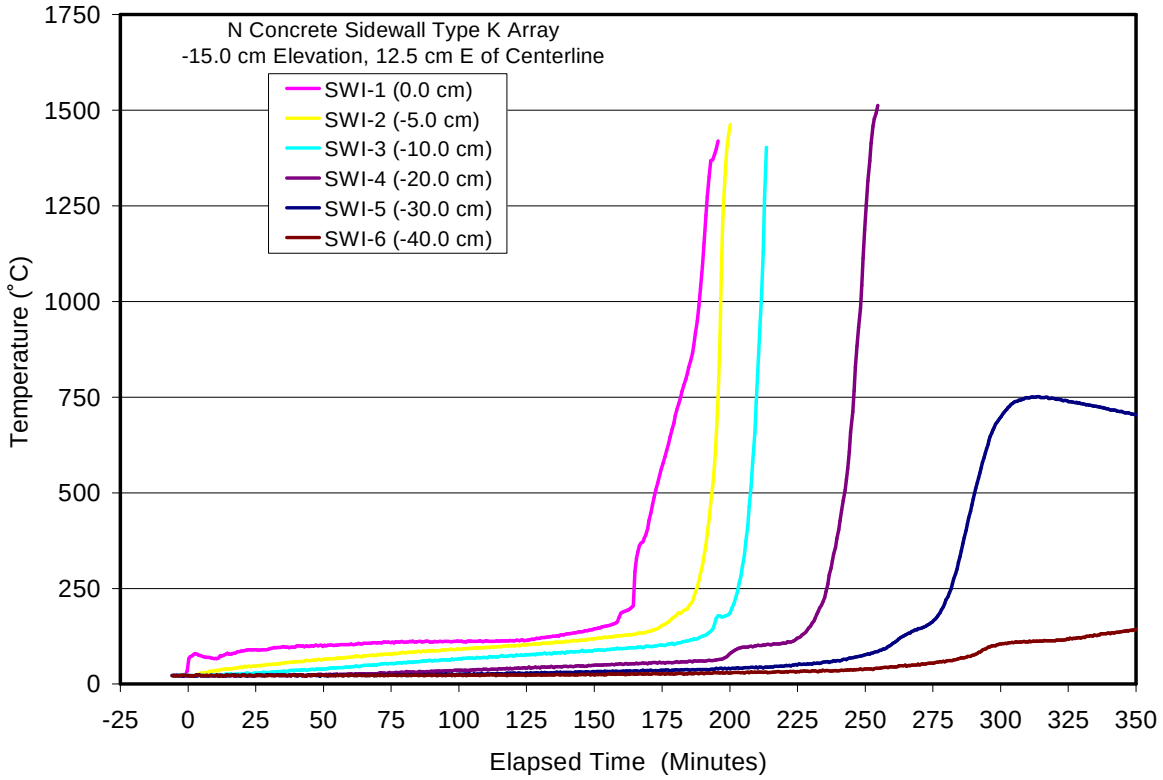

Figure B-22. North Sidewall Type K "SWI" Array Data.

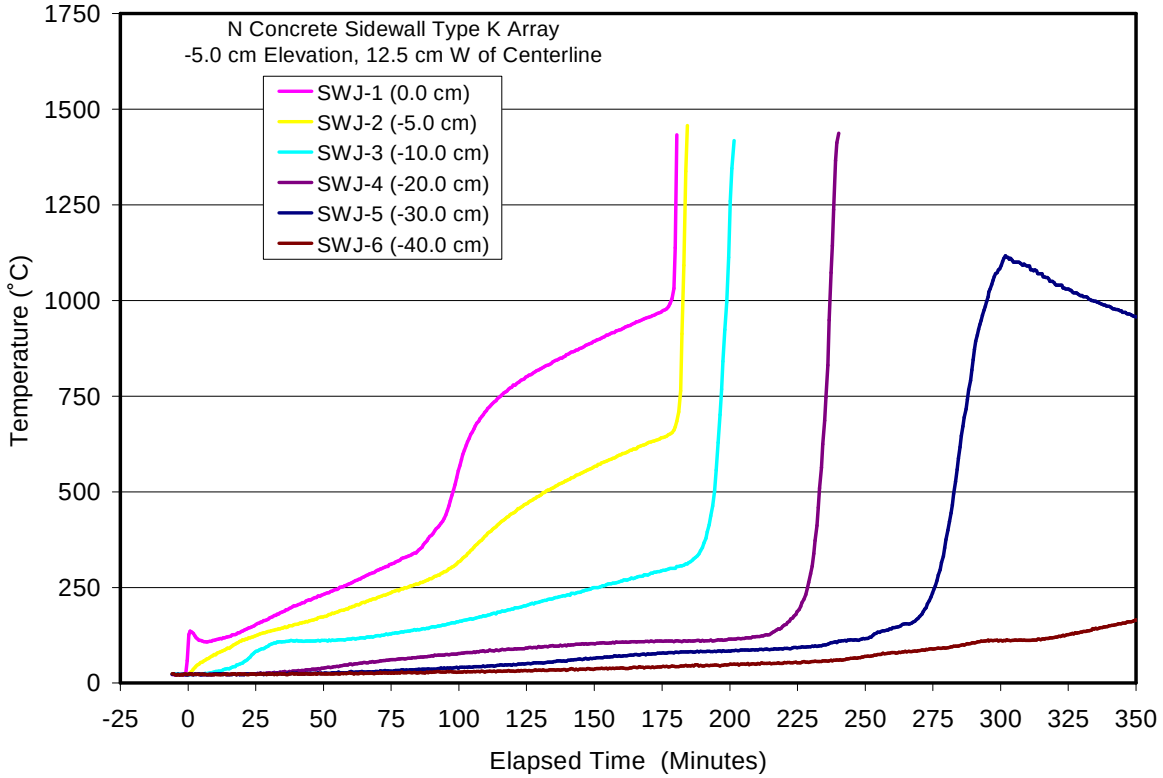

Figure B-23. North Sidewall Type K "SWJ" Array Data.

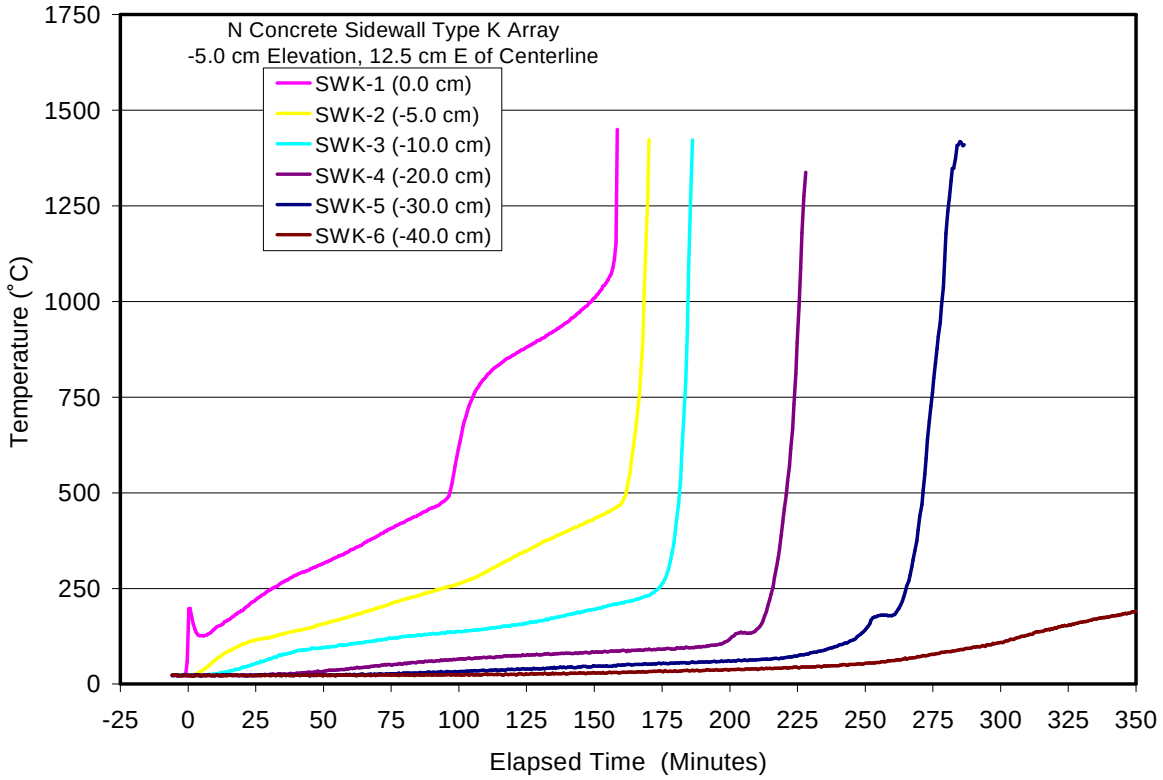

Figure B-24. North Sidewall Type K "SWK" Array Data.

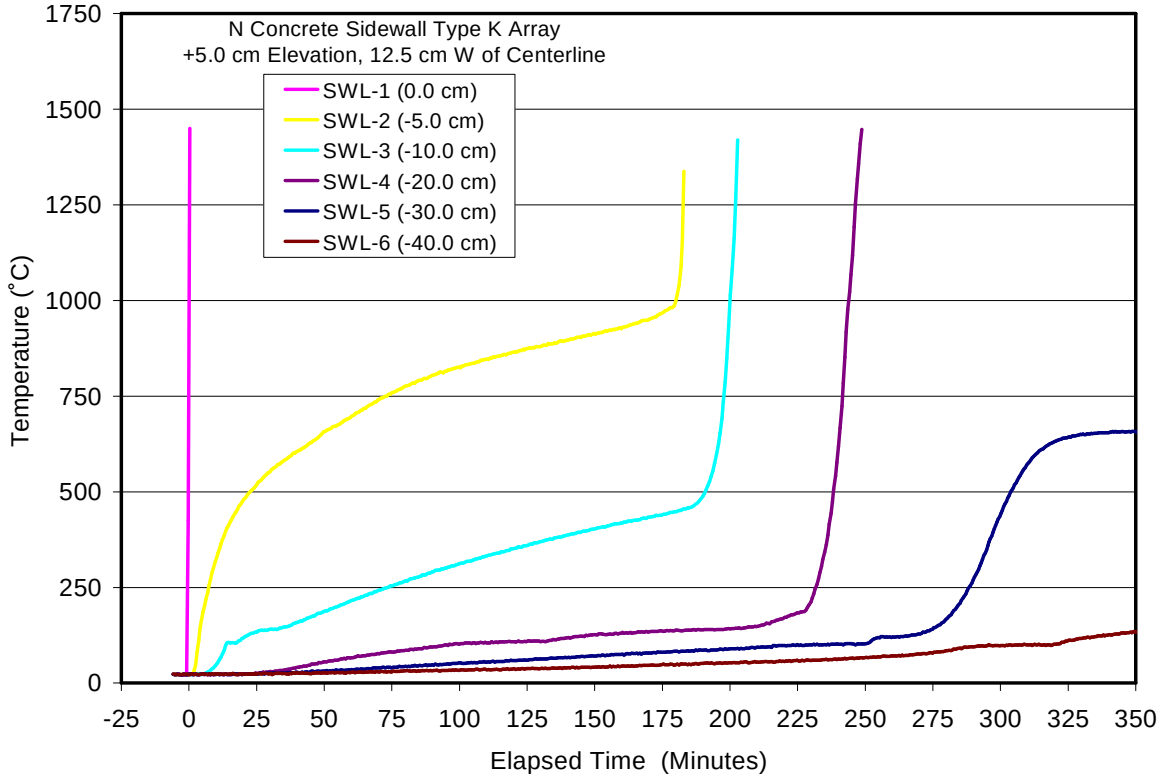

Figure B-25. North Sidewall Type K "SWL" Array Data.

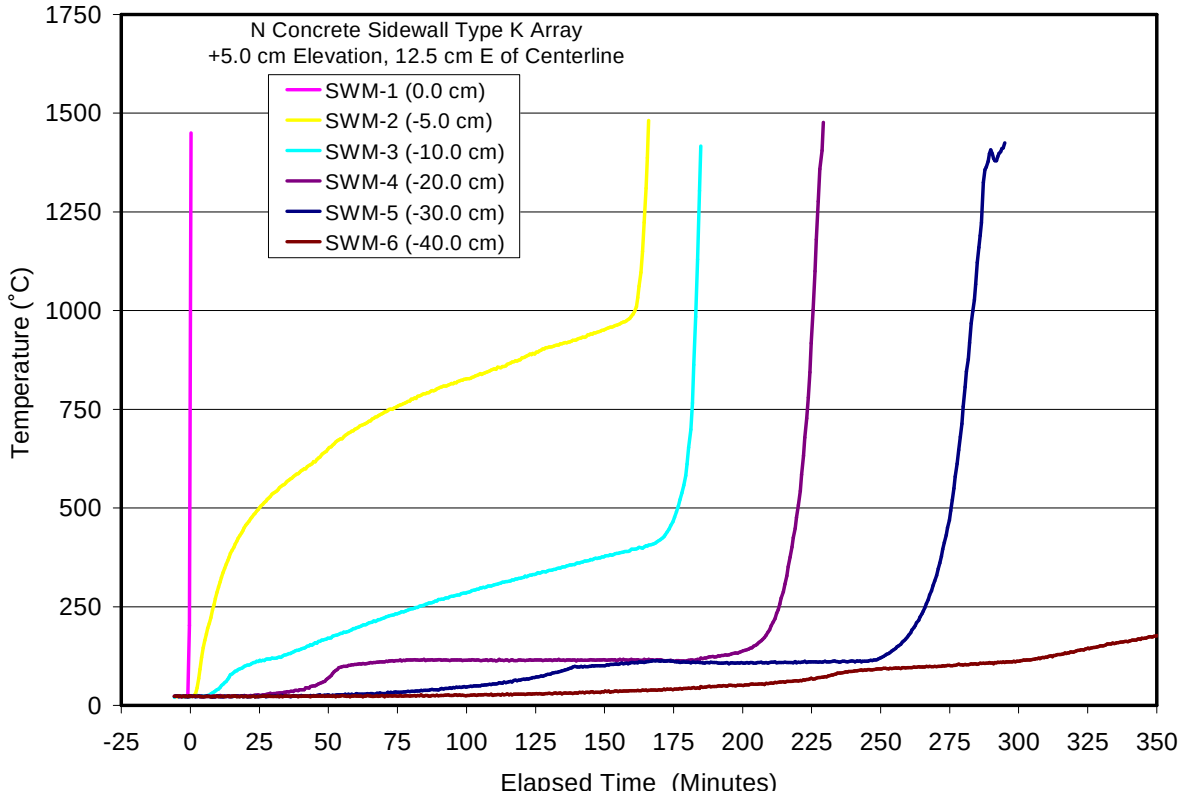

Figure B-26. North Sidewall Type K "SWM" Array Data.

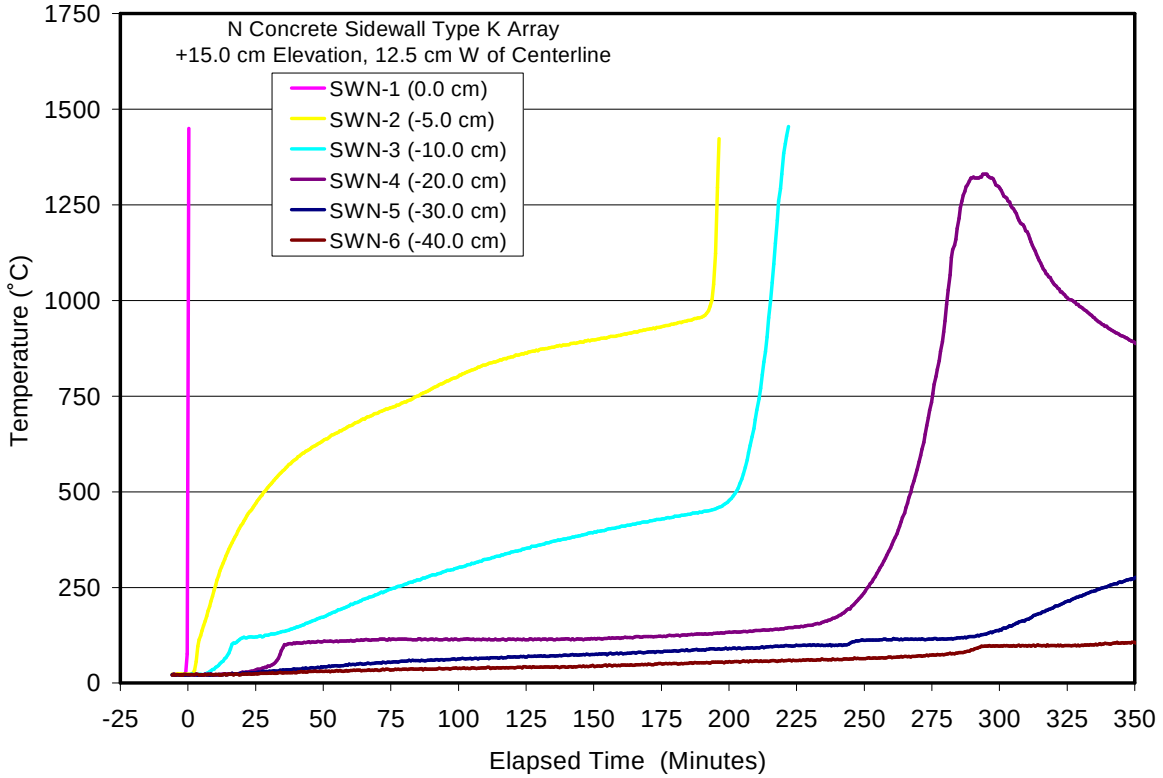

Figure B-27. North Sidewall Type K "SWN" Array Data.

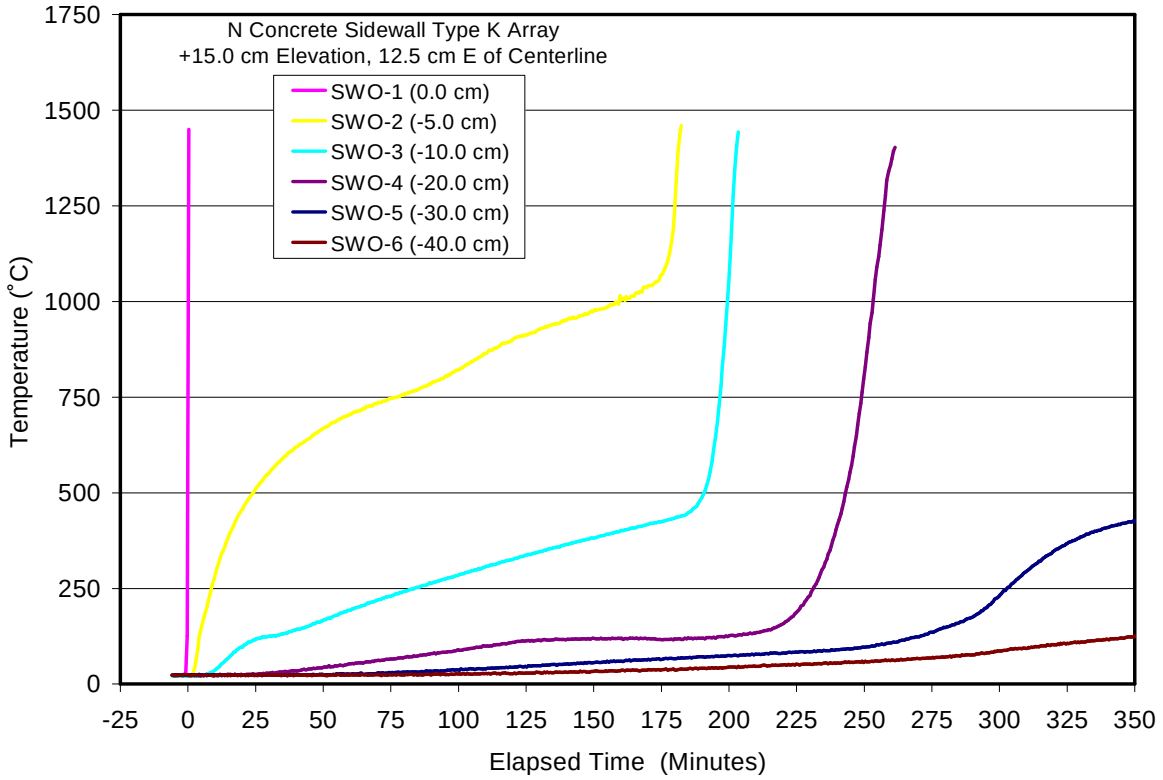

Figure B-28. North Sidewall Type K "SWO" Array Data.

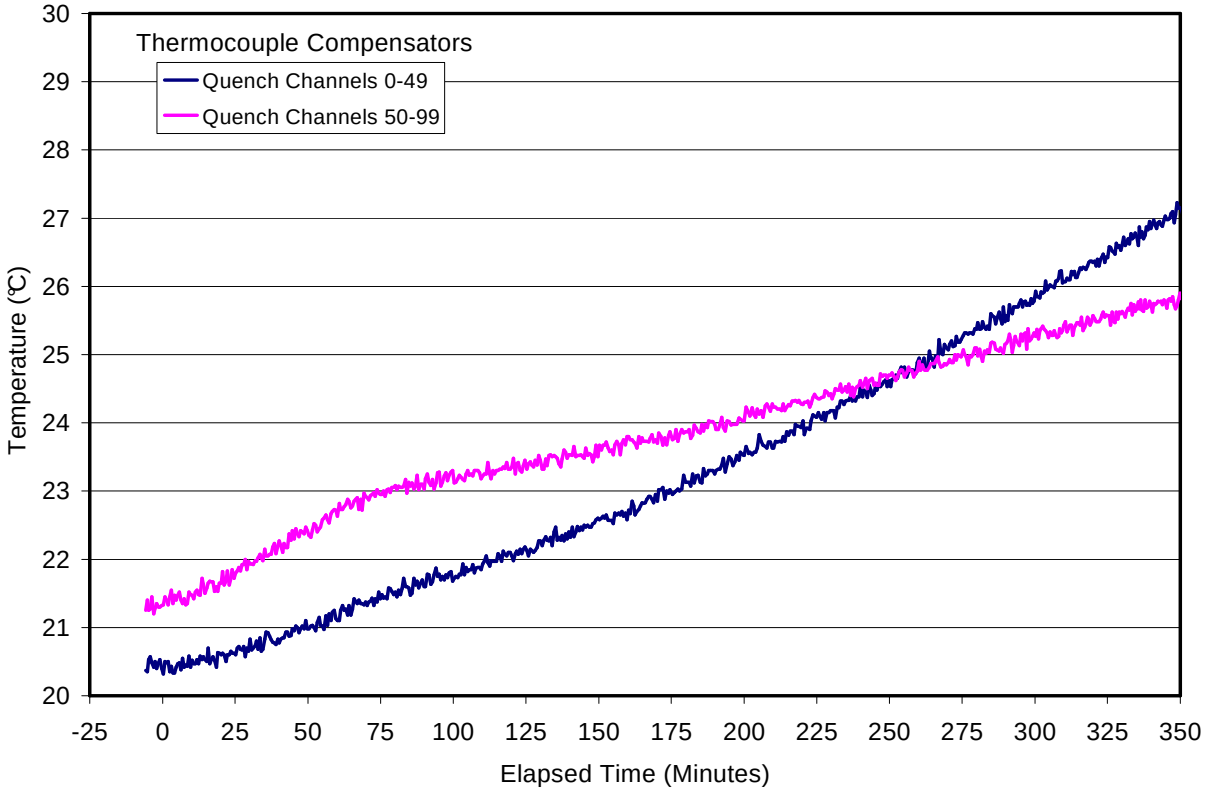

Figure B-29. Thermocouple Compensator Data for Channels Q0-Q49 and Q50-Q99.

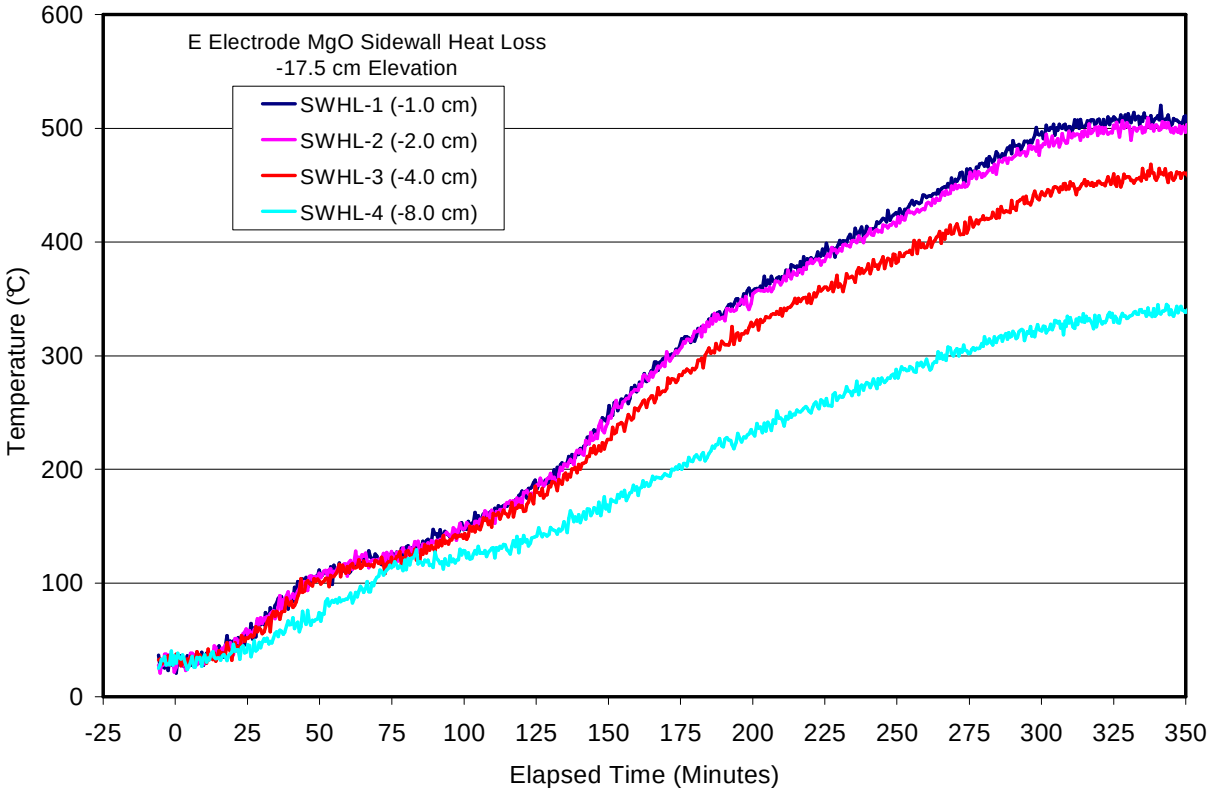

Figure B-30. Test Section Sidewall Heat Loss Data at -17.5 cm Elevation.

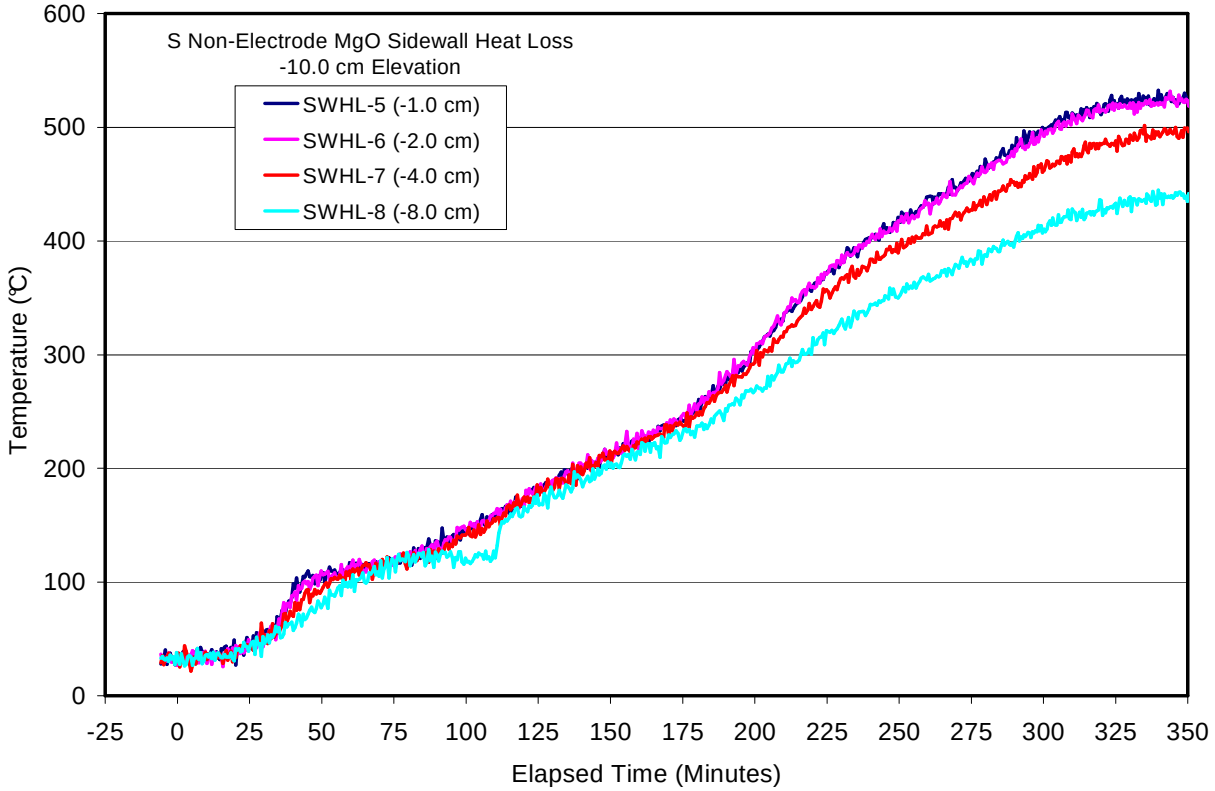

Figure B-31. Test Section Sidewall Heat Loss Data at -10.0 cm Elevation.

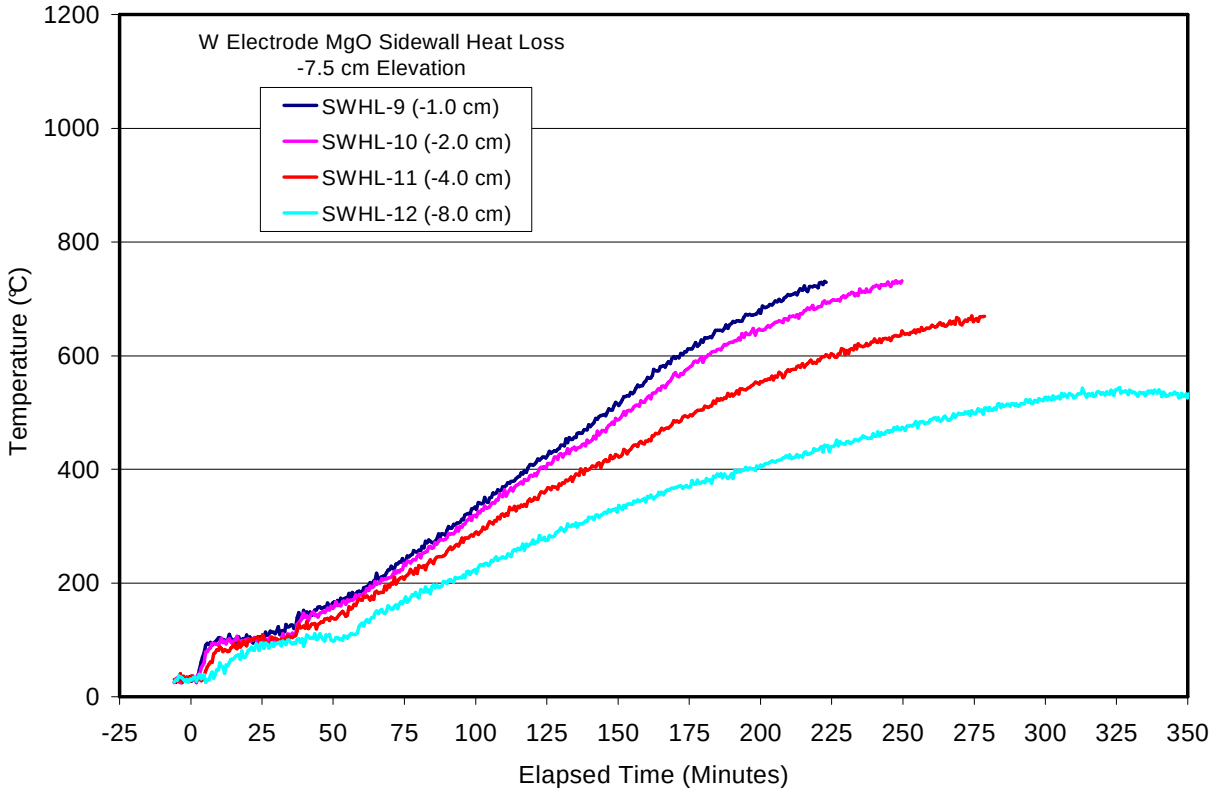

Figure B-32. Test Section Sidewall Heat Loss Data at -7.5 cm Elevation.

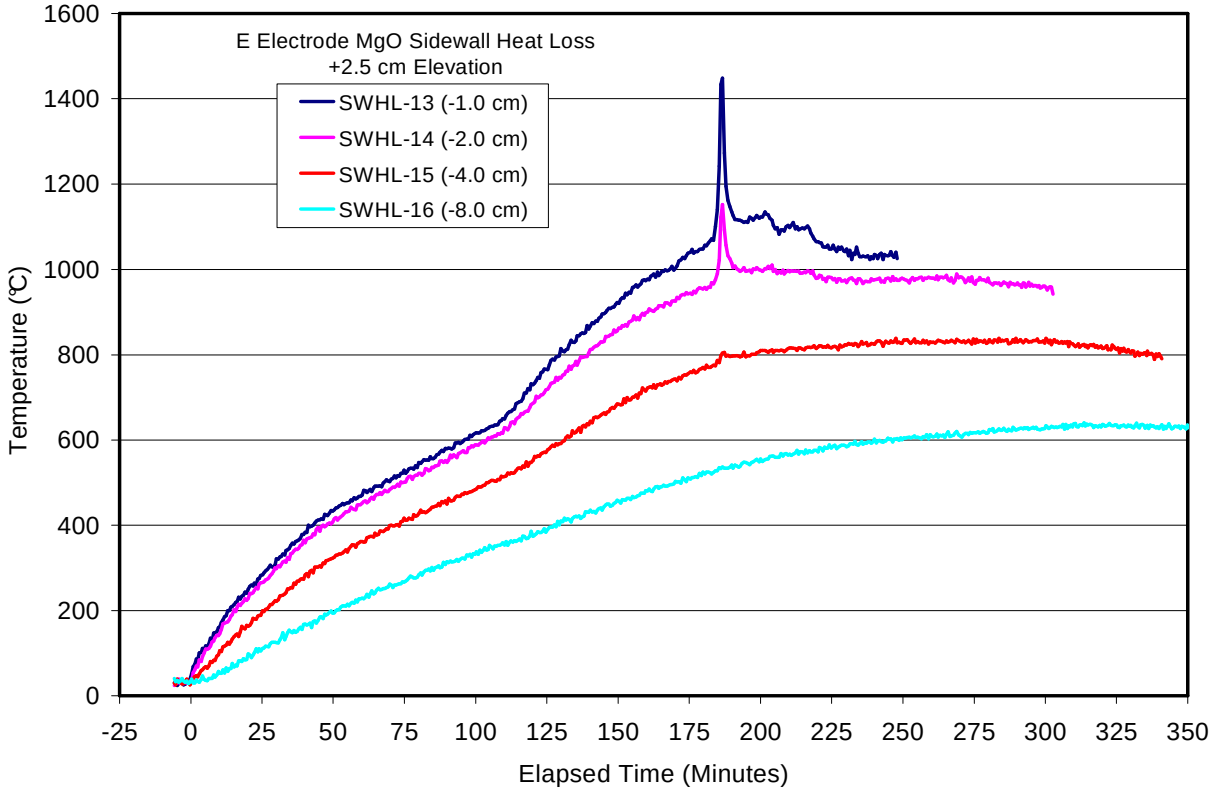

Figure B-33. Test Section Sidewall Heat Loss Data at +2.5 cm Elevation.

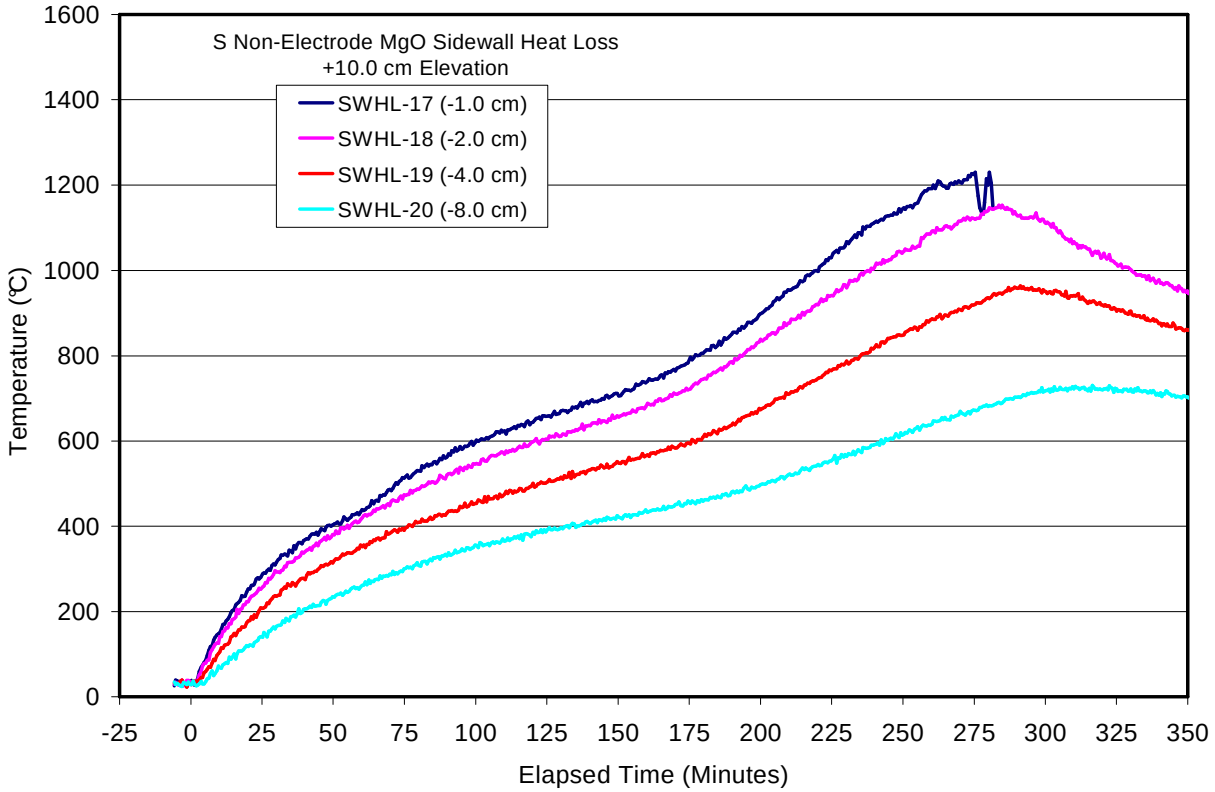

Figure B-34. Test Section Sidewall Heat Loss Data at +10.0 cm Elevation.

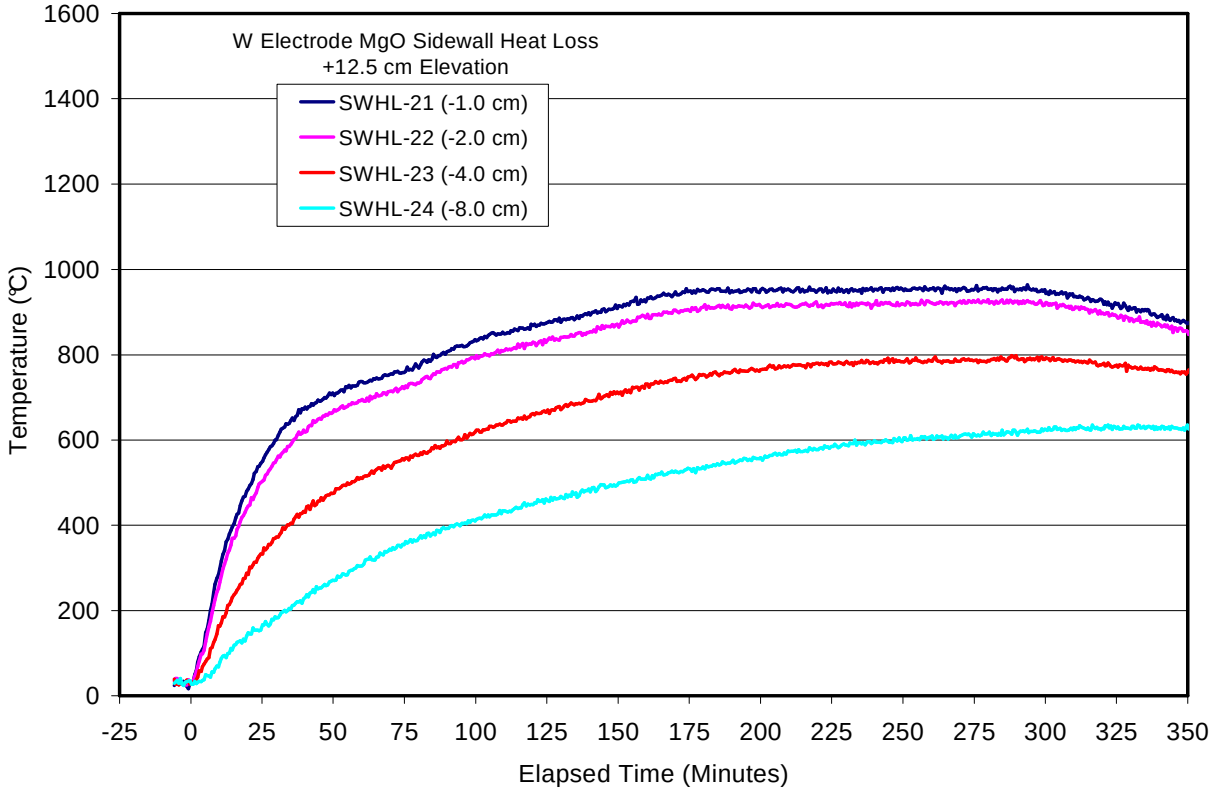

Figure B-35. Test Section Sidewall Heat Loss Data at +12.5 cm Elevation.

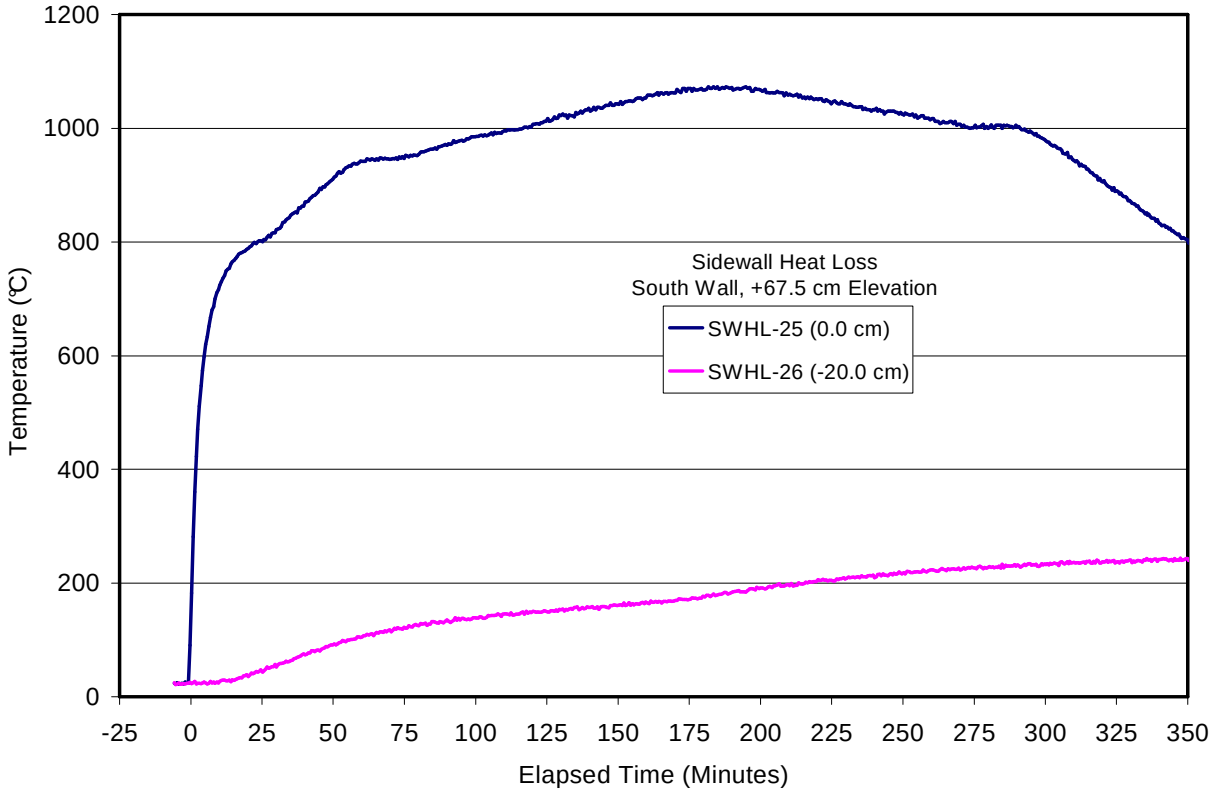

Figure B-36. Test Section Sidewall Heat Loss Data at the +67.5 cm Elevation.

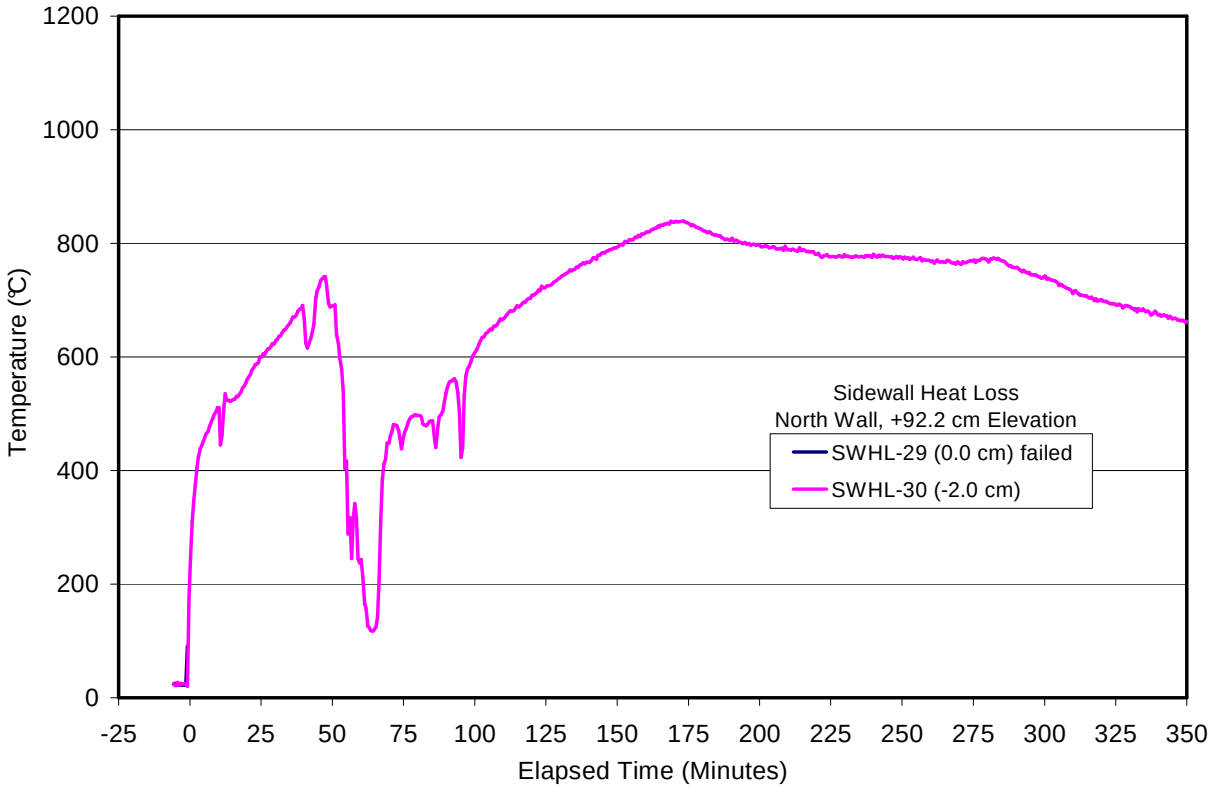

Figure B-37. Test Section Sidewall Heat Loss Data at the + 92.2 cm Elevation.

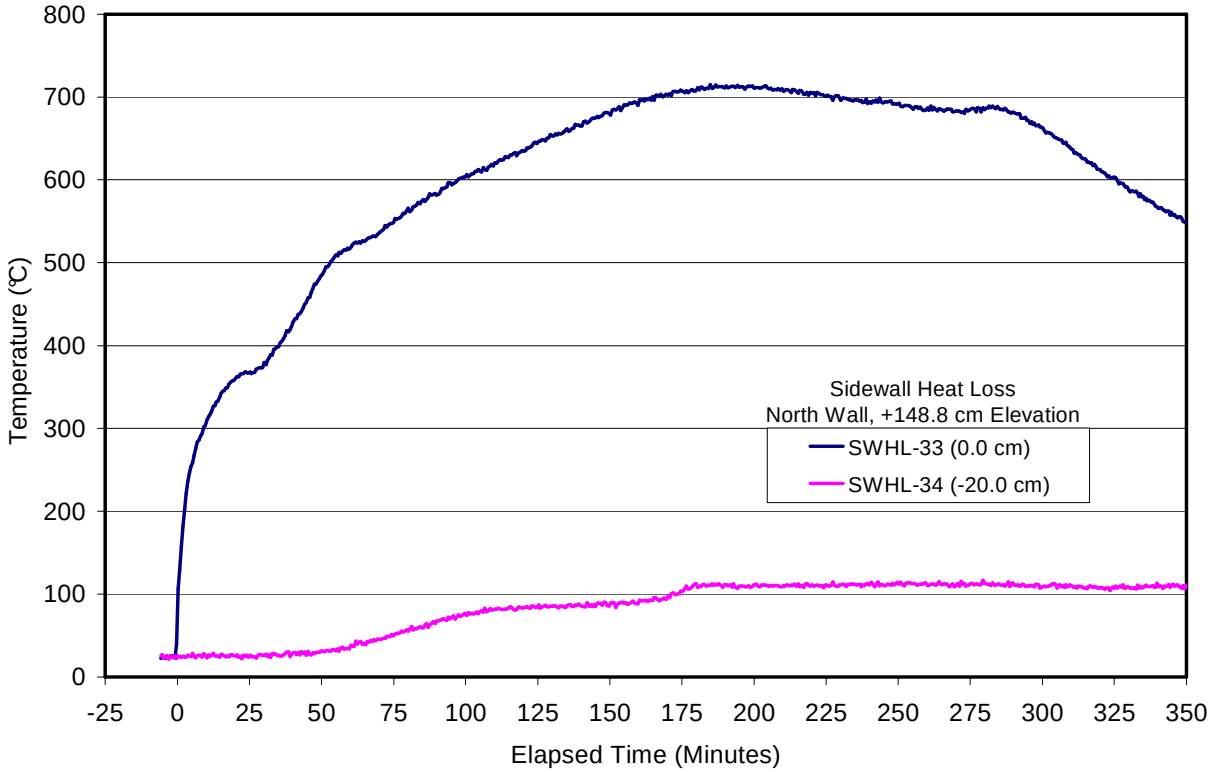

Figure B-38. Test Section Sidewall Heat Loss Data at the + 148.8 cm Elevation.

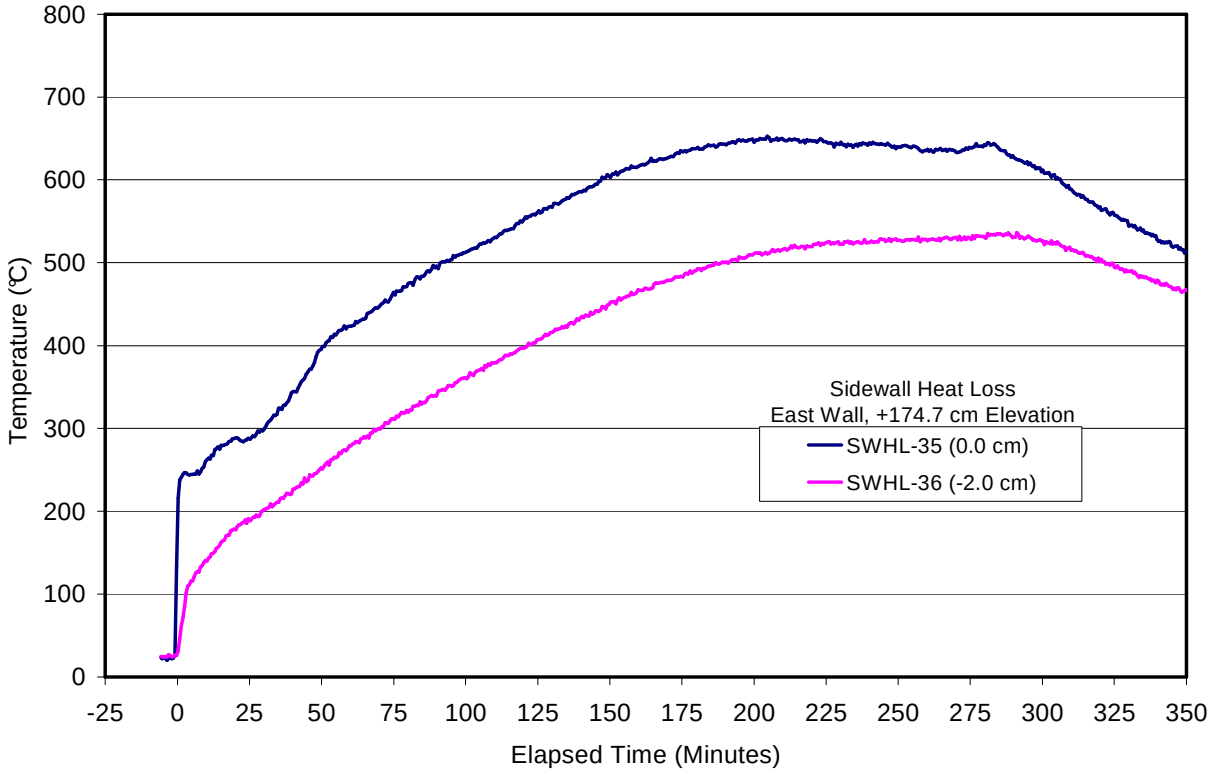

Figure B-39. Test Section Sidewall Heat Loss Data at the + 174.7 cm Elevation.

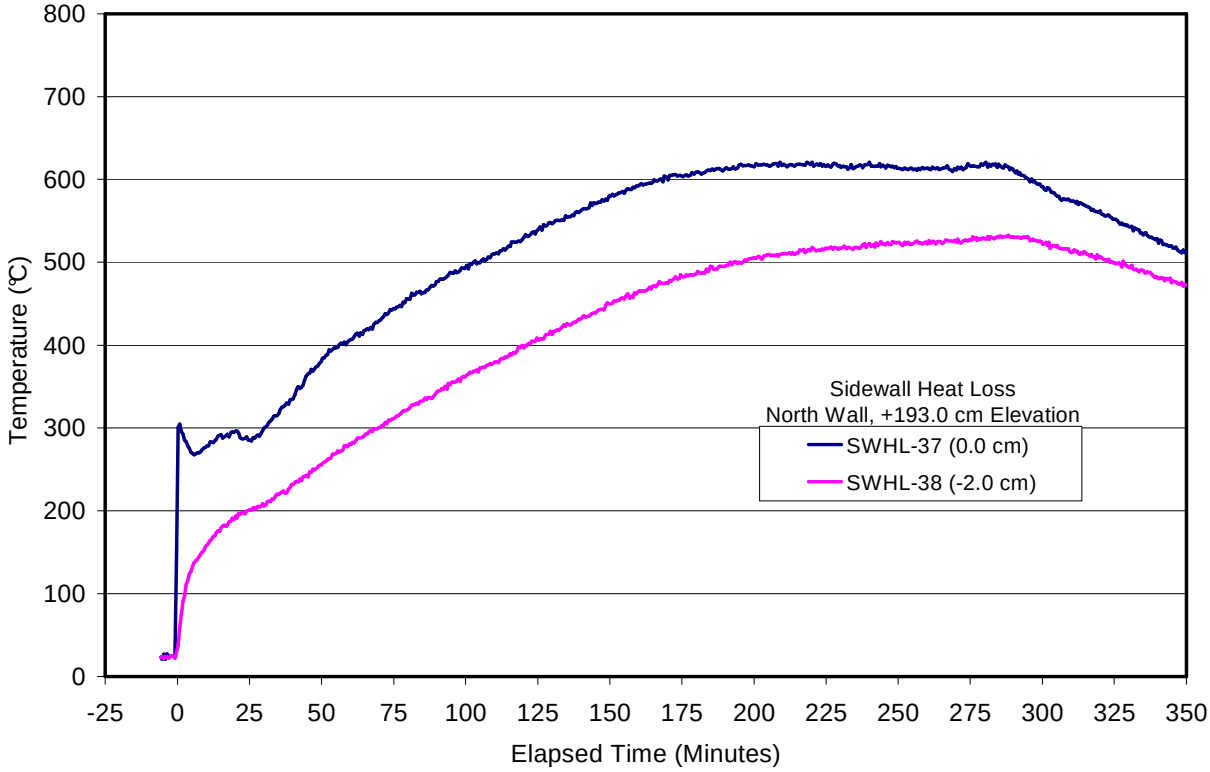

Figure B-40. Test Section Sidewall Heat Loss Data at the + 193.0 cm Elevation.

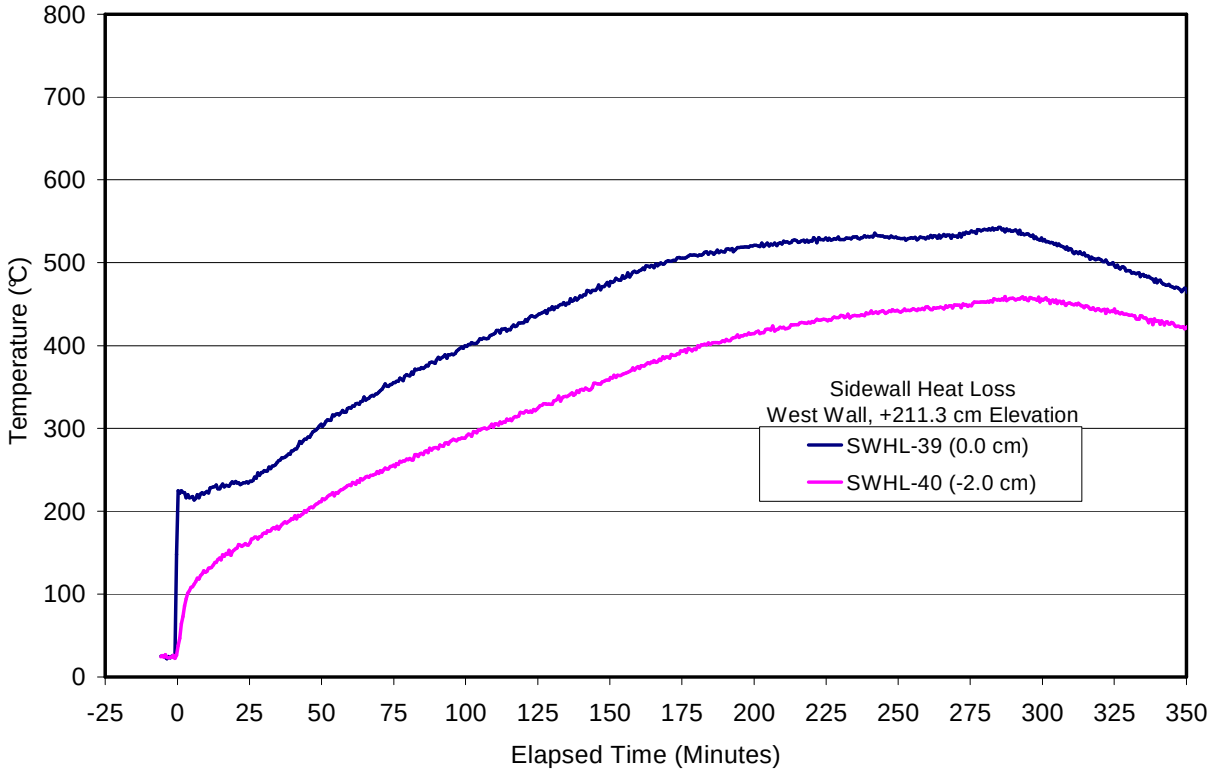

Figure B-41. Test Section Sidewall Heat Loss Data at the + 211.3 cm Elevation.

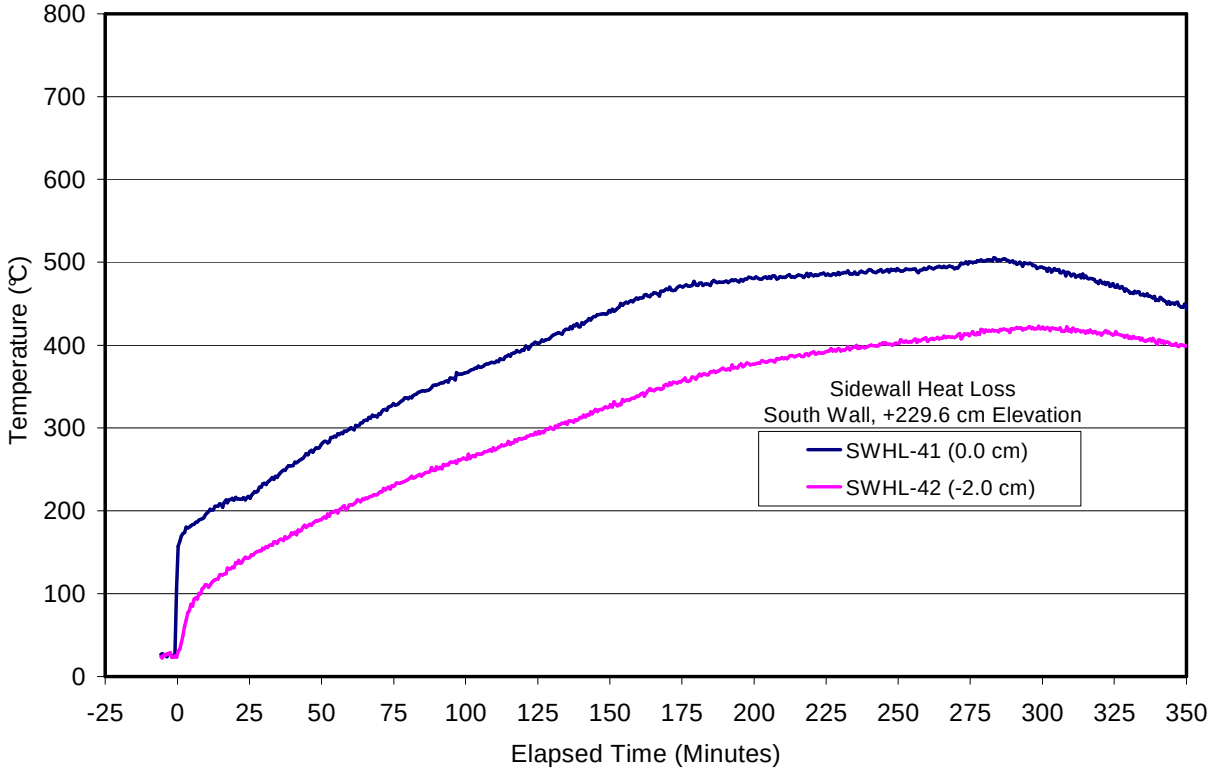

Figure B-42. Test Section Sidewall Heat Loss Data at the + 229.6 cm Elevation.

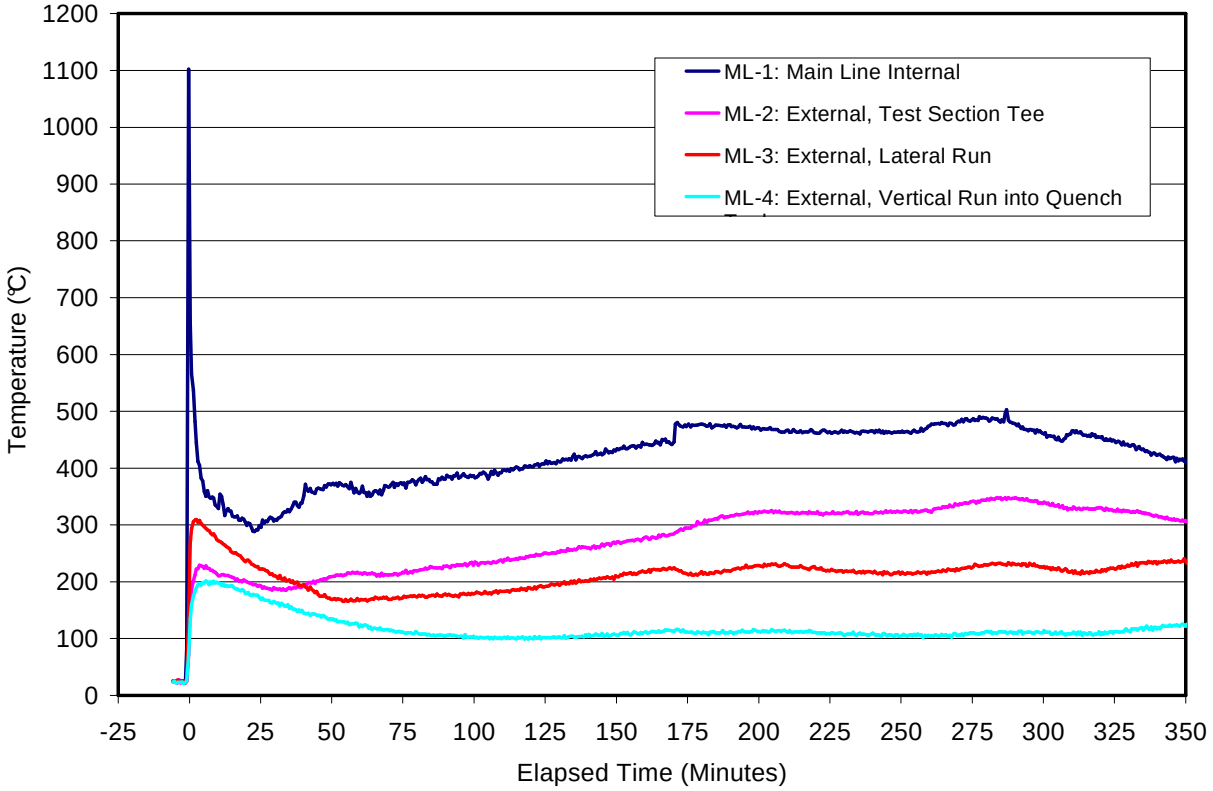

Figure B-43. Test Section Mainline Thermocouple Data.

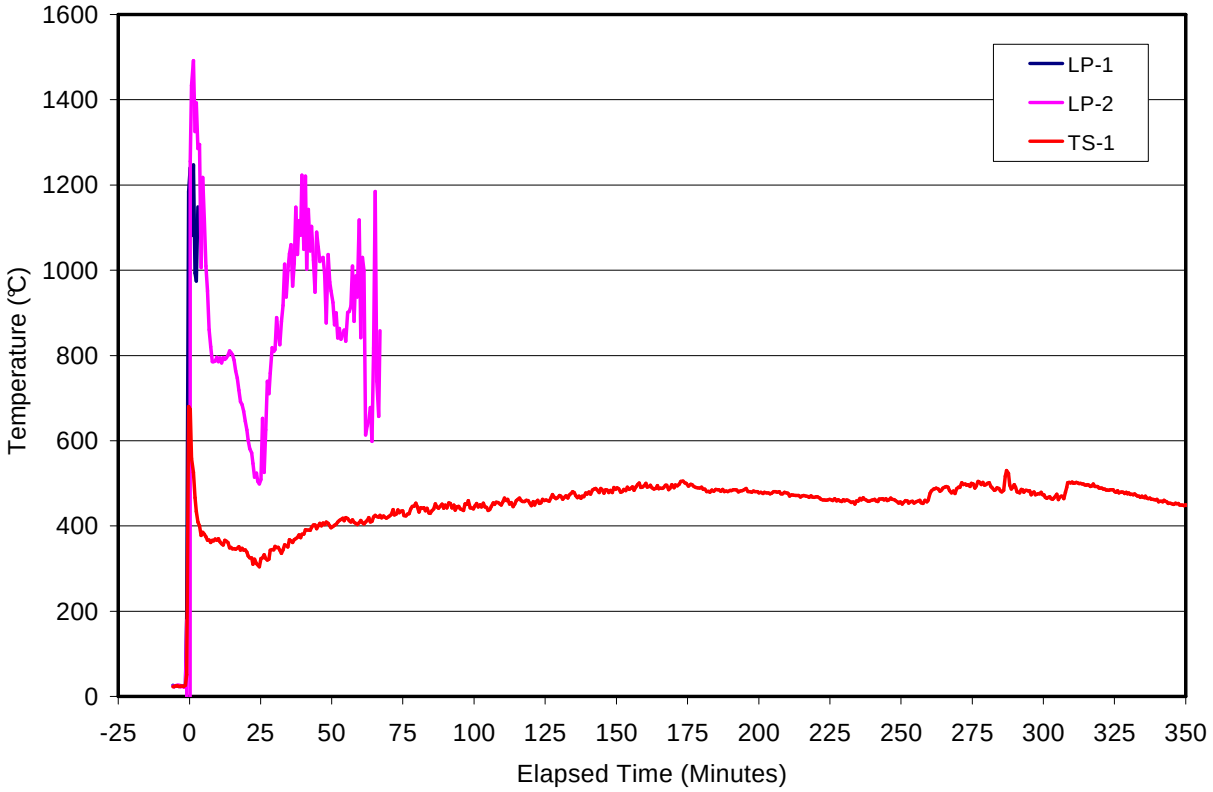

Figure B-44. Test Section Plenum and Insertable Water Probe Thermocouple Data.

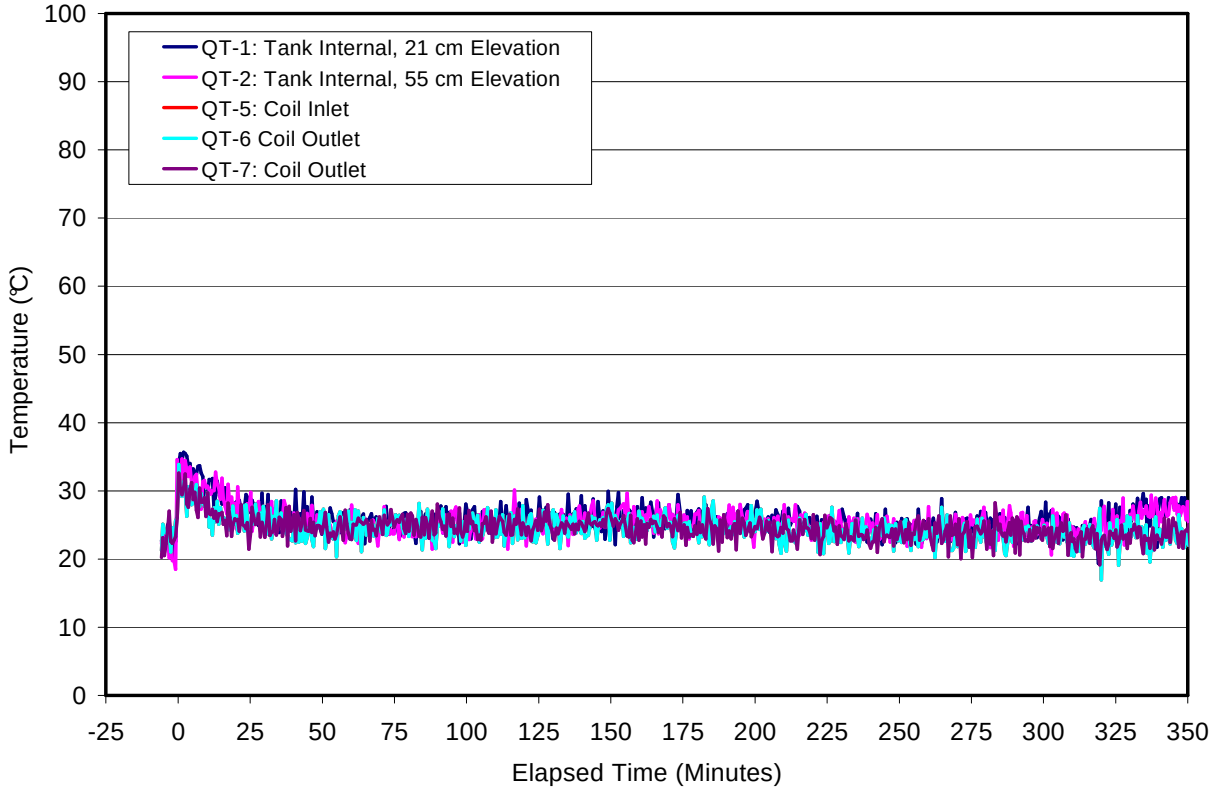

Figure B-45. Quench Tank Water Volume, Coil Inlet, and Coil Outlet Temperatures.

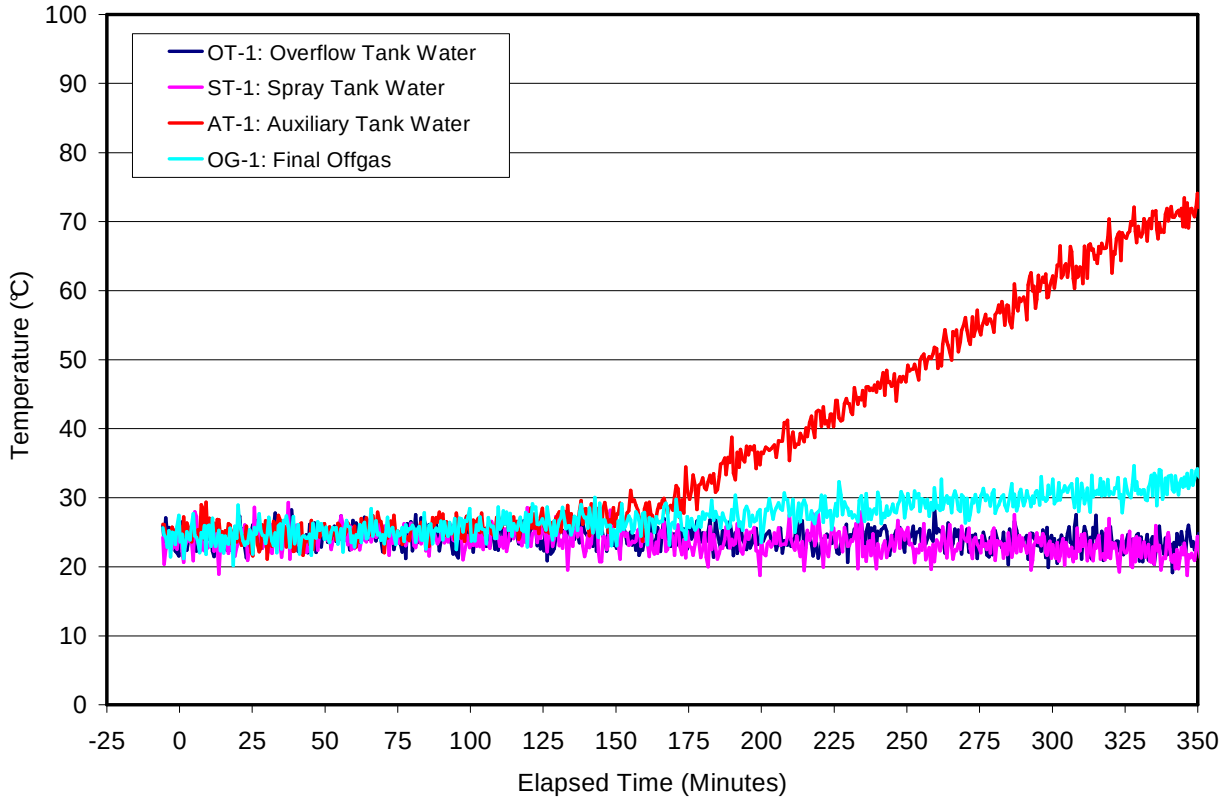

Figure B-46. Temperatures in Water Supply, Quench, and Off Gas Systems.

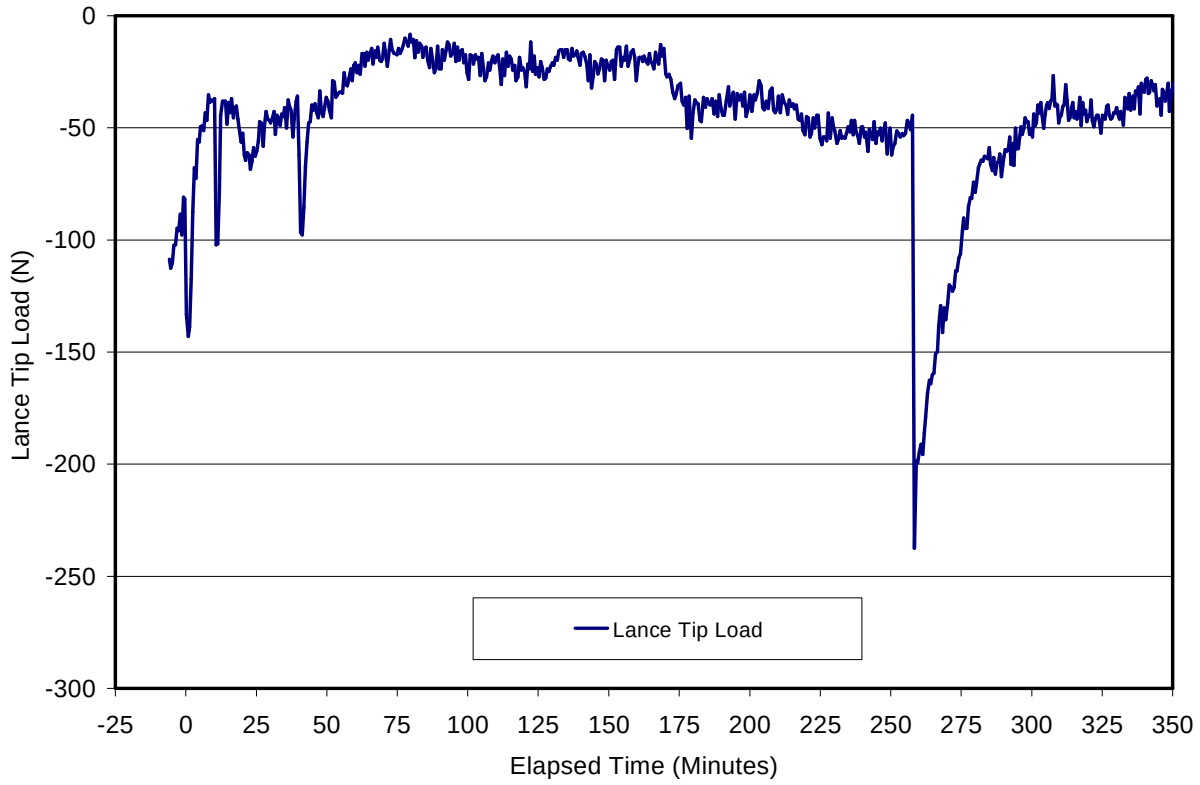

Figure B-47. Crust Lance Load Cell Data.

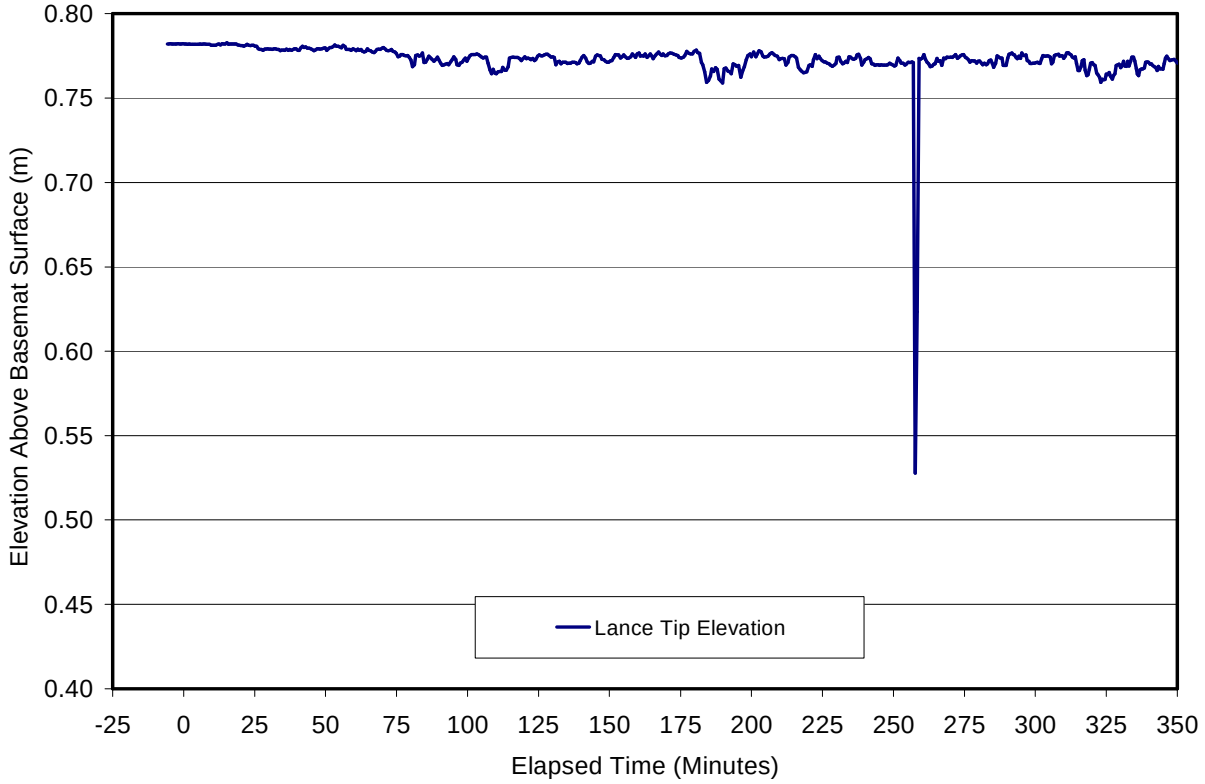

Figure B-48. Lance Position Indicator Data.

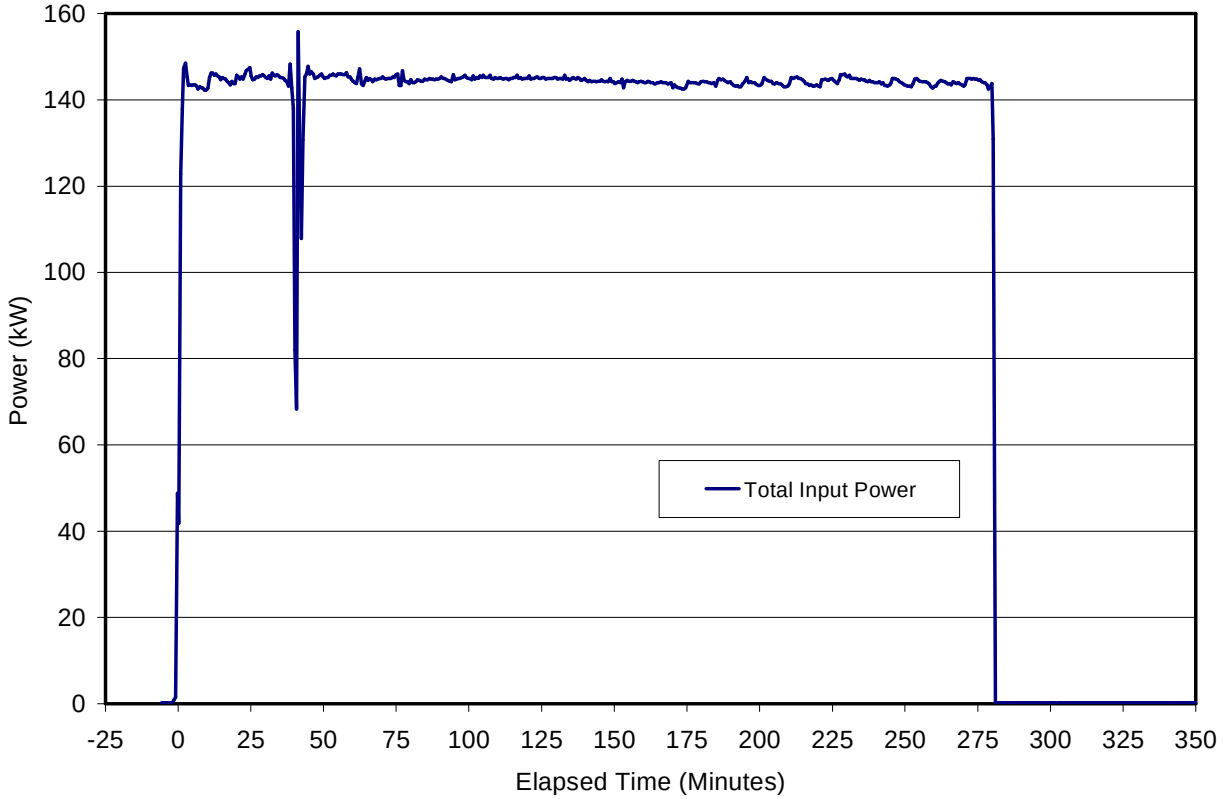

Figure B-49. Total Power Supply Power.

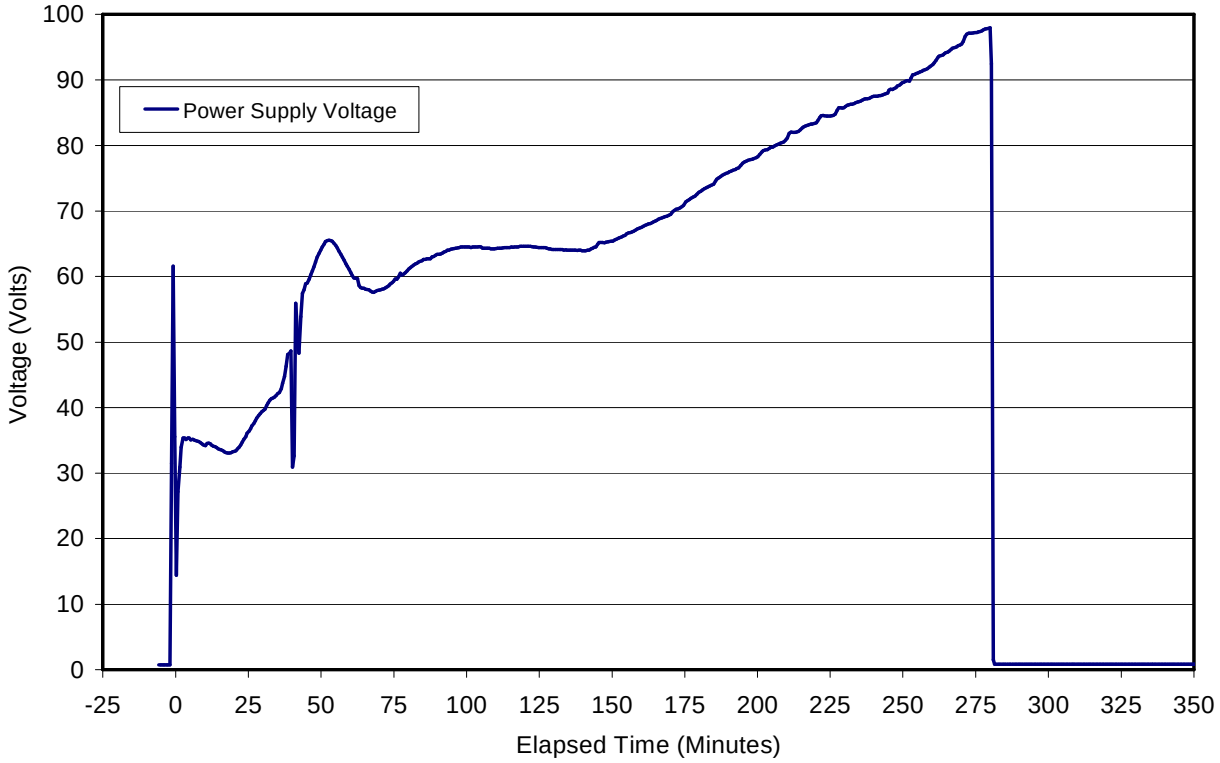

Figure B-50 Power Supply Voltage Data.

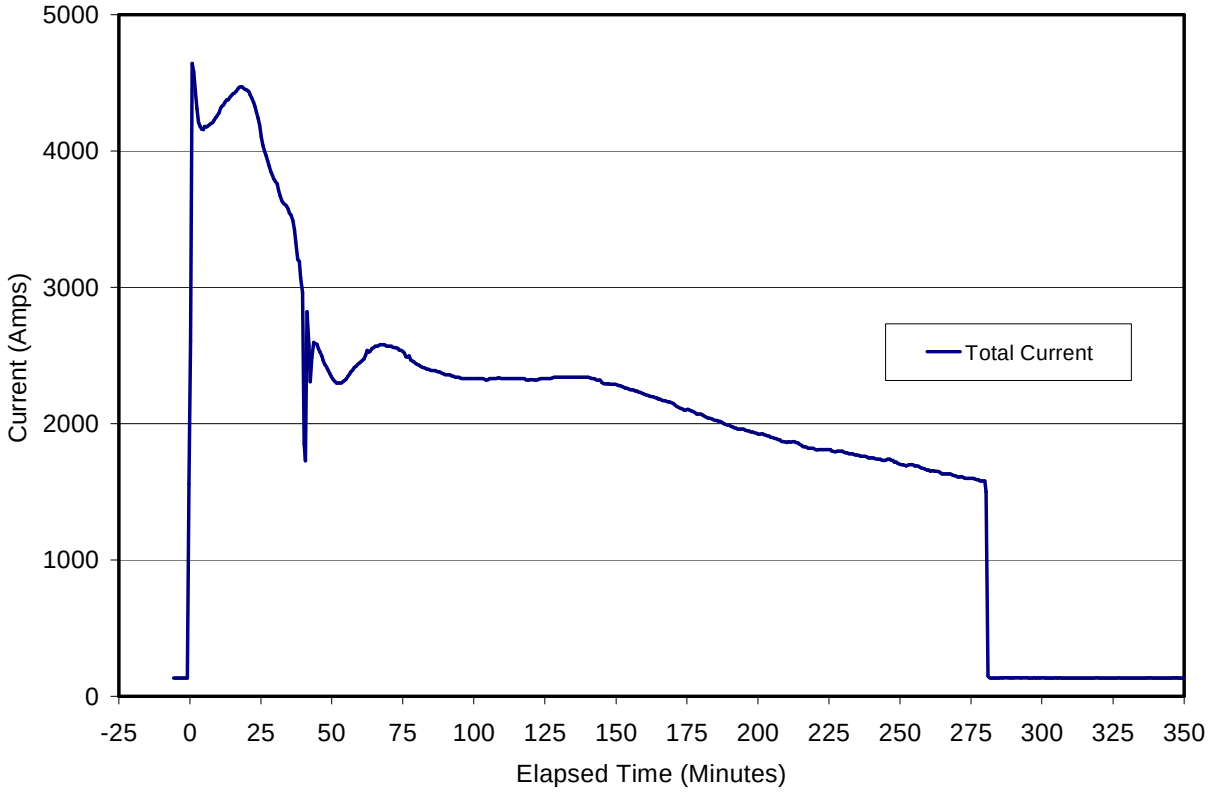

Figure B-51. Total Power Supply Current Data.

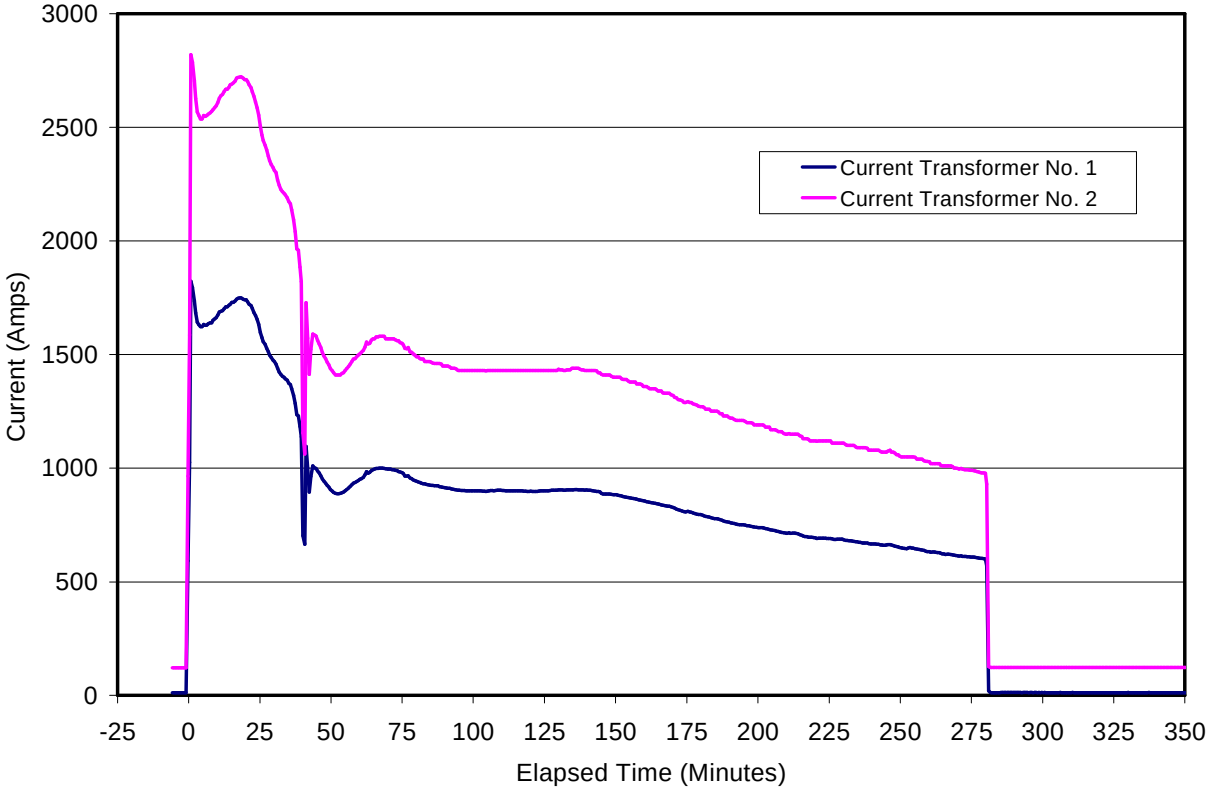

Figure B-52. Power Supply Current Transformer Data.

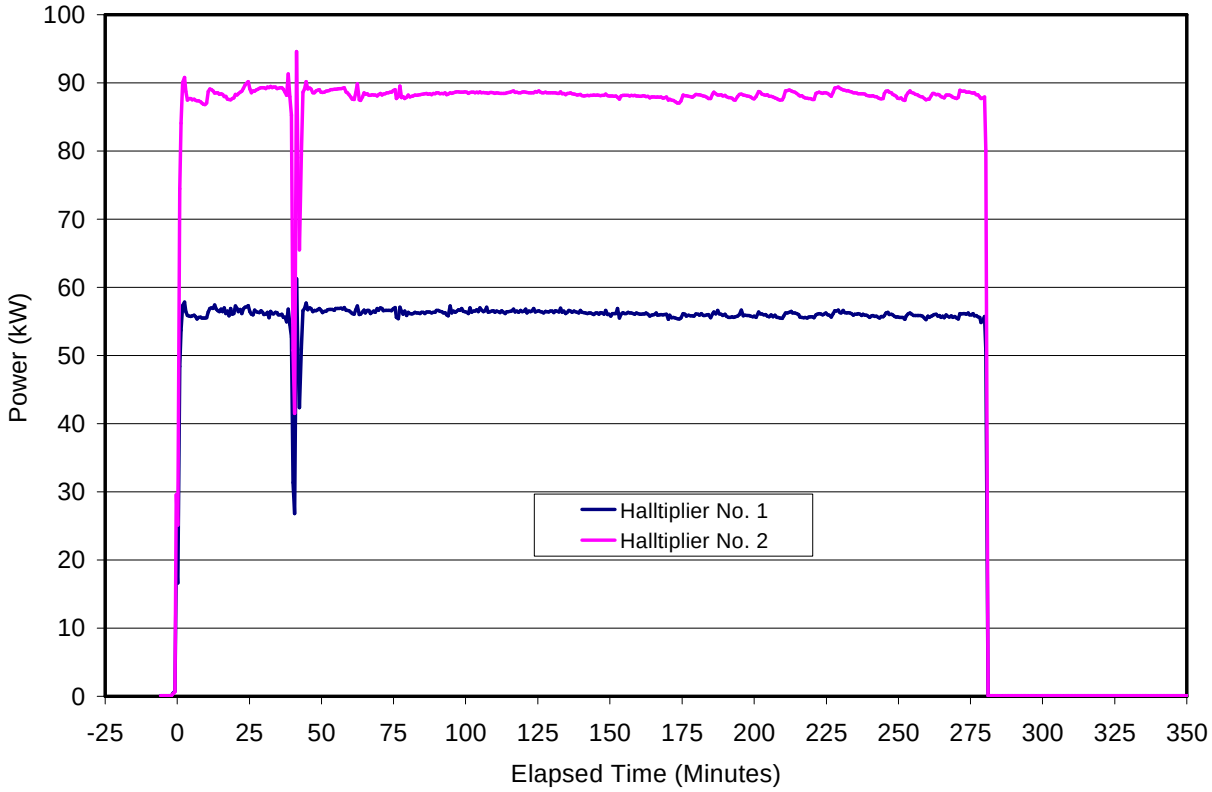

Figure B-53. Hall Effect Meter Data.

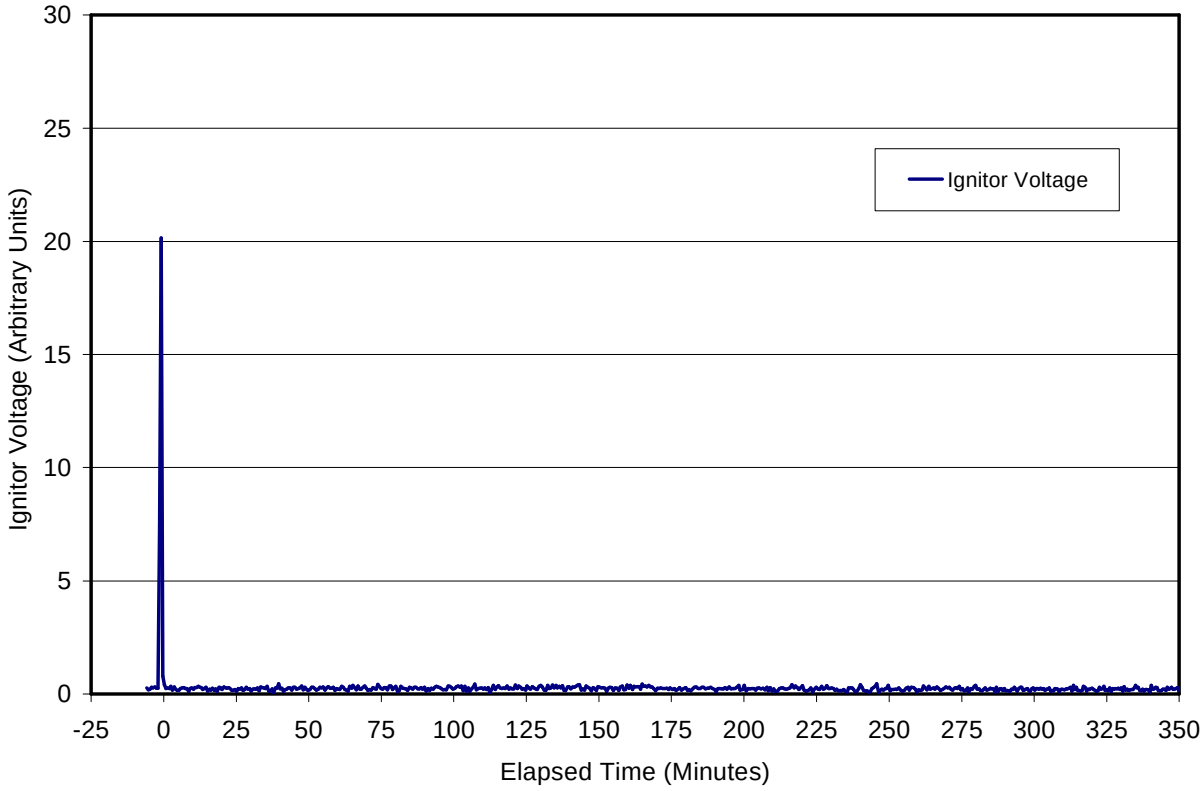

Figure B-54. Voltage across Igniter Shunt.

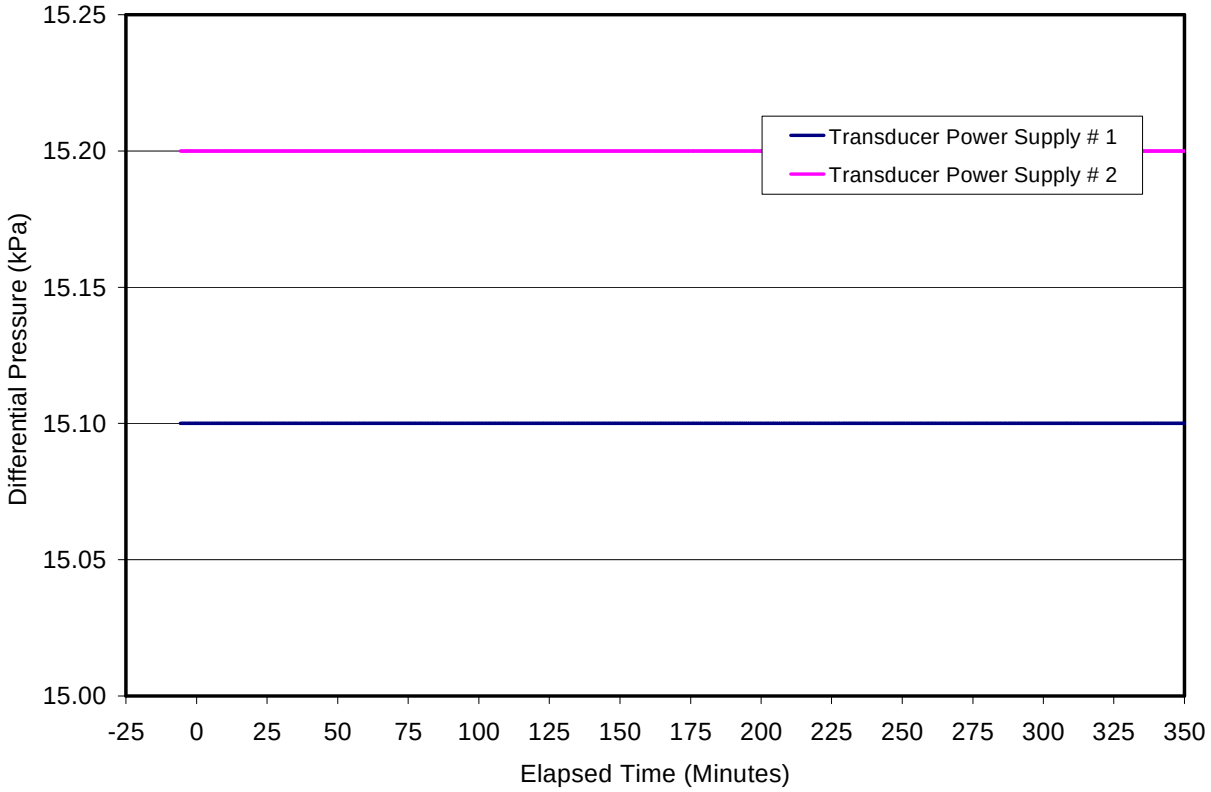

Figure B-55. Pressure Transducer Power Supply Voltages.

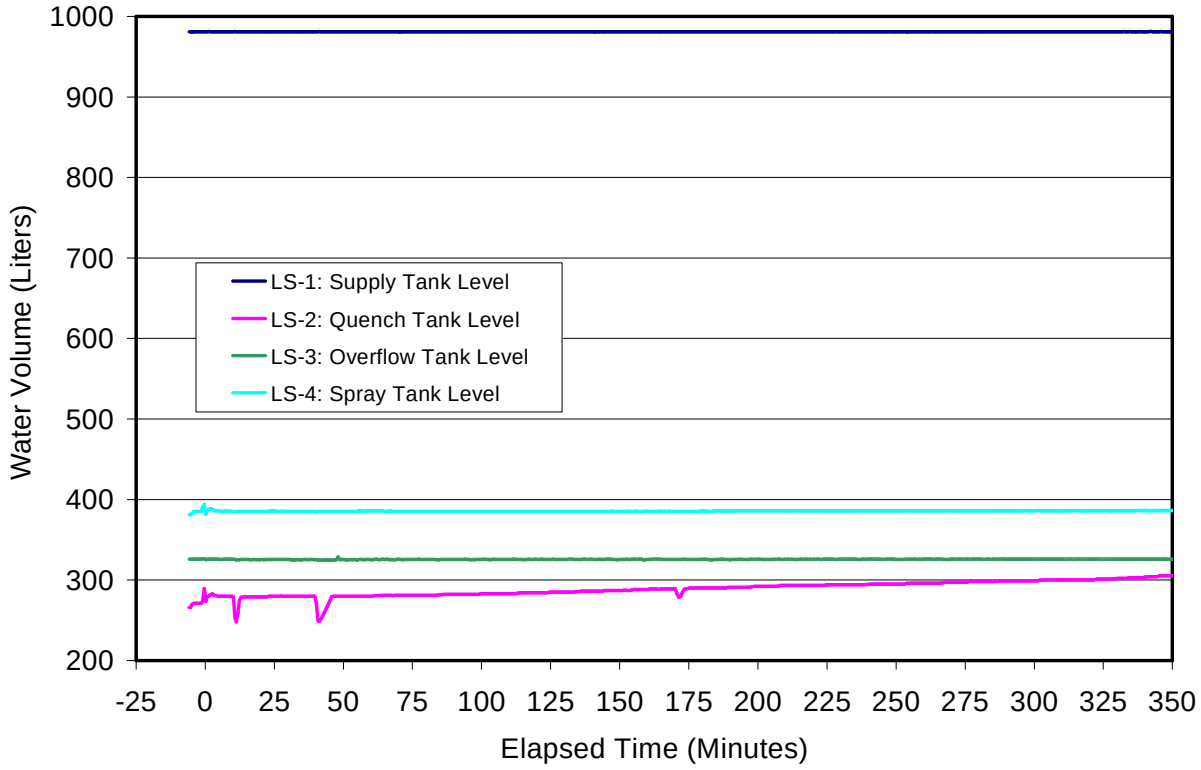

Figure B-56. Tank Water Volume Data.

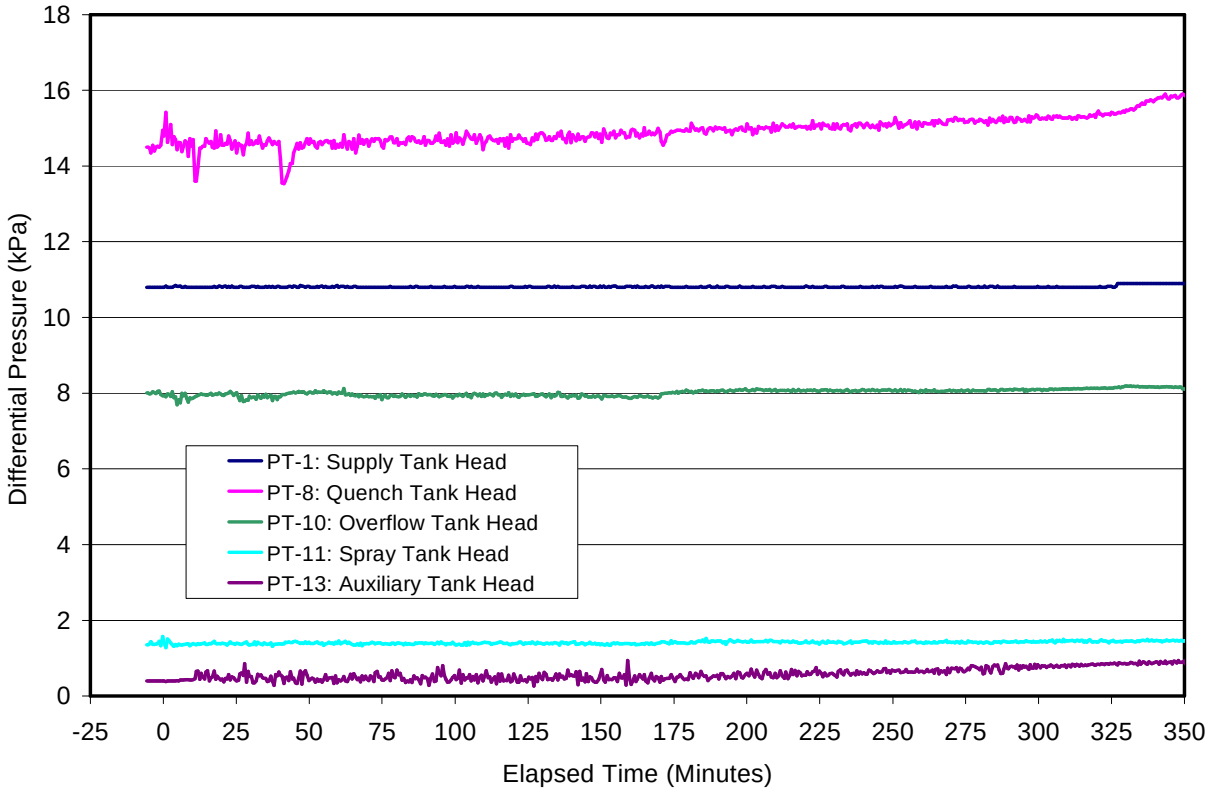

Figure B-57. Supply and Quench System Tank Head Data (Backup).

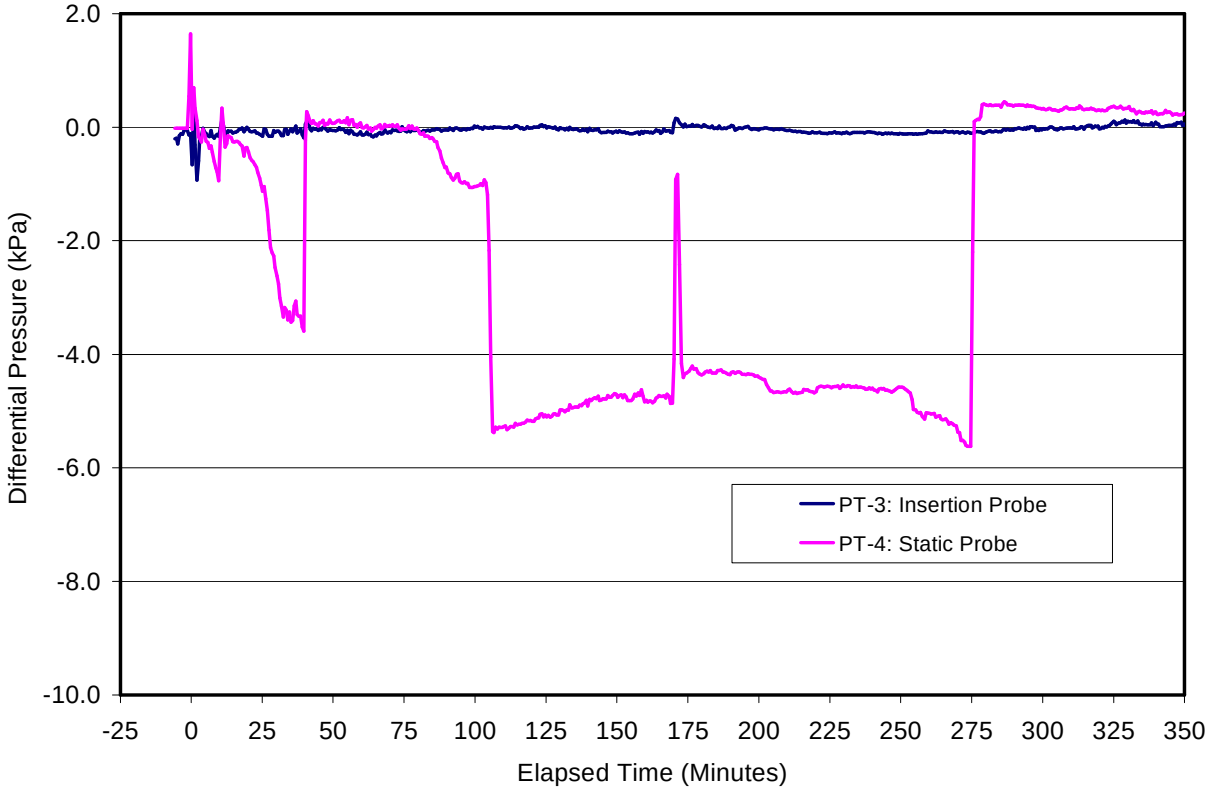

Figure B-58. Test Section Water Head Transducer Data.

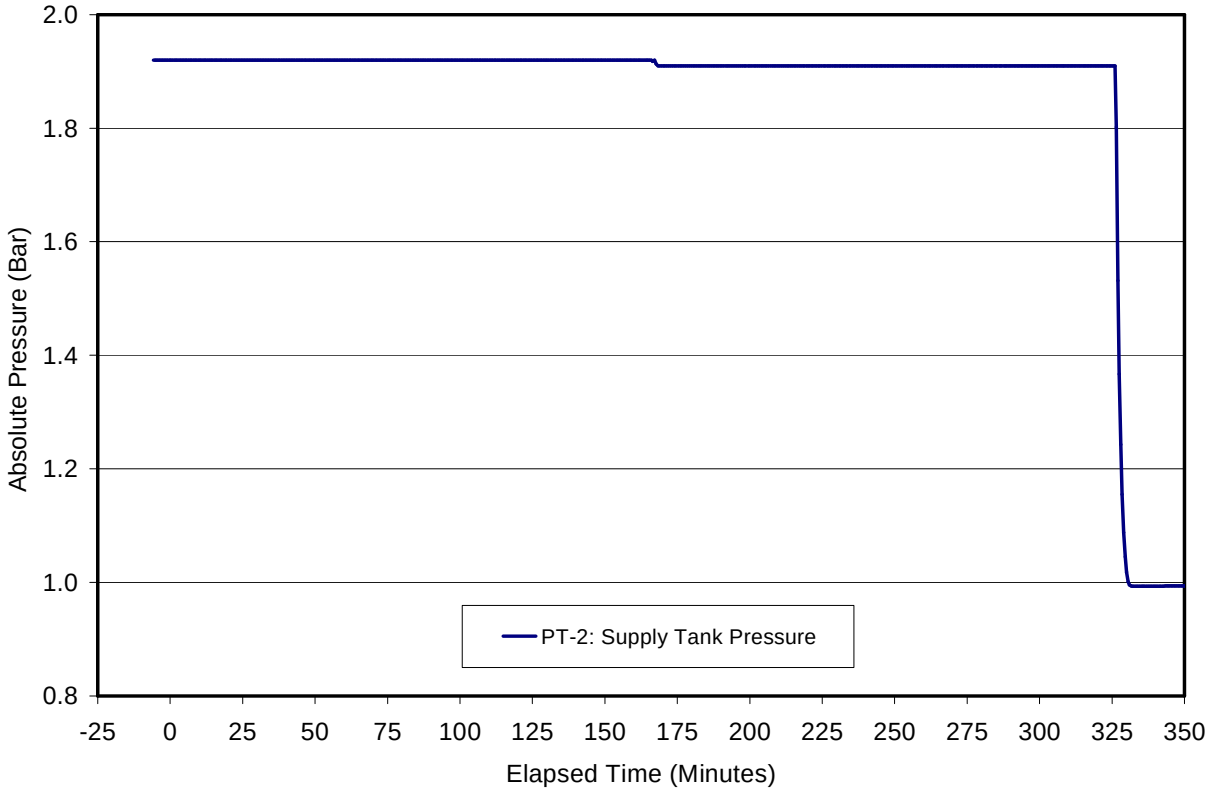

Figure B-59. Water Supply Tank Pressure.

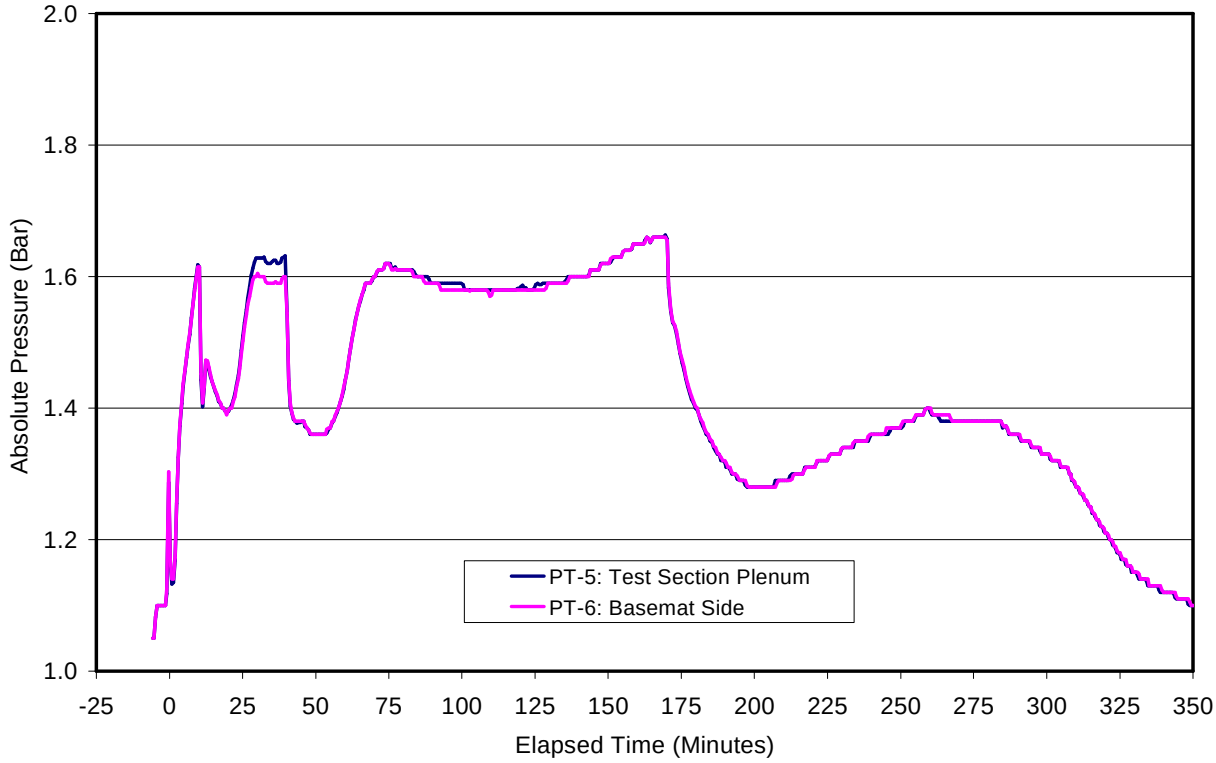

Figure B-60. Test Section Pressure.

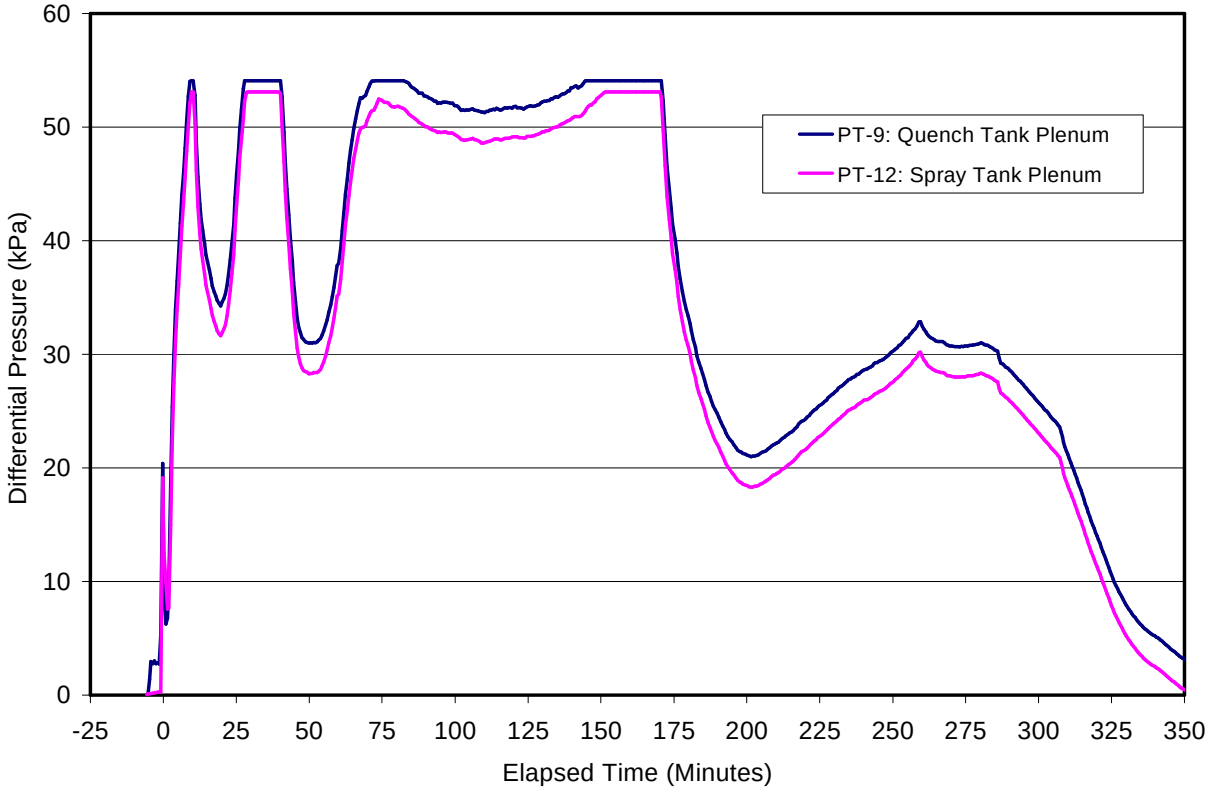

Figure B-61. Quench/Overflow and Spray Tank Plenum Differential Pressures.

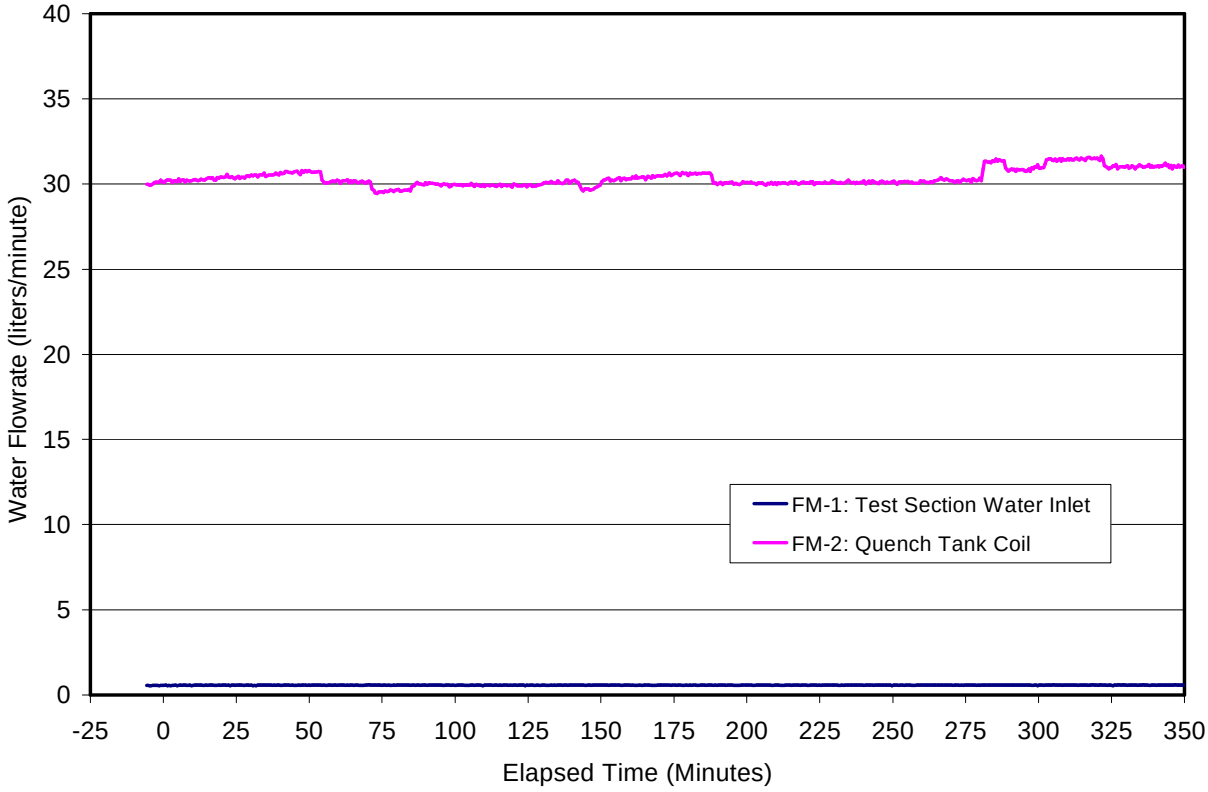

Figure B-62. Water Flow Rates.

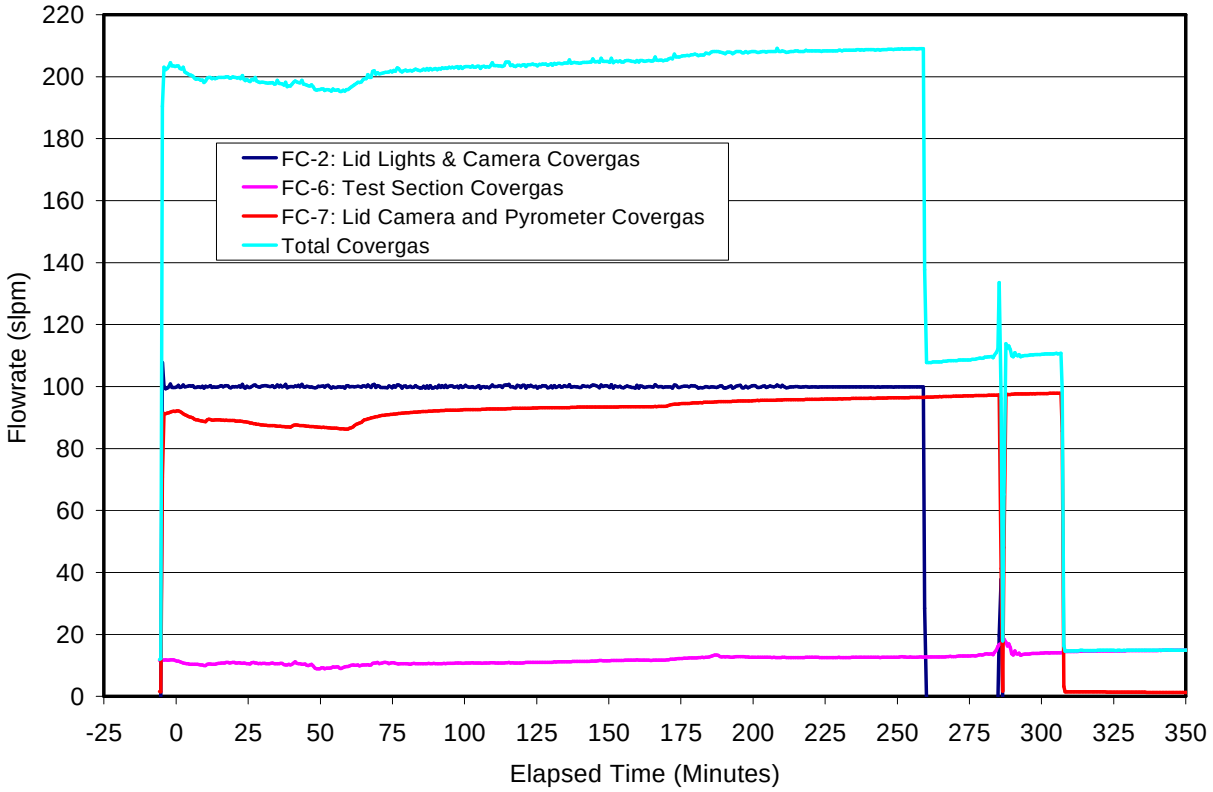

Figure B-63. Test Section Helium Cover Gas Flow Rates.

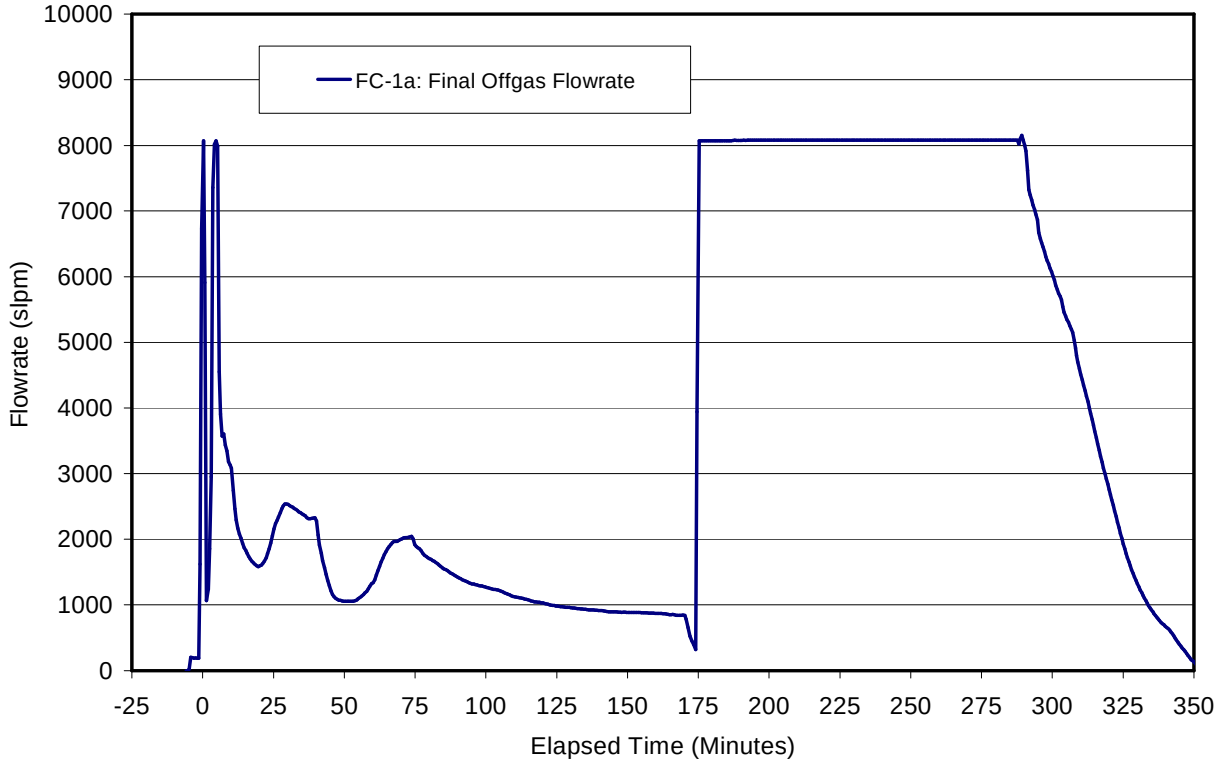

Figure B-64. Final Off Gas Flow Rate.

APPENDIX C
Chemical Analysis Results

This Appendix provides the raw data from the chemical analysis of the five corium samples that were collected as part of the posttest examinations for CCI-5. Sample locations are described in Section 4.4 of this report.

All samples were analyzed using Inductively Coupled Plasma Atomic Emission Spectroscopy (ICP/AES). The analysis was carried out by the Analytical Chemistry Laboratory (ACL) at Argonne National Laboratory. Results are provided in Table C-1. The ICP/AES analysis provides concentrations of selected elements; the elements have been converted to assumed oxide forms in the table. The resultant mass balance should sum to within the measurement error (reported as ± 10 % of the reported elemental concentration for each constituent) if the assumed oxide forms are reasonable and all key sample constituents have been included in the element scan list. As shown in Table C-1, all oxide mass balances fall within this range except sample CCI-7, which was collected from the dense oxide near the core-concrete interface at the center of the test section (see Figure 4-10). The mass balance for this sample is only ~ 85 %, indicating that a significant element was excluded from the scan (unlikely), or the assumed oxide form(s) are not entirely correct. Also note that this sample had a high amount of tungsten (i.e. ~5.8 wt % in elemental form) relative to the other samples. The tungsten would have been introduced into the melt through dissolution of the tungsten electrodes and thermowells that were in contact with the melt during the experiment.

Table C-1. Raw Data from CCI-5 Sample Analyses. (All constituents with elemental concentrations of > 0.1 wt% are shown)

Element	Oxide Form	Sample Number											
		CCI-5		CCI-7		CCI-8		CCI-9		CCI-9 (Dup)		CCI-10	
		Wt% Elem.	Wt% Oxide	Wt% Elem.	Wt% Oxide	Wt% Elem.	Wt% Oxide	Wt% Elem.	Wt% Oxide	Wt% Elem.	Wt% Oxide	Wt% Elem.	Wt% Oxide
Al	Al_2O_3	1.02	1.92	0.85	1.61	1.00	1.90	1.09	2.06	1.07	2.02	1.21	2.28
Ca	CaO	8.06	11.28	7.25	10.14	7.99	11.18	8.49	11.88	8.46	11.84	9.46	13.24
Cr	Cr_2O_3	0.13	0.20	0.08	0.12	0.14	0.20	0.19	0.27	0.18	0.26	0.23	0.34
Fe	Fe_2O_3	0.62	0.89	0.59	0.85	0.62	0.89	0.66	0.94	0.64	0.92	0.71	1.01
Hf	HfO_2	0.05	0.06	0.02	0.02	0.05	0.06	0.06	0.07	0.05	0.06	0.06	0.07
Mg	MgO	0.36	0.60	0.28	0.47	0.36	0.59	0.38	0.62	0.37	0.62	0.41	0.69
Mn	MnO	0.03	0.03	0.02	0.03	0.03	0.03	0.03	0.03	0.03	0.03	0.03	0.04
Ni	NiO	0.02	0.02	0.06	0.08	0.02	0.02	0.02	0.03	0.02	0.03	0.02	0.02
K	K_20	0.36	0.44	0.34	0.41	0.36	0.43	0.39	0.46	0.38	0.46	0.43	0.52
Si	SiO_2	15.49	33.14	14.22	30.42	15.64	33.45	16.31	34.90	16.31	34.90	18.25	39.05
Na	Na_2O	0.22	0.30	0.19	0.26	0.22	0.30	0.23	0.31	0.23	0.31	0.26	0.35
Sr	SrO	0.02	0.02	0.01	0.02	0.02	0.02	0.02	0.02	0.02	0.02	0.02	0.02
Ti	TiO_2	0.18	0.31	0.12	0.20	0.18	0.30	0.19	0.32	0.19	0.31	0.21	0.35
U	UO_2	26.35	29.89	22.62	25.67	25.65	29.10	24.26	27.53	23.78	26.98	20.42	23.16
W	WO_3	1.06	1.34	5.79	7.31	0.92	1.15	0.87	1.10	0.86	1.09	0.99	1.25
Zr	ZrO_2	7.98	10.77	5.72	7.72	7.95	10.74	8.20	11.07	8.15	11.01	8.48	11.46
Total			91.23		85.31		90.37		91.61		90.87		93.84